POLITECNICO DI MILANO
Dottorato di Ricerca in Bioingegneria
Ph.D. in Bioengineering

Francesco De Gaetano

Design, manufacturing and *in-vitro* testing of an innovative biomorphic heart valve made of a new thermoplastic elastomeric biomaterial

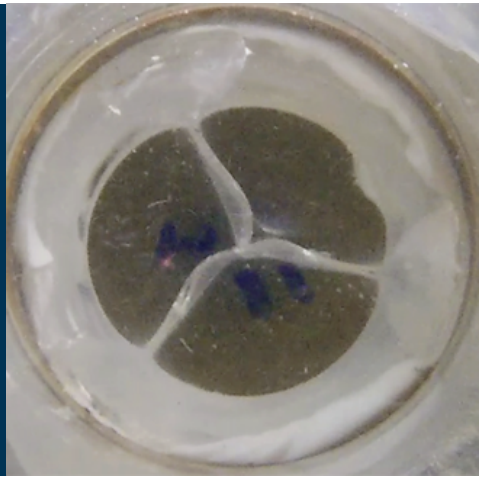

POLITECNICO DI MILANO
Dottorato di Ricerca in Bioingegneria
Ph.D. in Bioengineering

Design, manufacturing and *in-vitro* testing of an innovative biomorphic heart valve made of a new thermoplastic elastomeric biomaterial

Francesco De Gaetano

Supervisor:
Prof. Maria Laura Costantino

PhD Coordinator:
Prof. Andrea Aliverti

Advisor:
Prof. Silvia Farè

XXIX Cycle
March 2017

"*If you're going to try, go all the way. Otherwise, don't even start.*"

Henry Charles Bukowski

"*If you can not measure it, you can not improve it.*"

Lord Kelvin

Acknowledgements

First, I would like to express my sincere gratitude to my supervisor Prof. Maria Laura Costantino. Thank you for guiding my work in these years, your scientific and technical expertise was fundamental to me in successfully developing my research skills. Thank you so much also for the immense trust you have always demonstrated in me.
I would like to thank Prof. Geoff Moggridge, Dr. Joanna Stasiak, Dr. Jacob Brubert and Dr. Marta Serrani from the Department of Chemical Engineering and Biotechnology of the University of Cambridge. Thank you for helping me during these years and thank you so much for sharing your competencies and your precious data, this work would not have been fully complete without your support.
I would like to thank Prof. Dominik Obrist and David Hasler from the ARTORG Biomedical Research Center at the University of Bern, thank you for helping me with the Tomo-PIV experiments.
I would like to thank all the present and past students of LaBS for their sympathy and friendship and for sharing the good as well as the bad moments. Thank you for all the coffees, lunches, beers and most important for making LaBS a second home, I will never forget you.
A very huge thank goes to my family and in particular to my parents: they always support me during these years with encouragement. I thank my "second" family: Francesca, Leonardo, Maria Francesca e Giuseppe. Without them this work would have been much harder and boring.
I thank all my Friends, which are always present when I need.
And last but not least I would like to thank Grazia. This is for you because you always supporting me, being inspiring and pushing me to obtain my best.

Francesco

Abstract

In this work an innovative biomorphic heart valve made of a new thermoplastic elastomeric biomaterial was designed, manufactured and *in-vitro* tested.
Nowadays, only mechanical and biological heart valve prostheses are commercially available. The former ensures long lasting durability but anticoagulant therapy is required all life long; the latter displays better fluid dynamic performance in the short term but does not guarantee adequate durability.
Inspired by the anisotropic architecture of collagen in the natural valve, the use of new polystyrene based block copolymers (BCPs) could be helpful to this purpose. Three styrene BCPs were selected due to their haemocompatibility, low tendency to calcification and better inflammation response if compared to polyester and pericardium. Mechanical tensile and small angle X-ray scattering of these styrene BCPs were performed to assess their properties.
A numerical model replicating the injection moulding technique was developed in order to assess the best configuration of the injection locator to well fill the cavity promoting a mainly circumferentially orientation of the micro-chains. Using simultaneous injection locator at the centre of the free edge of each leaflet, a bioinspired orientation was obtained.
Hydrodynamic testing were performed following the ISO5840:2015 guidelines. An *ad hoc* pulse duplicator was designed and built. All the prototypes manufactured by both injection and compression moulding resulted to meet the minimum requirements in term of both EOA and regurgitation. The results were compared with one mechanical valve and one tissue valve currently on the market. The fluid dynamic field was assess by means of 2D PIV and Tomo-PIV.
Quasi-real time and accelerated fatigue testing were performed on injection moulded SEPS-22 prototypes which show the best short term performances. The fatigue performance was inadequate due to a manufacture imprecision which made the leaflet to be thinner than prescribed by the design. The optimisation of the production technique, would make the proposed bioinspired styrene based heart valve prosthesis to have the potential to overcame the issue of durability and need for anticoagulation therapy.

Glossary of Acronyms

0D	Zero-dimensional
3D	Three-dimensional
AV	Atrio-Ventricular
BHV	Bioprosthetic Heart Valve
BCP	Block copolymer
BP	Back Pressure
CAD	Computer-aided design
CFD	Computational fluid dynamics
CO	Cardiac output
CT	Computer tomography
ECG	Electrocardiogram
FE	Finite element
FEM	Finite element method
FSI	Fluid-structure interaction
HV	Heart Valve
HVP	Heart Valve Prosthesis
MHV	Mechanical Heart Valve
MSPD	Mean Systolic Pressure Difference
μCT	Micro Computed Tomography
PCU	Polycarbonate Urethane
PHV	Polymeric Heart Valve
PIV	Particle Image Velocimetry
PTFE	Polytetrafluoroethylene
PU	Polyurethane
PEU	Polyether Urethane
PEUU	Poly(Etherurethane-Urea)
QLV	Quasi-Linear Viscoelastic
RHD	Rheumatic Heart Disease
SAXS	Small Angle X-ray Scattering

SBCP	Styrenic Block Copolymer
SEPS	Poly(Styrene-Ethylene-Propylene-Styrene)
SIBS	Poly(Styrene-b-Isobutylene-b-Styene)
SV	Stroke Volume
TAVI	Transcatheter Aortic Valve Implantation
TEHV	Tissue engineered heart valve
Tg	Glass Transition Temperature

Contents

Chapter 1

Aims

In the present chapter, the motivations that led to develop this work and the aims are presented. In particular, a detailed description of the different steps carried out to design the new polymeric heart valve and in which chapter to find the different steps are given as well.

1.1 Motivation

FROM **Chapter 2** emerges that the ideal heart valve prosthesis does not exist yet and there are still improvement action to be done on the prostheses currently available. Nowadays two major types of implantable artificial heart valve are accessible to substitute severe insufficient or stenotic native valve: mechanical and bioprosthetic heart valves. The former are made of hard material (i.e. pyrolytic carbon) and show greater durability; on the other hand they have non physiological flow profiles and require daily anticoagulant treatment to avoid blood clotting. The latter are made of biological material and display better fluid dynamic behaviour and good haemodynamic performances but are characterised by limited durability and a significant risk of failure due to tissue degradation (Schoen and Gotlieb, 2016). As a matter of fact, porcine and bovine bioprostheses undergo chemical treatment to reduce immunologic response, which reduce mechanical properties.
To overcome the problems of the prostheses, researchers are studying different solution and innovative design.
Tissue engineering heart valves were born with the goal of generating a living valve replacement that would obviate the complication of conventional valve prostheses (Ghazanfari et al., 2015; Matheny et al., 2000). These innovative, fascinating devices have the potential to grow in a growing patients. However, to obtain the right chemical and physical stimuli to allow cells growing is critical and *in-vitro* studies (Schoen and Gotlieb, 2016; Syedain et al., 2016, 2015) have not been reported success in long-term function.
Another solution widely studied in the past were the polymeric heart valve prostheses. Fully polymeric heart valves have attracted considerable interest in the past due to their potential to combine the haemodynamic performances of biological valves with the durability of mechanical valves.
This interest has waned due to the long track record of initial promises followed by failures at the preclinical stages.
Despite several authors contributed to the development of polymeric heart valves, their use is limited to pulsatile ventricular assist devices or, however in other application where good performance in the long lasting are not necessary. To overcome the problem of bad long lasting performances, a new design capable to optimise both the geometry of the device and the mechanical properties of the material is necessary.
The manufacturing of fully polymeric heart valves still remains a challenge and they have great potential to revolutionize the treatment of heart valve disease.
In recent years, revolutionary advance in nanotechnologies propose novel ma-

terials very useful for biomedical application. Block copolymers are a new polymeric class capable to tailor their mechanical properties by using different polymer fragments. The styrene based block copolymer, like polystyrene-b-polyisobutylene-b-polystyrene (SIBS), is an emerging new material belonging to this class, with encouraging mechanical behaviour.
Several experimental and computational studies (Balguid et al., 2007; Billiar and Sacks, 2000; Claiborne et al., 2013b; Martin and Sun, 2012) show the functional role of the anisotropy of the biological tissue in the reduction of the stresses in the leaflet during closure and in the stabilisation during opening. Stasiak et al. (2009) demonstrated the anisotropy of this polymer and its capability to orient the internal micro-structure, if properly manufactured.
Showing good haemocompatibility, biocompatibility and log-term stability (Pinchuk et al., 2008), SIBS material seems to be suitable to be used to build heart valve prosthesis. Cacciola et al. (2000); De Hart et al. (1998) have proposed that fibres could be embedded into polymeric matrices to mimic the anisotropy mechanical properties of the native valve, but these attempts failed due to debonding of the fibres from the bulk.
Another trileaflet polymeric valve has been developed by Wang et al. (2010) using SIBS with an embedded reinforcement of polyethylene terephthalate, but, even in this case, the SIBS valve failed in animal testing because of material failure and calcification. Indeed, following cracking of the SIBS coating layer, the underlying PET fibres became exposed in animal tissue where they were tested, triggering chronic inflammation that led to excessive tissue encapsulation.
Another way of achieving anisotropy, as showed by Stasiak et al. (2010), could be to properly orient the microstructure. Modifying the volume fraction of the styrene block and the thermo-mechanical parameters during the manufacture, it is possible to tailor the mechanical response of the material and to orient the styrene micro-chain. At present, only few works are reported in literature using styrene block copolymer to obtain polymeric heart prostheses (Claiborne et al., 2011; Duraiswamy et al., 2008; Gallocher et al., 2006), but none of these has treated the material to orient the micro chain. Several studies were performed to understand the effects of fibre orientation on the stress distribution inside the leaflet (Cacciola et al., 2000; De Hart et al., 1998; Liu et al., 2007), but only Zaffora (2011) created a computational method for the optimisation of the micro chain orientation for the design of a polymeric heart vale prosthesis.

1.2 Aims

As described in **Chapter 2**, heart valve prostheses (HVP) cover a large spectrum of design. Each design was obtained starting from specific requirements to overcome different problems (i.e. obtain good fluid-dynamics, reduce inflammatory response, enhance biocompatibility etc.).
The aim of this work is to develop and test a new HVP entirely made by a co-polymer block of styrene with the capability to mimic the oriented microstructure inside the natural aortic valve leaflet. To accomplish this goal, an engineering design process was mixed with a scientific method.
The classic engineering design process (applied to obtain a new device) mixed with the scientific method (used to better understand how to control the micro-chain orientation in styrene based co-polymer) were used to define the process chart (Figure 1.1) and by consequence the different steps required to achieve the desired results. The first step to achieve this result is to choose the most suitable material and the manufacturing process capable to orient the microstructure. Several polymers have been considered for use in the past by different research groups (see Section 2.6) but only few materials could be micro and nano oriented. Based on the literature data, three different types of styrene based block copolymers were chosen. In **Chapter 3** mechanical tests and micro-chain orientation analyses are performed on samples of materials to evaluate the mechanical properties of the polymers and the micro-chain orientations inside. Based on the results of these tests, the polymer could be chosen or discarded.
In **Chapter 4** the main parts constituting the polymeric aortic valve prosthesis are described. Basically an heart valve prosthesis is based of two parts: the *leaflets* and the *stent*. The leaflet is the most critical component but the stent design, especially if made of polymeric material, should not be overlooked. However, to design a polymeric HPV it is necessary to take great care also to the design of the leaflet, keeping in mind the claim for reduce regurgitation, pressure loss and enhance long term duration of the implantation. The shape of the leaflet could drastically influence the short term performance (energy loss, vorticity, blood shear stress, etc.), on the other hand, the stent shape could extremely influence the long term performances. For these reasons different leaflet and stent shapes (and materials) have been proposed by different research groups (see Section 2.6).
After selecting material, leaflet and stent geometry a mould was made to produce statistically significant number of prototypes to be tested. This work is based on a collaboration with the research group of the Professor Geoff G. Moggridge belonging to the Department of Chemical Engineering and Biotechnol-

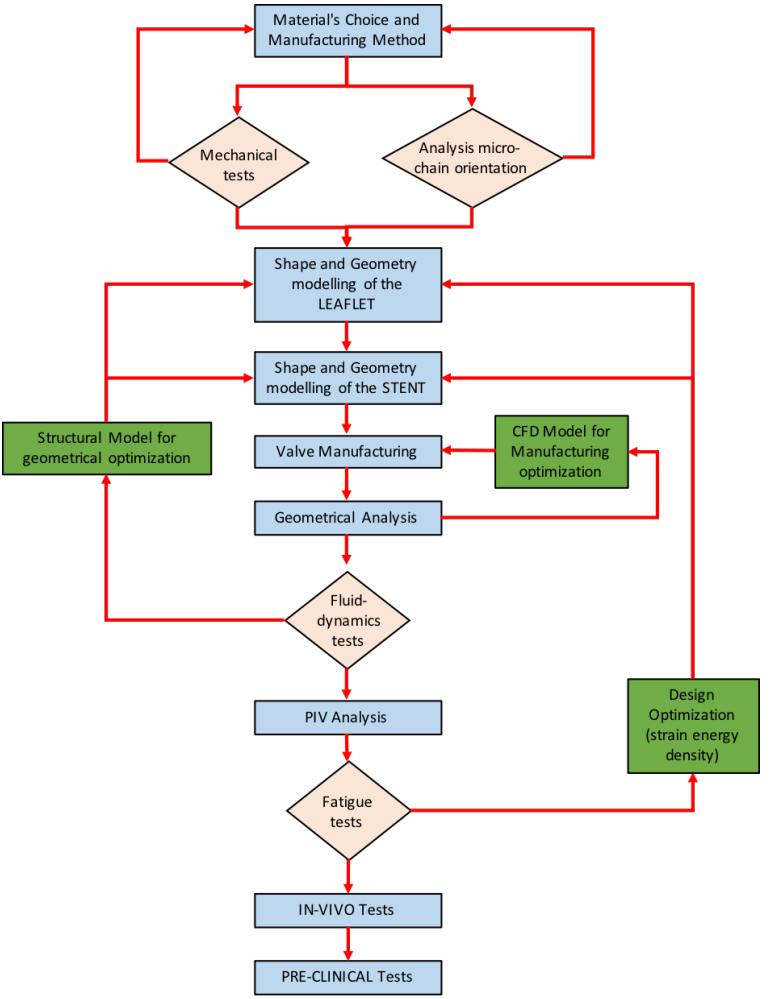

Figure 1.1 Engineering process design work flow.

ogy of the University of Cambridge. They have facilities in the manufacturing of these styrene based materials. All the required fluid dynamic tests to assess the short term performance of the different prototypes are describe in **Chapter 6**. If fluid dynamic tests failed, a structural model was used to modify the geometry of the leaflet, of the stent or of both of them. On the other hand if

the micro-chains orientation inside the leaflet is not altogether satisfactory, a computational fluid dynamic (CFD) model could be used to better set all the parameter involved in the manufacturing technique.This finite element model were as well describe in **Chapter 5**. On the contrary, if both fluid dynamics tests and micro-chain orientations analyses provide good results, further investigations could be made. In particular, micro computed tomography (μCT) or other surface analyses techniques, was used to inspect the external structure and to analyse accurately the morphology of the prototypes to better understand if there are difference between the theoretical model (CAD) and the real prototypes.
On these prototypes, a particle image velocimetry (PIV) was performed to compare the velocity profile distribution passing through the polymeric prototype and an HVP considered as a gold standard for its good fluid dynamic (like a bio-prosthetic heart valve, see Section 2.4.2). In order to obtain significant results, the two prostheses must have the same tissue annulus diameter.
The last *in-vitro* tests to perform before to carry out the *in-vivo* tests are the fatigue tests. The achievement of an adequate device lifetime remains the main challenge in the development of a clinically viable polymeric prosthesis. Accelerated testing of prosthetic heart valves allows simulation of wear and fatigue sustained by the heart valve prostheses, and to estimate the valves life expectancy in human body.
Morphology inspection, particle image velocimetry tests and fatigue tests were set out in **Chapter 6** Only if the PHV withstands a reasonable number of cycles (given by the International Standards) it is possible go ahead to perform the *in-vivo* and *pre-clinical* tests. If the prosthesis lifetime is not acceptable, an optimisation regarding the microstructure of the leaflet, the design of the stent or how these two component are filleted, is required. A numerical model of the polymeric valve, based on the strain energy density, was performed. As a matter of fact, the strain energy density is a widely used criterion to predict elastomers lifetime; this result suggests a possible increase of the device durability if the polymer microstructure is optimised.
To sum up, in the design process to obtain a new polymeric heart valve, multiple iterations were taken into account to obtain the best solution. A prototype is an operating version of a solution. It is often made with different materials than the final version, and generally it is not as polished but prototypes are a key step in the development of a final solution, allowing the designer to test how the solution will work. All the general results and limitations of this work are deepened in **Chapter 7**.

Chapter 2

Background

This introduction provides a description of the aortic heart valve anatomy and physiology before analysing the pathologies which lead to the native heart valve failure. Different kinds of handling and replacement, before turning to the prosthetic implants are considered.
A review of different types of heart valve prosthesis present in the literature is described.

2.1 Anatomy and Physiology of the Aortic Heart Valves (Guyton and Hall, 2006; Hansen, 2010)

THE heart is a hollow muscular (cardiac muscle), whose main function is to provide a pulsatile blood stream to both the pulmonary (oxygenation) and systemic circulation (nutrients, metabolic waste products, hormones to and from tissues, etc).

The heart is enclosed within a fibroserous (composed of both fibrous and serous elements) pericardial pouch that extends and blends into the adventitia of the great vessels that enter or leave the heart. The pericardium has a fibrous outer layer that is lined internally by a serous layer (parietal serous layer), which then reflects and is continuous with a visceral serous layer that is the outer covering of the heart itself (also known as the epicardium). These two serous layers form a potential space known as the pericardial sac (cavity).

The human heart has four chambers, each with unique internal features related to their function (Figure 2.1). The heart can be considered as essentially consisting of two muscular pumps in series. The right side of the heart is composed of the right atrium and right ventricle. These chambers receive blood from the systemic circulation and pump it to the pulmonary circulation for gas exchange. The left atrium and left ventricle receive blood from the pulmonary circulation and pump it to the systemic circulation. The atria contraction is synchronous, followed by contraction of the two ventricles.

During the heart cycle, each ventricle exchanges blood with the corresponding atrium and the corresponding artery through natural orifices. The cardiac cycle consists of a period of relaxation called diastole, during which the heart fills with blood, followed by a period of contraction called systole. Figure 2.2 shows the different events during the cardiac cycle for the left side of the heart.The top three curves show the pressure changes in the aorta, left ventricle, and left atrium, respectively. The fourth curve depicts the changes in left ventricular volume, the fifth the electrocardiogram, and the sixth a phonocardiogram, which is a recording of the sounds produced by the heart, mainly by the closure of the heart valves. In order to maintain unidirectionally flow, each orifice is occupied by special structure called *heart valves* (HV).

From the anatomical point of view, two kinds of heart valves can be identified: *atrioventricular* HV and *semilunar* HV (Figure 2.3). The atrioventricular valves (the tricuspid and mitral valves) prevent backflow of blood from the ventricles to the atria during systole, while the semilunar valves (the aortic and pul-

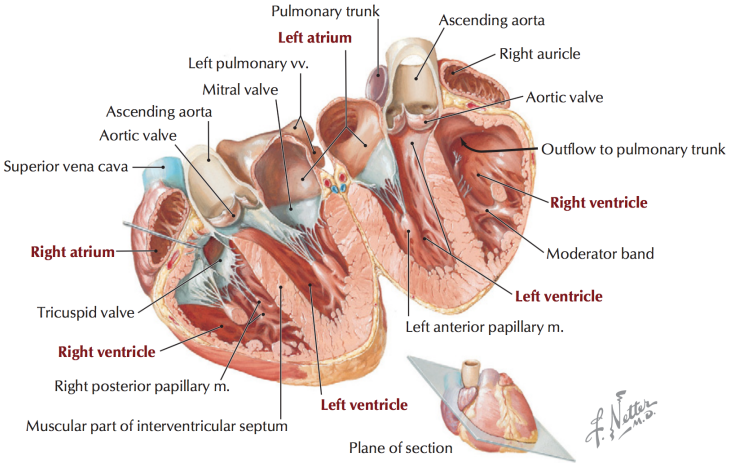

Figure 2.1 Chambers of the heart (Hansen, 2010).

monary artery valves) prevent backflow from the aorta and pulmonary arteries into the ventricles during diastole. These valves close and open passively. Two or three thin membrane structure, called *leaflet*, prevent the backflow by coaptation. They close when a backward pressure gradient pushes blood backward, and they open when a forward pressure gradient forces blood in the forward direction. The aortic and pulmonary artery semilunar valves function quite differently from the atrioventricular valves. First, the high pressures in the arteries at the end of systole cause the semilunar valves to snap to the closed position, in contrast to the much softer closure of the atrioventricular valves. Second, because of smaller orifice area, the velocity of blood ejection through the aortic and pulmonary valves is far greater than that through the much larger atrioventricular valves. Also, because of the rapid closure and rapid ejection, the edges of the aortic and pulmonary valves leaflet are subjected to much greater mechanical abrasion than are the atrioventricular ones. Finally, as above reported, the atrioventricular valves are supported by the chordae tendineae, which is not true for the semilunar valves. The aortic and pulmonary valves must be constructed with an especially strong, flexible fibrous tissue base to withstand the extra physical stresses.

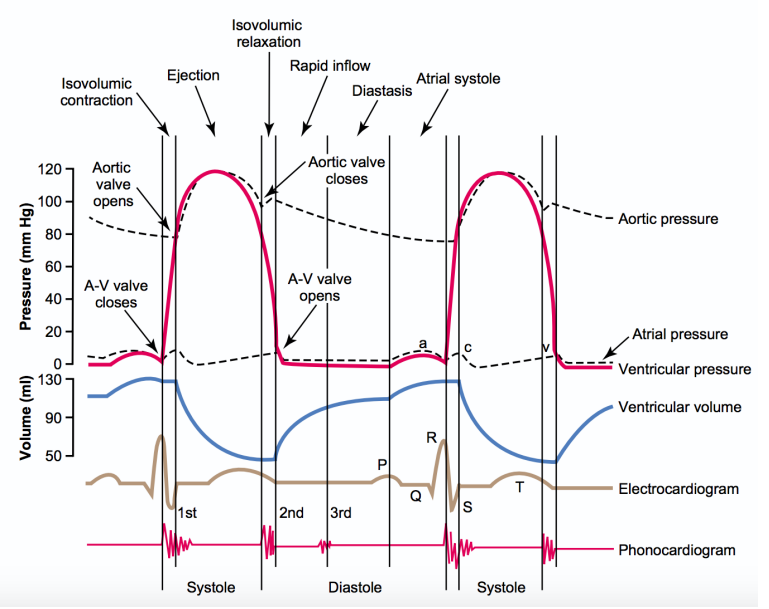

Figure 2.2 Events of the cardiac cycle for left ventricular function, showing changes in left atrial pressure, left ventricular pressure, aortic pressure, ventricular volume, the electrocardiogram, and the phonocardiogram. Modified from Guyton and Hall (2006)

2.2 Biomechanics of the Aortic Valve

In this section the physiology and the microstructure of the natural aortic valve is deeply described. This work is focused on the development and test of a new aortic prostheses and the reason that supports this choice will be described in Section 2.3. When the left ventricle contracts, the ventricular pressure increases rapidly until the aortic valve opens. Then, after the valve opens, the pressure in the ventricle rises much less rapidly because blood immediately flows out of the ventricle into the aorta and then into the systemic distribution arteries. Downstream the aortic valve, the aortic pressure increases to about 120 $mmHg$ (maximal pressure called *systolic pressure*). At the end of systole, the elastic walls of the arteries maintain a high pressure in the arteries, even during diastole when the aortic pressure usually decreases slowly to about 80 $mmHg$ (*diastolic pressure*) because the blood stored in the distended elastic arteries flows continually through the peripheral vessels back to the veins (Figure 2.2).

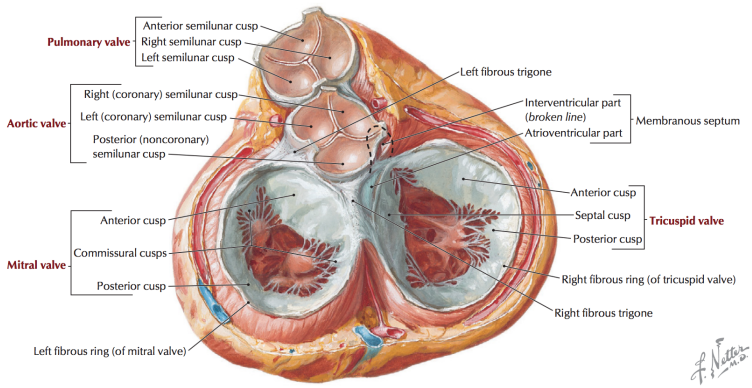

Figure 2.3 Heart in ventricular diastole viewed from above without atrial chambers (Hansen, 2010).

Now, the pressure inside the left ventricle decreases to about 0 $mmHg$ and the pressure gradient across the closed aortic vale is about 100 $mmHg$. At rest, the systolic phase lasts $^1/_3$ of the cycle period and the diastolic phase for the remaining $^2/_3$. Moreover, in physiological condition, a typical resting heart rate is 70 bpm, whit an average cardiac output (CO) of 5 $l \cdot min^{-1}$. In this conditions, the aortic valve opens and closes 40 million cycles each years. It appears clear how the microstructure of the leaflet have to be well organised to support these loads for most of the time (Figure 2.4).

The aortic valve is made of three flexible leaflets. The aortic leaflet corresponding to the ostium of the right coronary artery is called the right leaflet, the one corresponding to the left coronary ostium is called the left leaflet and the non-coronary leaflet is called the posterior (Figure 2.5). The tissue of the leaflet is composed of biomechanically responsive extracellular matrix (ECM) and valve cells, which actively adjust valve structure and behaviour in both health and disease states (Schoen and Gotlieb, 2016).

The aortic valve leaflets are composite, laminated structures, consisting in three layers: *ventricularis*, *spongiosa* and *fibrosa* (Figure 2.6). The fibrosa and ventricularis layers are located towards the aortic and ventricular surface of the leaflet, respectively, and are separated by a gelatinous layer: the spongiosa (Vesely and Noseworthy, 1992). Spongiosa consists of highly hydrated glycosaminoglycans (GAGs) and proteoglycans (PGs) as well as some loosely arranged collagen and elastin. It enables shearing between the two layers during loading and unloading (Hasan et al., 2014).

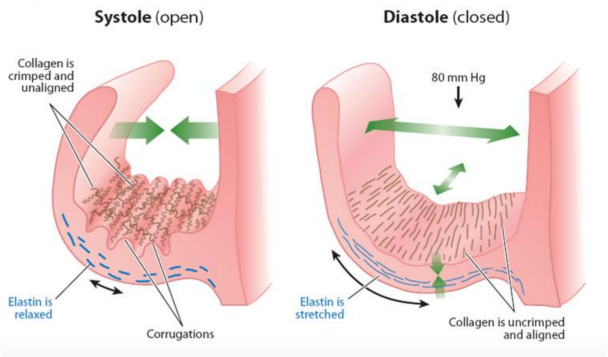

Figure 2.4 Schematic representation of architecture and configuration of aortic valve cusp in cross section and of collagen and elastin in systole and diastole. Modified from Duan et al. (2014).

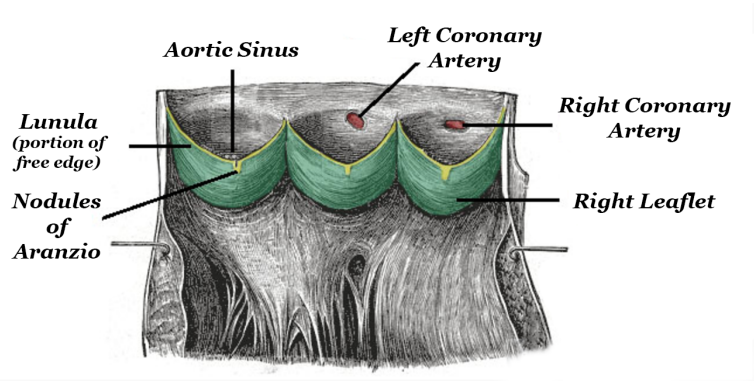

Figure 2.5 The aortic valve leaflet, aortic sinuses, and the origin of the coronary arteries. It is possible to observe the lunula, one of each portion of the free edge divided by the nodule of Aranzio (Hansen, 2010).

The fibrosa and ventricularis layers are themselves made of multiple layers of collagen fibres and elastin properly oriented (Billiar and Sacks, 2000; De Hart et al., 2004; Martin and Sun, 2012; Vesely, 1997; Vesely and Noseworthy, 1992), while the spongiosa is rich of proteoglycans.The behaviour of soft tissues is well know to exhibit a highly non-linear stress-strain relationship, undergoes large deformations, and complex viscoelasticity (Sacks et al., 2010).
The fibrosa, by virtue of its greater thickness and higher elastic modulus, un-

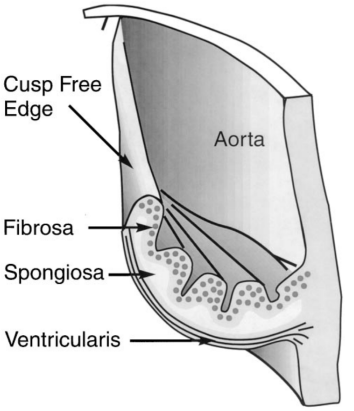

Figure 2.6 A cutaway through the leaflet and aortic wall showing the internal configuration of the fibrosa, spongiosa and ventricularis. Near the central portion of the leaflet, the fibrosa exists as a folded sheet that unfolds as the leaflet stretches radially. Modified from (Gallocher et al., 2006).

doubtedly provides the greatest contribution to resisting tensile forces in the circumferential direction. Its radial modulus, however, is identical to that of the ventricularis (Vesely and Noseworthy, 1992). Both layers therefore possess a similar amount of radial collagen fibres, and may equally contribute to limit the radial extensibility of aortic valve leaflet. The anisotropic mechanical properties of fibrosa and ventricular (Figure 2.7), due to the anisotropic orientation of the collagen fibres, are accountable for the mechanical behaviour of the whole leaflet (Sacks et al., 2010; Tseng and Grande-Allen, 2011; Vesely and Noseworthy, 1992). The fibrosa layer shows a higher degree of orientation while the ventricularis is more randomly oriented. The degree of fibre orientation for both layers became more similar during the diastole. When the transvalvular pressure exceeds 60 $mmHg$, the orientation inside the layers is almost not detectable (Sacks et al., 1998). The highly aligned aortic valve fibre architecture is responsible of the non-linear stress-strain relationship in the entire cusp. As a matter of fact, the same behaviour of fibrosa and ventricularis is observed on the whole leaflet in both uniaxial tensile tests (Vesely et al., 1990) and biaxial test condition (Billiar and Sacks, 2000; Martin and Sun, 2012). As a consequence of this particular fibre distributions, the leaflet circumferential stiffness is much higher than the radial stiffness, about 15 MPa and 2 MPa, respectively (Balguid et al., 2007; Mavrilas and Missirlis, 1991). A complete qualitative and

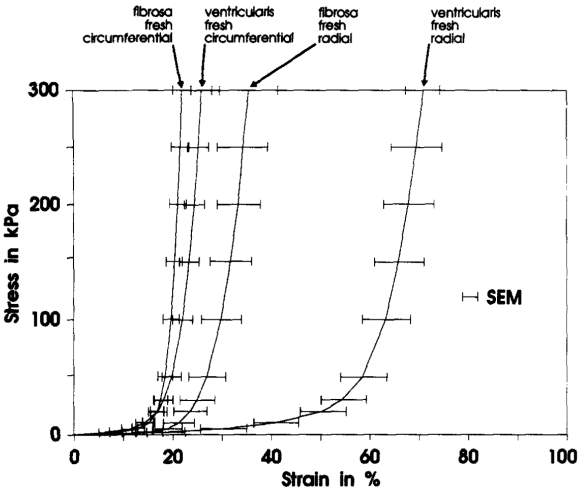

Figure 2.7 Mean stress-strain curves for fresh fibrosa and ventricularis components tested in circumferential and radial directions. The error bars represent the computed standard error of the mean. Note the significantly greater extensibility of the fresh ventricularis in the radial direction, and the near isotropic elasticity of the fibrosa. Modified from Vesely and Noseworthy (1992).

quantitative analyses of the whole valve and leaflet fibre bundle branching patterns using a novel imaging system was performed by Rock et al. (2014). They made different fascinating polarised light images of the aortic leaflets (Figure 2.8), where is possible to observe the major fibre bundle orientation. Not only the *in-plane* response but also the *time dependent* and *flexural* behaviours of the aortic valve leaflets were investigated, in the past, by different authors. How confirmed by the uniaxial test performed by the Carew's group (Carew et al., 2000, 1999), Quasi-Linear Viscoelastic (QLV) theory, well represents the mechanical response although it is one dimensional and does not take into account material anisotropy. Stella et al. (2007) investigated time dependent aortic valve behaviour under physiological biaxial loading states. The results show the independence between stress-strain response and strain rate. Moreover, the aortic valve leaflets exhibit significant stress relaxation, while the creep over the 3h test duration was negligible. The aortic valve leaflets undergo bending every cycle, flexing within and against the natural curvature. Being a three layered structure, fibrosa, ventricularis and spongiosa have different strain.

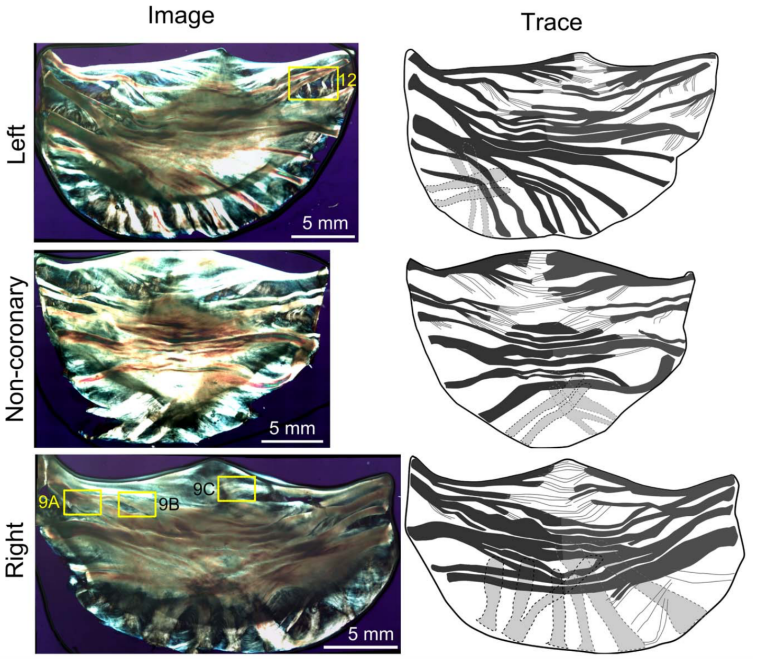

Figure 2.8 Polarised light images of three representative aortic valve leaflets. Images of three representative leaflets (left) along with traces of the major fibre bundles (right) to clarify primary structures of the leaflets. Fibre bundles appear yellow-orange and membranes appear blue as a result of the use of transmitted elliptically polarised light imaging. Clear differences in the fibre bundle arrangement were shown in the three leaflets. The left leaflet was the most asymmetric, while the non-coronary and right leaflets were more symmetric. Fibre bundles were most distinct at the edge (root) and branched or spread out towards the belly of the leaflet. Overall, fibre bundles appeared to present a cross-hatched, overlapping structure with thin connecting membranes. [Reprinted from (Rock et al., 2014) with permission by Elsevier].

The contribution of each layer is *a priori* unknown. To assess the flexural behaviour, bending tests on radial and circumferential strips of porcine aortic heart valve leaflets were performed by Sacks et al. (2010) both in 3-point and cantilever configuration. The results showed that the fibrosa layer is slightly stiffer than ventricularis (the neutral axis of bending is located at 0.55-0.60 normalised tissue thickness, that is in fibrosa layer) and, there is no evidence of slipping between layers. The results suggest that the leaflets behave as a whole and the

three layers undergo a maximum strain equal to 7%. In conclusion, the effectiveness of the aortic heart valve is the results of a combination of different mechanisms. The anisotropic behaviour of the leaflet helps the valve to better withstand the loading state, while the layered structure allows the valve to bend easily in any directions: the results is a superior flexibility and high strength with low thickness.

2.3 Aortic Valve Disease and Treatment

Although each valve may be involved in disease, the mitral and aortic valves are the most commonly affected. As explained in Section 2.1 these two valves are subjected to higher pressure than the tricuspid an pulmonary valves. Major problems include *stenosis* (narrowing) or *insufficiency* (compromised valve function, often leading to regurgitation). Mitral stenosis leads to left atrium dilation; usually caused by rheumatic heart disease (RHD) while mitral regurgitation can be caused by abnormalities of valve leaflets, rupture of papillary muscle or *chordae tendineae*, papillary muscle fibrosis or left ventricular enlargement.
Aortic stenosis, the second leading cause of cardiovascular mortality in USA (17,000 deaths annually), is generally caused by RHD, calcific stenosis and congenital bicuspid valve (1-2% of the population) and leads to left ventricular overload and hypertrophy. Aortic regurgitation (Figure 2.9), also called insufficiency or incompetence, is caused by congenitally malformed leaflets, RHD, ankylosing spondylitis, Marfan syndrome and aortic root dilation. Marfan syndrome is an autosomal-dominant disorder of connective tissue caused by mutations in the fibrillin-1 (FBN1) gene, located on chromosome 15q15-31 with an estimated prevalence of 1 in 3,000-5,000 leading to multi-systemic clinical problems (Lee et al., 2016b). In patients with Aortic root aneurysm, aortic dissection or annular aortic ectasia, especially in cases where Marfan disease is present, the aortic valve structure may be normal and valve incompetence is the result of leaflet being stretched open by a dilated aortic root (Feindel and David, 2004). In these case, it is possible to preserve the natural aortic valve by removing the surrounding diseased aortic tissue.
Therapies generally rely on surgery, including valve repair or valve replacement, both of which continue to have limitations. Although conservative medical therapy in case of valve disfunction is preferred, HV replacement therapy is a standard treatment in case of acute disease. Moreover, due to the lack of effective medical therapies and the evolution of cardiac valve replacement and repair procedure, approximately 100,000 heart valve substitutions every year in

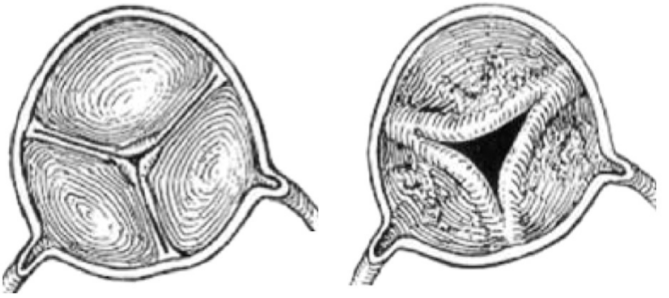

Figure 2.9 Comparison between closure of healthy (a) and insufficient (b) aortic valve

the United Stated (and nearly 300,00 worldwide) were performed (Schoen and Gotlieb, 2016), and this number is projected to reach 850,000 by the year 2050, as the average age of the population increases (Hasan et al., 2014). It's crucial, therefore, to obtain a valid and reliable device able to reproduce the function of the natural heart valve. Different techniques were developed in these years with the purpose to replace faulty aortic valve. The Ross procedure is a type of specialised aortic valve surgery where the patient's diseased aortic valve is replaced with his or her own pulmonary valve. The pulmonary valve is then replaced by cryopreserved cadaveric pulmonary valve. In children and young adults, or particularly active elder patients, this procedure offers several advantages over traditional aortic valve replacement with manufactured prostheses. Longevity of the pulmonary autograft in the aortic position is superior to bioprostheses such as porcine valves, which tend to degenerate after only few years in patients under 35 years of age. Furthermore, anticoagulation is not required as with mechanical valves. Thus, individuals can lead an active life without the risks associated to anticoagulation therapy. This is especially important for women of child bearing age needing aortic valve replacement, as anticoagulation is contraindicated in pregnancy. Unfortunately, due to the lack of cadaveric pulmonary valves that could well fit for different size of patients, the Ross procedure is seldom utilised. As matter of fact, this procedure is well accepted only in active, young adult patients ($<$ 50 years of age) with aortic stenosis and a normal size of the aortic root (Bansal et al., 2015). Nowadays, operative mortality for routine valve replacement is less than 4% for aortic valve replacement (AVR) (Nishimura et al., 2014), and 5-9% for mitral valve replacement (MVR) (Yanagawa and Christakis, 2012). Moreover, following AVR with either mechanical or tissue valves, the probability of a 10- year survival is about

70% (Schoen and Butany, 2016). Also for that reason, valve replacement is the widely used elective therapy. Currently, two typologies of heart valve prosthesis (HVP) can be implanted: mechanical HVP or biological HVP. Mechanical valves, while long lasting, require life-long anticoagulation therapy. Biological valve, on the other hand, while not requiring anticoagulation, expose the patient to the potential need for a re-operation in 10-15 years. A major disadvantage of both types is that they do not allow for somatic growth or remodelling after implantation.

2.4 Currently Used Heart Valve Prostheses

The main purpose of the heart valve prostheses is to obtain equivalent performances of the natural heart valves. Due to the impossibility of obtaining both performances and durability similar to the natural heart valve, in the years many researcher are focused to find the right compromise between correct fluid-dynamic behaviour and reliability. The main design specification are:

- *fluid-dynamic*: the flow passing through the prosthesis should be undisturbed and strictly unidirectional, with low pressure drops and minimal energy loss;
- *durability*: the durability should be as high as possible, so as to reduce as low as possible the need for a new intervention.
- *thrombogenesis*: the probability to form thrombi should be as low as possible in order to avoid the need for a constant and massive dose of anticoagulant drugs;
- *haemolysis*: it is important to well design the valve and assess a good *fluid-dynamic* behaviour in order to reduce the shear stresses that lead to red blood cells (RBCs) damage as low as possible.

Currently, surgeons can implant three types of valve: *mechanical*, *bioprosthetic* or *biological* heart valve and *transcatheter* valve. Mechanical HVPs, made from hard materials, ensure good reliability manifested by long lasting of the implantation, however daily therapies based on anticoagulant treatment are required to control blood damage and clotting. Biological valves don't need an anticoagulant treatment due to their good fluid-dynamic biocompatibility. On the other hand, the chemical treatment used to get biocompatibility of the heterologous biological tissue increased the risk of failure due to the tissue degradation and calcification. The transcatheter heart valves are substantially biological valves implanted via a catheter in a less invasive way.

2.4.1 Mechanical Heart Valve Prostheses

Regardless of their type, the mechanical heart valves (MHVs) are made of three parts: the *occluder*, the *housing* and the *sewing ring*. The occluder is the mobile part of the prosthesis and due to the pressure difference between ventricle and aorta, it should be able to open and close. The housing is the fixed part in which the occluder is free to move. The sewing ring allows the connection of the prosthesis to the patient's tissue.
Different kinds of MHVs were design in the last fifty years and they can be classified according to morphology into three subcategories: *caged-ball valves*, *tilting disc valves*, and *bileaflet* valves. Each of these valves, can be design with different materials, geometry and open/close mechanisms. There are a lot of different materials like titanium, cobalt, low temperature isotropic (LTI) pyrolytic carbons, polyoxymethylene (Delrin®), polytetrafluoroethylene (Teflon®), polyethylene terephthalate (Dacron®) and many others (Mohammadi and Mequanint, 2011), that could be used to manufacture the different part of a MHV. The first MHV (Figure 2.10) called cage-ball, was developed in 1952, while the first implant took place in 1960, when the Starr-Edwards prosthesis was used (Mohammadi and Mequanint, 2011). This valve had a spherical or disc shape occluder made of silicon or metallic material surrounded by a Stellite alloy (a range of cobalt-chromium alloys designed for wear resistance, it may also contain tungsten or molybdenum and a small but important amount of carbon) cage stitched up to a Teflon®or Dacron®ring. Even if these valves showed good durability, their centrally obstruction design resulted in a larger pressure drop and poor haemodynamics characteristic across the valve in the open position. Moreover their relatively large profile increased the possibility of interference with anatomical structures after implantation. The non-tilting disc valves (Figure 2.11) were devised with the intent to overcome the slowness during the movement of cage-ball valves, due to its great inertial effects. In the effort to reduce the profile of such valve, a flat disc, instead of a ball, was used. However, non-tilting disc valves were still associated with haemodynamic problems of having a leaflet that remained obstructive in the open position. The most important non-tilting disc was the Kay-Shiley, introduced during 1965. Due to their small size if compared to the caged-ball, the non-tilting disc valve were implanted in both mitral and aortic position. However, because of their bad haemodynamic, they were put aside shortly. In 1967 one of the most important MHVs made its entry into the market: the Bjork-Shiley tilting disc (Figure 2.12). In this valve the concept of the occluder has been completely revolutionised. This valve was made of a free-floating disc, which in the close position tilts to an angle that depends on the design of the strut where the disc

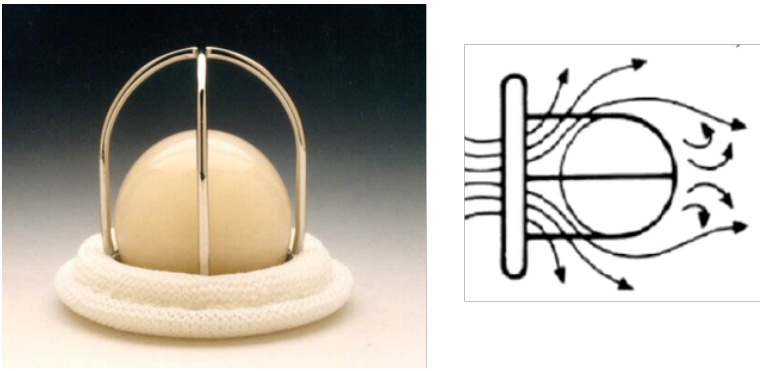

Figure 2.10 Starr-Edwards MHV and haemodynamic profile. It is possible to observe the occluder made by silicone material, the housing made by Stellite alloy and the Dacron ring sutured in the end. Modified from Mohammadi and Mequanint (2011)

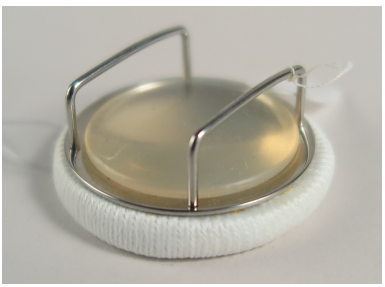

Figure 2.11 A type of Kay-Shiley non-tilting disc valve, the most common type of Kay-Shiley valve. It has four vertical struts form two parallel bars made of Stellite, and the disc is made of a radiolucent silicone rubber.

is hinged. In the open position, the blood flowing over and around the disk, lowering flow abnormalities. The leaflet of the original Bjork-Shiley was made by Delrin®, which was later replaced by pyrolytic carbon.

Although tilting disc MHVs have better haemodynamic than the ball-caged valves, this is still far from the fluid dynamics of the natural valve. The fluid passing through the tilting disc prosthesis is forced to go against the aortic wall causing shear force such as to results in aneurysm formation or wall damage. In 1978 St. Jude Medical Inc. tried to overcome this problem introducing the first bileaflet MHV (Figure 2.13). (Mohammadi and Mequanint, 2011).

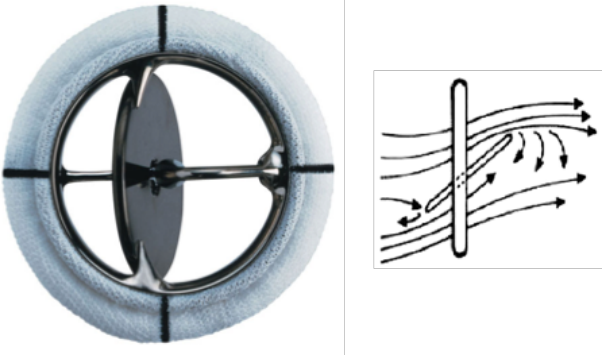

Figure 2.12 Tilting disk MHV and haemodynamic profile. Modified from Mohammadi and Mequanint (2011)

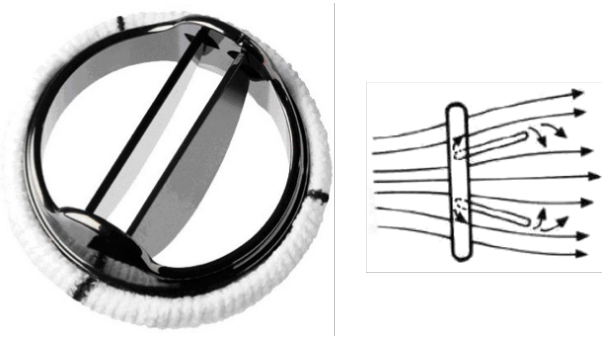

Figure 2.13 Bileaflet MHV and haemodynamic profile. Modified from Mohammadi and Mequanint (2011)

They are made of two semicircular leaflets placed within the ring by hinges. In the open position bileaflet MHVs clutter less then tilting disc valve and their fluid dynamic is better because the two open leaflets are positioned in the middle of the blood stream showing much more similar fluid dynamics to the physiological one. As a matter of fact, the large effective orifice area contributes to obtain a flat, nearly physiological flow profile with much less abnormalities if compared to the early generation of MHVs. During diastole, the leaflet are enclosed within the ring. In the last thirty years, additional new designs of bileaflet valve have been introduced by different manufacturers but cavitation and thromboembolism effects with or without anticoagulant therapy remain an

unsolved problem. Lifelong anticoagulation is still necessary also with these fluid dynamic efficient HV.

2.4.2 Bioprosthetic Heart Valve

Bioprosthetic heart valves (BHVs) are made of porcine aortic valves or bovine pericardial tissue (Figure 2.14) that are mounted on a rigid metallic or polymeric stent, to mimic the natural heart valve architecture. Cross species implantation of animal tissues is clearly prone to immune reaction and rapid tissue degeneration. To avoid the possible immune rejection, the biological tissue should be treated with glutaraldehyde, a not expensive chemical reagent, soluble in water, capable of producing stable cross-links, which almost completely reduce tissue antigenicity (Mohammadi and Mequanint, 2011).
The treatment can, however, considerably modify the functional characteristics of the extra-cellular matrix, drastically altering the biochemical and biomechanical properties. These devices are therefore less thrombogenic than MHVs and do not require long-life anticoagulation treatment. This is the main advantage of the biological prosthesis.
The average duration of tissue valves, is around 10 or 15 years: clinical follow-

(a) (b) (c)

Figure 2.14 Bioprosthetic heart valves: (a) an example of porcine aortic valve and two pericardium valve currently on the market. (b) LivaNova MITROFLOW with PRT (phospholipid reduction treatment) and (c) Carpentier-Edwards PERIMOUNT Magna Ease Aortic Heart Valve. The black vertical line on the Dacron ring is one of the three suture markers aid in valve orientation and suture placement

ups indicated that more than 50% of patients with BHV implants develop complication within 10 years (Ribeiro et al., 1986). As a matter of fact, degenerative processes may occur because of the chemical cross-linking which is required to give stability to collagen fibres after the decellularization. The slow release of unreacted glutaraldehyde, which is present in the matrix after the treatment, can

cause, however, serious problems: cytotoxicity, inflammatory response, calcification. In addition, glutaraldehyde, prevents the re-endothelialization hindering the integration of the device.
The bovine pericardial prosthesis if compared to the porcine has the main advantage of being able to be designed, ideally, for every size.
The choice between BHVs and MHVs is not univocal. Before 1975 the mechanical valves were largely used, but then more attention on BHVs had been placed. In general, MHVs are implanted in 60 years or older patients, because the prosthesis can last for the rest of the patient's life. Conversely, more BHVs are implanted in younger patients and children even if their higher tendency to calcify tissue implants could reduce the life of the device.
Other bioprosthetic valves include stentless valve, human valve allograft, and pulmonary-to-aortic valve autografts. Stentless valves are made of glutaraldehyde-pretreated porcine aortic root and valve without a rigid support stent. Aortic or pulmonary valve transplanted from one individual to another (homografts or allografts) are usually derived from cadavers or diseased heart removed at transplantation and then cryopreserved (Schoen and Gotlieb, 2016). Replacement of the aortic valve or root using the patient's own pulmonary valve is an uncommon but well accepted option in particular patients. These solutions typically suffer degeneration or replacement in the frame time comparable to those of conventional bioprosthetic valve. Moreover, the poor availability of human valves is the main disadvantage of these prostheses.

2.4.3 Transcatheter Aortic Valve

Transcatheter aortic valves (Figure 2.15) are heart valve substitutes delivered through a catheter and implanted in a manner generally not involving direct visualisation and generally involving a beating heart. The main advantage of this surgical technique is to be less invasive than traditional valve replacements requiring sternotomy. Transcatheter aortic valves implantation (TAVI) is now regarded as the treatment option in otherwise inoperable patients and selected high risk population (Schoen and Gotlieb, 2016). Sometimes TAVI can be applied as a bridge to valve replacement in patient in whom the surgery needs to be delayed, but there is a pressing need to repair a dysfunctional bioprosthesis valve by placing a new valve via catheter into the orifice of the existing failed bioprosthetic valve (Figure2.16).
TAVI is most frequently accomplished through peripheral arterial access, with the device introduced into the femoral artery up to the aorta to the aortic valve annulus, where it is deployed pushing the diseased valve to the periphery of the

(a) (b) (c)

Figure 2.15 Three transcatheter aortic valve: (a) Edward Sapiens, (b) Sapiens XT and (c) Medtronic CoreValve

Figure 2.16 Medtronic CoreValve used in a valve-in-valve procedure

valve orifice. Percutaneous valves are made of two components: an outer stent structure (similar to the endovascular stent) and attached leaflets which can be folded into the catheter. Often some transcatheter aortic valves differ from each other for the stent design. The most frequent complications in TAVI include misplacement, paravalvular leak, vascular injury, stroke, cardiac injury such as heart block, coronary obstruction, and cardiac perforation. Embolisation is a rare but serious complication during TAVI.

2.5 Tissue Engineered Heart Valve

The basic idea of the tissue engineering is to replicate *in vitro* an environment suitable for the healthy life of the cells of the tissue (cell culture), and to stimulate the construction of the new tissue by means of an appropriate pattern of solicitations.
Tissue engineered heart valves (TEHVs) are biological prostheses with the primary goal to reproduce the geometry and the function of the native heart valve by combining living cells with a biocompatible scaffold.
To allow cells growing on the designed scaffold, exogenous physical/chemical stimulations (i.e temperature, pH), exchange of nutritive substance and mechanical stimuli (cyclic tensile and shear loading condition) should be provided in the micro environment, using a bioreactor. Only when a leaving tissue covers the scaffold with autologous cell, the prosthesis is ready to be implanted (Figure 2.17).

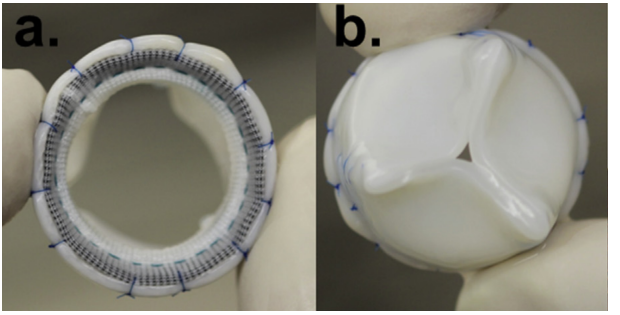

Figure 2.17 Tissue engineered aortic valve mounted on Sorin's Mitroflow® Frame with a. bottom and b. top view shown. Modified from Syedain et al. (2015)

To date, two distinct approaches are currently used in the tissue engineered heart valve research (Kheradvar et al., 2015). In the first, traditional approach, a TEHV is created seeding cells on a synthetic scaffold and the cell growth takes place on the scaffold in a bioreactor. The second approach is based on the ability of the human body to populate the unseeded scaffold after implantation, using the body as a bioreactor. The latter approach is intended to transform gradually the scaffold into a living structure. On one side this technique offers an off-the-shelf availability of the prosthesis but, on the other hand, the scaffold should immediately have the mechanical properties to withstand stimuli present in the human body at the time of implantation. Moreover, the control

of cells recruitment and tissue formation inside the body is the main challenge of this approach (Bouten et al., 2011). Early scaffolds were made of polyglycolic acid (PGA), but to overcome problems concerning thickening and more stiffness of the TEHVs compared to native valve, a combination of PGA and poly-4-hydroxybutyrate (P4HB) was used (Kheradvar et al., 2015). This kind of TEHVs showed mechanical properties and internal structure similar to that of native valve but long-term durability were unknown. In these years, Tranquillo's group is doing a big effort in order to obtain a reliable TEHV (Syedain et al., 2015, 2013), with good results in preliminary preclinical evaluation in the sheep model (Syedain et al., 2016). The last TEHV created by this group was fabricated from a decellularized tissue tube mounted, using prolene suture, on a custom PEEK frame with three struts, which collapse into three coapting leaflet as a result of an applied backpressure (Figure 2.18). The tissue was manufactured by ovine fibroblasts dispersed within a fibrin gel. The fatigue tests in pulmonary position on these prototypes seem promising, but further investigations need to be performed.

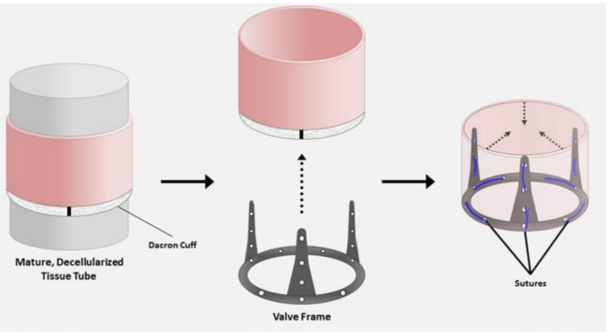

Figure 2.18 Schematic diagram of fabrication of a heart valve based on an engineered tissue tube. An engineered tissue tube with a Dacron cuff is decellularized and mounted on a custom PEEK frame using prolene suture. Modified from Syedain et al. (2013)

In conclusion, TEHVs shows promising as a regenerative patient specific model that could be very interesting in the future of valve replacement. However, due to the fact that TEHV depends on cell and their creation, to obtain the right chemical and physical stimuli in their microenvironment is critical. Even though there have been multiple studies (Syedain et al., 2015) using engineered tissue heart valve grown *in vitro*, there has been no reported success in demonstrating long-term function as an aortic valve replacement.

2.6 Polymeric Heart Valve

The principal requirements of replacement heart valve should be fluid-dynamic performances as good as the natural valve and long-term durability without the need for anticoagulation. Unfortunately these needs don't coexist in the currently used heart valve prostheses (see Section 2.4). The use of polymers to produce flexible heart valve prostheses could combine the characteristic previously described. Moreover, the relatively inexpensive mass production technique, if compared with the production costs of the mechanical, biological and, in particular, transcatheter valves, makes this kind of valve further appealing. For these reasons, polymeric valves have been studied since mid 1950s as mitral valve and 1960s as aortic prostheses (Bezuidenhout et al., 2015). Despite all the efforts and money invested in the polymeric heart valve research, to date they have not yet gained clinical acceptance and clinical use has remained limited to pulsatile ventricular assist device. The early polymeric valve were made of polyurethane. Since then, various polymer have been used like polysiloxanes, polytetrafluoroethylene family, and new emerging block copolymer materials.

Polyurethane

Polyurethane (PU) is a polymer composed of organic units joined by carbamate (urethane) links (Figure 2.19). While most polyurethanes are thermosetting polymers that do not melt when heated, thermoplastic polyurethanes are also available.

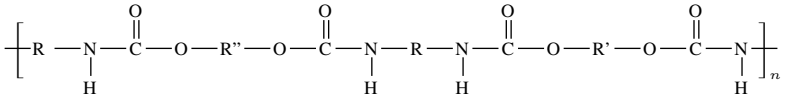

Figure 2.19 Structure of a polyurethane (PU)

Medical grade segmented polyurethane have been applied successfully in various cardiovascular devices, including artificial hearts, ventricular assist devices and blood pumps (Bernacca et al., 1997b) also due to their interaction with macrophages and bacterial cells (Visai et al., 2002). Polyurethanes make up the most popular form of polymeric heart valve due to the ease of production. Over the year, they were molecular linked up to several chemical group like polyester, polyether, polycarbonate and polysiloxane soft segment (Kheradvar et al., 2015).
However, the first generation of PU valves were plagued by calcification. Even

if *in vitro* tests showed good results, all the valves implanted in juvenile sheep and calf failed (Wisman et al., 1982).
Several generation of valves were made modifying the PU chain with polyether group, obtaining polyether urethane (PEU) and poly(etherurethane-urea) (PEUU) elastomers. Since 1992, Dr. Bernacca at the University of Glasgow (Scotland) has widely investigated calcification, mechanical behavior and hydrodynamical performance of different prototypes (Figure 2.20) of PU valves (Bernacca et al., 1997b, 2002a,b). He analysed the influence of thickness and

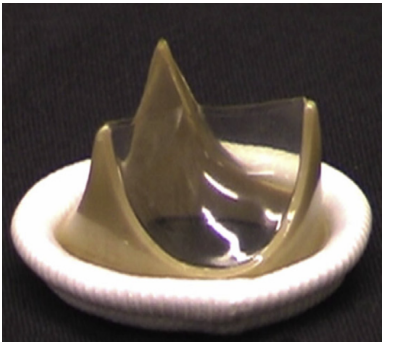

Figure 2.20 Polyurethane heart valves developed by the Glasgow group: Elliptohyperbolic Estane®dipcoated on a PEEK frame. Modified from Bezuidenhout et al. (2015).

Young's modulus of the leaflet in PHV and found that valve hydrodynamic function is not affected significantly by the material modulus but leaflet thickness is a highly significant factor (Bernacca et al., 2002a). In recent years, remarkable advancement in polymer synthesis has resulted in a more bio-stable PU. Durability of more than 800 million cycles *in vitro* tests at 12 Hz was achieved with a diamine-extended PEUU at optimal 150 μm thickness. Calcification in this valve was minimal and was observed where the material failed, indicating the intrinsic lower capacity for calcification of the polyurethane compared with bovine pericardium or porcine aortic valve biomaterials (Bernacca et al., 1997a). Further eight prototype trileaflet polyurethane valve were compared with mechanical and bioprosthetic valves for assessment of *in vivo* function, durability, thromboembolic potential and calcification. Also in these case, in the absence of valve-related death and morbidity, the PU valve was superior to the bioprosthesis and showed lower thrombogenicity compared with the mechanical valve (Wheatley et al., 2000). Wheatley and colleagues assert that a

biostable polyurethane valve could offer clinical advantage with the promise of improved durability and low thrombogenicity. Another group that made big efforts in the developments of new PU valves is the Reul's group at the University of Aachen, in Germany. First, they studied the calcification behaviour of medical grade polyurethanes and then, after having established their chemical stability and biocompatibility (Glasmacher-Seiler et al., 1992), they started to produce different prototypes (Figure 2.21). An aliphatic PCU, manufactured

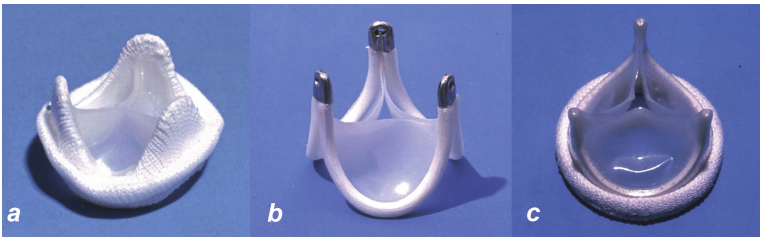

Figure 2.21 Trileaflet polyurethane valves developed by the Aachen group. (a) the Reul-Ghista trileaflet valve, (b) the Reul-Haussinger valve and (c) the Helmholtz Institute valve. Modified from Bezuidenhout et al. (2015).

by Jansen and Reul (1992), had very low energy losses, and lifetimes between 400 and 650 million cycles during *in vitro* accelerated testing. Nonetheless, mitral implants in young calf showed extensive thrombotic deposits and calcification. To overcome this problem, they produced different samples of a new material, obtained by the synthesis of polyurethanes from oligoetherdiol. Static seven-weeks-calcification testing in a synthetic calcification fluid did not indicate calcification by optical density measurements and by visual inspection and computer image processing of the X-ray films for PU (Szelest-Lewandowska et al., 2003). In 2004, Daebritz et al. (2004) developed a mitral (bileaflet) and aortic (trileaflet) prostheses (Figure 2.22) made entirely of polycarbonate urethane (PCU). *in vitro* fatigue testing of the PCU mitral valves proved durability for 600 million to 1 billion cycles, while *in vitro* fatigue testing of the PCU aortic valves proved durability for 450 million cycles. The performance of both prostheses in vivo was superior to that of biological mitral and aortic prostheses. Only animals with PCU aortic valves reached the end of the study period. The animals with biological valves died as the result of severe degeneration of the prostheses with calcification after less than 5 weeks. The PCU valves, explanted at an average of 20.7 weeks, showed mild moderate degenerative changes and minor to moderate calcification.

In conclusion, the results with mitral and aortic Adiam PCU valves are promis-

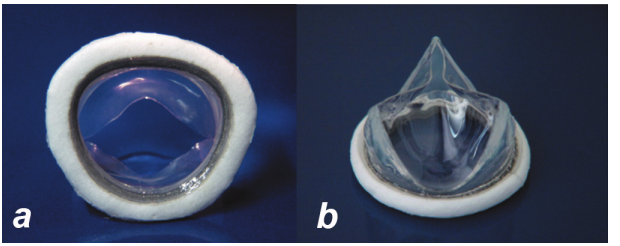

Figure 2.22 (a) The Adiam polycarbonate urethane (PCU) valve with special design for the mitral position and (b) the Adiam polycarbonate urethane valve with special design for the aortic position. Modified from Daebritz et al. (2004).

ing and, due to their superior durability compared to current bioprostheses in growing animal model, Sachweh and Daebritz (2006) think that this prostheses may be a future option for paediatric patients.

Polysiloxanes

Polysiloxanes are polymers with alternating silicon and oxygen atoms in the molecule structure, with the possibility to link different pendant groups (as methylene) to the silicon atom (Figure 2.23). These materials have been used in many medical devices, even as biosensor (Lee et al., 2016a), due to their biostability, biocompatibility and fatigue resistance (Bezuidenhout et al., 2015). These elastomers were widely used to design flexible leaflet valve with differ-

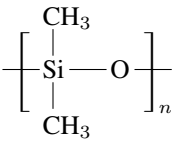

Figure 2.23 Structure of a polydimethylsiloxane

ent specifications. Different leaflet thickness were proposed: Roe et al. (1958) made a 380 μm thick leaflet housed in a silicone cylinder but long-term survival was not achieved. They made another version with thicker leaflet (430-500 μm) that shown very good *in vitro* fatigue result (over 700 million cycle). Unfortunately high mortality rate was observed during clinical trial. Performing the *in vitro* fatigue test at 58 Hz has given unrealistic expectation because were not

performing a correct opening and closing movement. The effect of variation of test frequency was well investigated by D'Souza et al. (2003).
Since 1980s silicone materials do not appear to have been used in the fabrication of aortic heart valve prostheses (Bezuidenhout et al., 2015), probably due to their suboptimal mechanical properties for thin leaflet manufacture.

Polytetrafluoroethylene

Polytetrafluoroethylene (PTFE) is a highly crystalline fluorocarbon as it is a high-molecular-weight compound consisting wholly of carbon and fluorine (Figure 2.24). It is also well know with the brand name of Teflon® and was discovered in 1938 by DuPont Corporation (DuPont Co., Wilmington, Delaware, USA). Its inertness and low surface energy leads to good biocompatibility and consequently it was widely used within medical device technology. In 1965

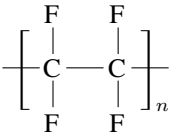

Figure 2.24 Structure of a polytetrafluoroethylene (PTFE)

Braunwald and Morrow (1965) made a clinical trial implanting in 23 patients a flexible trileaflef Teflon valve. These valves became stiff and regurgitant. The regurgitations was noted through holes in the leaflet due to tears. Moreover some calcific deposits was observed in the surface. Nistal et al. (1990) manufactured polymeric valves with the microporous form of PTFE, known as ePTFE, widely used in vascular graft. They implanted twelve prostheses in the tricuspid position in weanling sheep. The results suggest that the ePTFE valves have a moderate overall calcification rate and that calcium deposits appear to be always related to the commissural region, the junction between adjacent leaflet. PTFE material, due to their tendency to calcify and stiffen, has become less and less appealing to manufacture heart valve prosthesis, but it is still used in the fabrication of artificial conduits (Dacron based).

A Novel Material

Revolutionary advances in nanotechnology propose novel materials with superior properties for biomedical application. Block copolymers (BCPs) are a

particular class of polymer belonging to the family of soft materials. They can be considered as being made by two or more chemical homogeneous polymer fragments (block) joined together by covalent bonds. In the simplest case of two different monomer, linear diblock (XY), triblock (XYX), multiblock or star-block copolymer can be prepared (Lecommandoux et al., 2006). An emerging new elastomeric BCP is poly(**s**tyrene-b-**i**so**b**utylene-b-**s**tyene) known as **SIBS** (Figure 2.25), produced by Innovia LCC (Miami, FL, U.S.A).

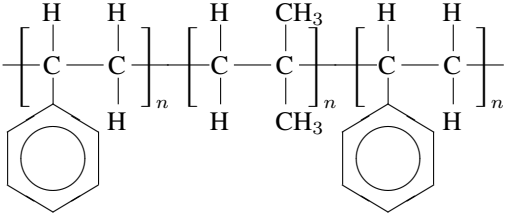

Figure 2.25 Structure of poly(styrene-b-isobutylene-b-styene) composed by an hard-soft-hard segment

Several studies (Duraiswamy et al., 2008; El Fray et al., 2006; Pinchuk et al., 2008) have demonstrated the ability of using this polymer as material to manufacture heart valve prosthesis. SIBS polymer has just been used as stent-graft, coating on metallic stents and drug-eluting coronary stent (Boden et al., 2009) showing good haemocompatibility, biocompatibility and long-term stability in contact with metal (Pinchuk et al., 2008).
To date, few research groups work on aortic heart valve made by SIBS. Yin et al. (2005), from the Biomedical Engineering Department of the Stony Brooke University, assess measurement of platelet activation among a mechanical valve (St. Jude Medical MHV-SJM Master Series), a porcine bioprosthetic heart valve (St. Jude Toronto SPV) and an Innovia LCC Trileaflet (Innovia, Miami, FL, U.S.A) composite polymeric valve. The leaflet of the polymeric valve have an embedded polyester mesh and an average leaflet thickness of approximately 240 μm. The results shown a platelet activation in near-real time without statistically significant differences among the three valves.
In 2010 Wang et al. (2010) implanted four SIBS valves with an embedded reinforcement polyethylene terephthalate (PET) fabric and two commercial Magna tissue valves (as reference valves) into sheep. Only three animals surviving through the target duration (20 weeks): one with the polymeric valve and the two with the commercial Magna tissue valves. The other three animals died

after few weeks due to material failure (stent deformation, cracks and extrinsic calcification on the leaflets). Although SIBS is a biostable and biocompatible material, the valve failed in animal testing due to material failure and calcification. It is important to underline that the valves failed in the study of Wang et al. (2010) were made by SIBS with PET fibre obtaining a composite material. On the contrary, the studies performed by Pinchuk et al. (2008) and El Fray et al. (2006) that showed a long-term stability of the material, were performed on single SIBS layer. As a matter of fact, fatigue failure in composite materials is a progressive rupture, which is manifested by the formation and propagation of defects. In 2011 Claiborne et al. (2011) performed thrombogenic tests between an improved polymer valve design (Innovia LCC) made from SIBS, a commercially available biological valve. The results showed a fivefold lower platelet activation in the SIBS valve in regard to the biological one, demonstrate a significant improvement in thrombogenic performance of the polymer valve compared to their previous study (Yin et al., 2005). Then Claiborne et al. (2013a), analysing the failure modes that were observed in the pre-clinical animal trials previously reported (Wang et al., 2010), improved the polymeric heart valve design. They made a parametric study (Claiborne et al., 2013b) to optimise different parameter as shape (modified from cylindrical to hemispherical), leaflet thickness (modified from uniform to variable thickness) and valve's stent (Figure 2.26). The hydrodynamic performances of this optimised polymeric

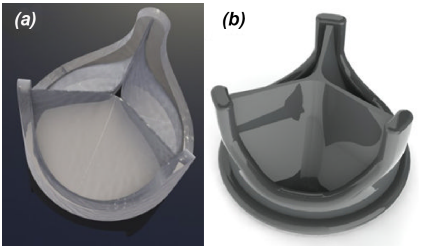

Figure 2.26 CAD images of the valves: (a) original Innovia composite SIBS-Dacron polymer PHV, and (b) the optimised xSIBS-PHV. Modified from Claiborne et al. (2013b).

valve are comparable with the performances of Carpentier-Edwards Perimount Magna tissue valve. However *in vivo* tests have not been yet performed. Nowadays, many polymeric heart valves have been designed and developed but none of these have long term performances such as to allow their use in the clinical application, and hence on the market.

Chapter 3

Polymer Selection and Test

This Chapter aims at describing the first fundamental step to design a new polymeric aortic valve: the material choice. A class of materials identified as promising material are presented. After a brief introduction (Section 3.1), tensile tests that were done on three materials (Section 3.2.1), differing in styrene percentage and manufacturing technique are described. Finally, in Section 3.2.2, the description of how micro-chain orientation were assessed using SAXS technique is given.

3.1 Polymer selection

BLOCK copolymers, belonging to the general class of thermoplastic elastomers, might be considered as of the "alloys" of the polymer world due to their properties to mix several polymeric material in the same solid solution. From the mechanical behaviour point of view, the most important feature of these materials is related to mechanical anisotropy at the macroscale that could be tuned by using different manufacturing technique. This anisotropic behaviour could be used to mimic the anisotropy of the natural heart valve leaflet (Stasiak et al., 2010). Advances in controlled polymerisation technique (Lecommandoux et al., 2006) have actually permitted to arrange BPCs in different architectures, including not only linear block but also branched system. Among the linear copolymer, diblock and triblock copolymers are the most studied architectures. Self-assembling morphologies in di- or triblock copolymers present four ordered microstructures including: spheres, cylinders, gyroids and lamellea (Figure 3.1). These microstructures depend on the percentage of the monomer block present in the material.

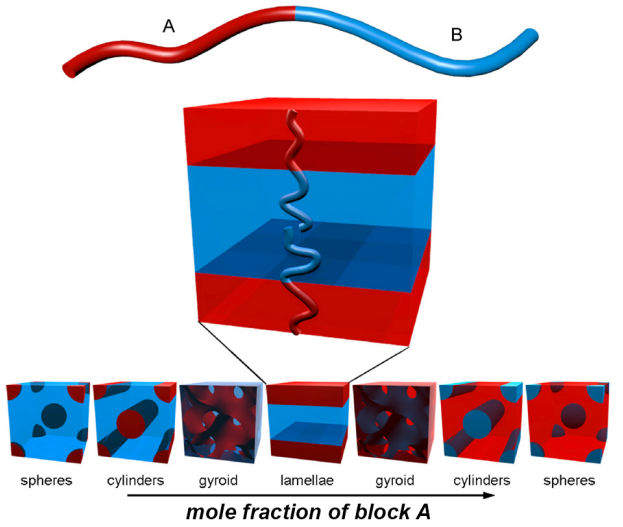

Figure 3.1 Schematics diblock copolymer phases. In the A-B diblock copolymer, the structure was determined primarily by the relative fraction of the polymer blocks. Modified from Darling (2007)

The cylindrical morphology from a mechanical point of view is the most interesting structure because by aligning the micro-chain it may be possible to obtain anisotropic material.
Polymers which might be suitable for a prosthetic heart valve should display several properties: they must exhibit phase separation at room temperature, cylindrical morphology must have been reported, the polymers should not contain heavy metal ions, and neither block should be unstable in the presence of water, weak acid, or weak alkalis. In additions, they must be biocompatible and show low calcification in physiological habitat.
Among all block copolymers, styrene based copolymers were chosen because of their demonstrated stability, biocompatibility and low calcification (Brubert et al., 2016; El Fray et al., 2006; Gallocher et al., 2006; Pinchuk et al., 2008). They do not substantially activate platelets in the vascular system and degradation has not been observed in any living system to date (Pinchuk et al., 2008). Moreover, SBCPs were already used to fabricate via compression moulding prosthetic heart valves (cf. Section 2.6).
Finally, to achieve cylindrical morphology the polystyrene fraction of the polymer must be in the region of 18 to 30% (Brubert, 2015). As a matter of fact, cylindrical morphology microstructure could be useful to obtain polymeric materials with the same properties of natural heart valves leaflet.
At this stage, only commercially available BCP were considered, therefore triblock copolymers will be used because they are the most developed from a commercial point of view.
By taking into account all these factors, the SBCPs tested in this work are:

- poly(styrene-b-isoprene/butadiene-b-styrene),commercial product Kraton name D1171PT, with 19% wt polystyrene fraction, that from now will be referred to as SI/BS-19;
- poly(Styrene-Isoprene-Styrene), commercial product Kraton name D1164PT, with 30% wt polystyrene fraction, that from now will be referred to as SIS-30;
- poly(Styrene-Ethylene-Propylene-Styrene), with 22% wt polystyrene fraction, that from now will be referred to as SEPS-22.

All these polymers were obtained from Kraton^{TM} Performance Polymers, Inc. (Huston, Texas, USA) and are summarised in Table 3.1.

Table 3.1 List of commercial cylinder forming triblock copolymer using A, B and C to denote the three different blocks.

A	B	C	Styrene (% wt)	Moulding
Styrene	Isoprene	Butadiene	19	Compression
Styrene	Isoprene		30	Compression
Styrene	Ethylene	Propylene	22	Injection

In the segmented copolymers that form BCPs, one of the segments is considered hard (crystalline or glassy amorphous domain) and the other segment is considered soft (rubbery amorphous domain). When the temperature is lower than the glass transition temperature (Tg) of the hard segment, the hard segment domains serve as anchor points. In the BCPs listed in Table 3.1, the styrene is the hard segment while the others blocks are the soft part of the chain. The Tg of the polyisoprene, polybutadiene, polyisobutilene, polyethylene and polypropylene blocks is typically between -6°C and -90°C (Castano, 2016; Lee et al., 1998), while the polystyrene block Tg is 100°C.
At any temperature between about -90°C and 100°C styrenic copolymer will act as a physically cross-linked elastomer. Under processing conditions, as the temperature is raised above the Tg of the hard segment, the hard segment domains soften and the copolymer may undergo viscous flow, and therefore can be cast, moulded, or extruded into any desired form. When the temperature is cooled back below the Tg of the hard segment, the hard segment domains crystallize or vitrify and the copolymer regains elasticity and once again behaves like a vulcanized rubber. The polystyrene blocks form domains of nanometre size in the microstructure, and they stabilize the form of the moulded material.
Both SI/BS-19 and SIS-30 are obtained starting from pellet via compression moulding, while SEPS-22 is fabricated by injection moulding. Comparing the different manufacturing techniques, it is possible to assess how they influence the microstructure of the block ionomers. The SI/BS polymer series are unsaturated block copolymers that have isoprene and butadiene copolymerized in the midblock (S-(I/B)-S).
SEPS are the selectively hydrogenated versions of SIS and its microstructure consists of domains of polystyrene arranged regularly in a matrix of polyethylene/propylene. The main difference between SI/BS and SEPS is that SI/BS is made from polyisoprene, which has double bond in its chemical structure, so it is less stable (degrades with time due to chemical reactions via the double bonds). SEPS is built on ethyle-propylene, which does not have the double

bond back structure. It also means, that it is less prone to chemical reaction and therefore it is more stable, and in principle it should last longer.
In the following sections, SI/BS-19, SIS-30 and SEPS-22 were mechanically tested both parallel and perpendicular to the micro-chain direction. Then the real-microstructure was investigate by Small-angle X-ray scattering (SAXS) technique.

3.2 Material Characterization

All the samples were manufactures at the Department of Chemical Engineering and Biotechnology in the University of Cambridge (UK) by Dr. Moggridge's group.
Anisotropic samples of SI/BS-19 and SIS-30 were fabricated via compression molding at $160°$C, starting from pellets. Samples of SEPS-22 were injection moulded between two parallel plates to form discs of diameter 80 mm. The injection point was located at the centre of the top plate and the polymer melt was injected at $160°$C. The injection rates used were at least 10 times slower than would be used in a typical industrial injection moulding process.
While *uni-axial tensile tests* were performed on SIBS-19, SIS-30 and SEPS-22, the *micro-chain orientation analysis* were performed only on SEPS-22 because SI/BS-30 and SIS-30 have already been tested by Dr. Moggridge's group and other colleagues of the Politecnico di Milano.

3.2.1 Uni-axial Tensile Tests

In the following sections, a brief description of the adopted methods is given while significant result will be presented in Section 3.3.2. The mechanical properties of styrene based co-polymer have been widely studied (see Section 2.6), but the behavior of these materials can vary greatly modifying their microstructure with different manufacturing process. It is fundamental to investigate the mechanical properties of the styrenic block co-polymer obtained with the same manufacturing technique by which the polymeric heart valve will be created.
Both *cyclic loading and unloading* and *quasi-static tensile tests* were performed on confined dog-bone specimens, meaning that the ends of the strips were clamped with pneumatic grip, not allowing translational movement. The thickness of the samples were measured using a Digimatic Micrometer (Mitutoyo America Corporation, Aurora, IL, USA).
Dog-bone specimens type 1B (Figure 3.2) were cut from sheet of materials in both parallel and perpendicular fiber directions according to ASTM Standard D882-12 and EN ISO 527-3.
The anisotropic sample of SI/BS-19 and SIS-30 were obtained in two phases. First, pellets are compressed in a mould, heated to $160°$C and squeezed into a dense cuboid block, then the cuboid is compressed in a hot press at $160°$C in order to align the microstructure. From rectangular samples, dog-bone specimens were obtained in both direction.
Sheets sample of $0.5 \pm 0.1\ mm$ thickness were prepared by injection moulding of the SEPS-22 block copolymer melt at $160°$C and $2 \cdot 10^{-8}\ m^3 s^{-1}$ injection

rate to obtain anisotropic samples. From the disc shape sheet, dog-bone sample were obtained (Figure 3.3).

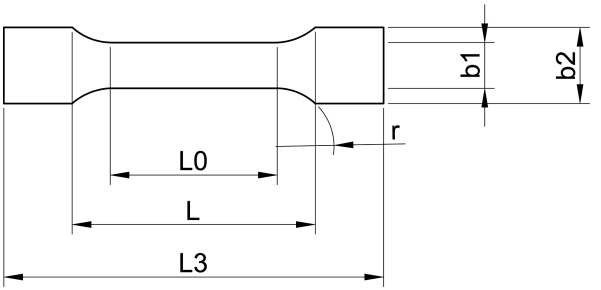

Figure 3.2 Dog-bone specimen type 1B. L3 is the total length of the specimen ($\approx 50mm$), L is the specimen length out of the test machine ($\approx$ 40 mm), L0 is the utilizable length ($\approx$ 30 mm), b1 is the width of the utilizable length ($\approx$ 7 mm), b2 is the total width of the specimen ($\approx$ 10 mm) while is the radius of curvature (30 mm)

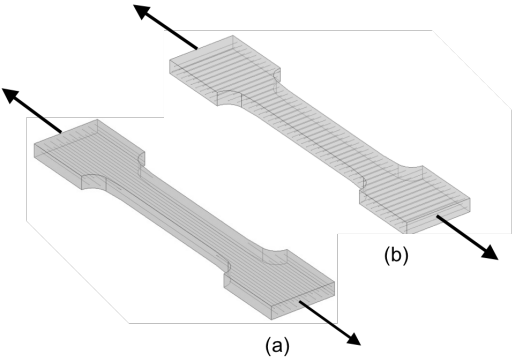

Figure 3.3 Styrene micro-chain orientation inside the dog-bone specimen in relationship of the the tensile force direction: (a) parallel and (b) perpendicular to the force direction.

Uniaxial tensile tests (MTS Synergie 200h, MTS System, USA) were performed up to 100% elongation at a speed of 1 mm/s, according to the Standards. To satisfy the accuracy imposed by the standard (1%), a 100 N full-scale load cell was used. Ten preconditioning cycles were performed in order to investigate stability and reach a reproducible stress-strain behavior between two

subsequent cycles. Anisotropic samples were tested and two orientations were considered: *parallel* and *perpendicular*[1] to the principal direction of the styrene micro-chains. A minimum of five samples were tested for each material in each direction to assess their repeatability.
Thus, the average nominal stress $\bar{\sigma}$ was calculated by the following formula:

$$\bar{\sigma} = \frac{1}{5} \cdot \sum_{j=1}^{5} \tilde{\sigma}_j(\varepsilon_i) \tag{3.1}$$

where ε_i is the *i-th* value of reference strain and $\tilde{\sigma}$ is the corresponding stress obtained from the interpolation of the experimental data by a third order Spline. The secant stiffness $E_x = \sigma(\varepsilon_x)/\varepsilon_x$ was evaluated at 20% and 80% of strain. In order to evaluate the degree of anisotropy, the ratio between the secant stiffness in both the directions at 20% and 80% of strain was calculated according to the formula:

$$R_x = 1 - \frac{E_x^{\perp}}{E_x^{\parallel}} \tag{3.2}$$

where R identifies the increment in stiffness in the direction parallel ($\parallel$) to cylinders axis with the respect to the transversal direction ($\perp$) at the *x* deformation.
From the curves, the ultimate tensile stress (UTS) at the 100% of the strain(ε_{max}) was determined.

3.2.2 Micro-Chain Orientation Analysis

Thanks to the collaboration between Politecnico di Milano and University of Cambridge, the micro-chain orientation of the compressed moulding samples were well investigated (Stasiak et al., 2010, 2009), and they are adopted as baseline for the procedures.
All these tests were carried out at the Diamond Light Source Ltd (Harwell Science & Innovation Campus, Didcot, Oxfordshire, UK) synchrotron. The synchrotron works like a giant microscope, harnessing the power of electrons to produce bright light that can be use to study anything from fossils to jet engines to viruses and vaccines. The machine speeds up electrons to near light speeds so that they give off a light 10 billion times brighter than the sun. These bright beams are then directed off into laboratories known as "beamlines" where the light was used to study a vast range of subject matter.

[1]Note on nomenclature: hereinafter parallel direction and perpendicular direction will be used to refer at the direction between the axial force used in the tensile tests and the direction of the styrene micro-chain in the samples.

SAXS is a powerful tool for investigating the deformation mechanism of a two-phase polymer system, especially for changes in the domain structure. The same method used in our previous work was applied (Stasiak et al., 2009).
SAXS patterns were recorded using a Bruker analytical X-ray system. Cu K α radiation (λ=1.54 Å) was generated by a Siemens ceramic tube operated at 45 kV and 45 mA. A collimator of three 0.1mm pinholes was used, and the specimen was placed 650 mm from the HiStar 2-D multiwire detector. Bruker SAXS data collection and analysis software was used. Polymer samples were observed with the X-ray beam perpendicular to all three planes of the sample. Oriented samples with cylindrical morphology were stretched both parallel and perpendicular to the cylinder axis. The X-ray exposure time was 20 min. The force in tension measurements of 2 mm thick film specimens were made using a Texture Analyzer TA-TX2 from Stable Micro System, at 1 mm/s stretching and relaxation rate, up to 200% of initial length.
The frequency of data collection was 10 points/s. Stretching was paused at particular deformations for the recording of X-ray patterns, during both elongation and relaxation. For better visualisation of the X-ray patterns, background scattering was subtracted from the scattered intensity.

3.3 Results

3.3.1 Uni-axial Tensile Tests

The *nominal stress* versus the *nominal strain* were analysed under the hypothesis of homogeneous material. All the tested materials showed an hysteretic behaviour, typically of the rubbery materials. Prior to perform uniaxial tensile test, ten cycle of loading and unloading until 100% of deformation were done. Only ten cycle were carried out because the stability is confirmed by the overlapping of the 9^{th} and 10^{th} cycles in the hysteretic behaviour (Figure 3.4(b) and Figure 3.4(d)). Figure 3.4 shows the hysteresis curve for the SIS-30 and similar results were obtained for SEPS-22 and SI/BS-19. It is interesting to observe the difference between the hysteresis of the first preconditioning cycle between the parallel and perpendicular samples (Figure 3.4(a) and Figure 3.4(c)). The difference between the subtended area of the loading and unloading trace in the $\sigma - \varepsilon$ graph, is a quantitative evaluation of the dissipation of the elastic energy. The first cycle in the perpendicular directions dissipates less energy than the first cycle for the parallel material in all the tested materials. BCPs exposed to tensile test, tend to extend the distance between two subsequent subphases proportionally to the microscopic elongation. The increment in the intermolecular distance has the effect of orienting the cylindrical structure of the material towards the stretching direction.
The initial energy to orient the styrenic chains, therefore, is greater when the samples are characterized in the direction parallel to these chains, that form the hard block. As a matter of fact, the elastic limit of the soft block (isoprene in SIS, isoprene with butadiene in SI/BS and ethylene with propylene in SEPS) is easily reached and the material start an internal rearrangement of the cylindrical fibre. Once load is removed, a new stable microarchitecture is obtained and the new microstructure turn stable and prone to effort the same elongation without further rearrangements (shear or slipping of cylinders over the styrene matrix). Perpendicularly to the chains direction, the stress will act mainly on the soft block, requiring less energy (and therefore less force) and producing less hysteresis area. All the samples show, as expected from the different hysteresis area, an anisotropic behaviour (Figure 3.5). These differences do not depend on the thickness because the thickness variation between the different samples are in a narrow range.
Zaffora (2011) observed differences in the mechanical properties varying the thickness sample from 0.16 mm to 0.82 mm. The thickness of all the samples tested in this work are equal to $(0.5 \pm 0.1)mm$.

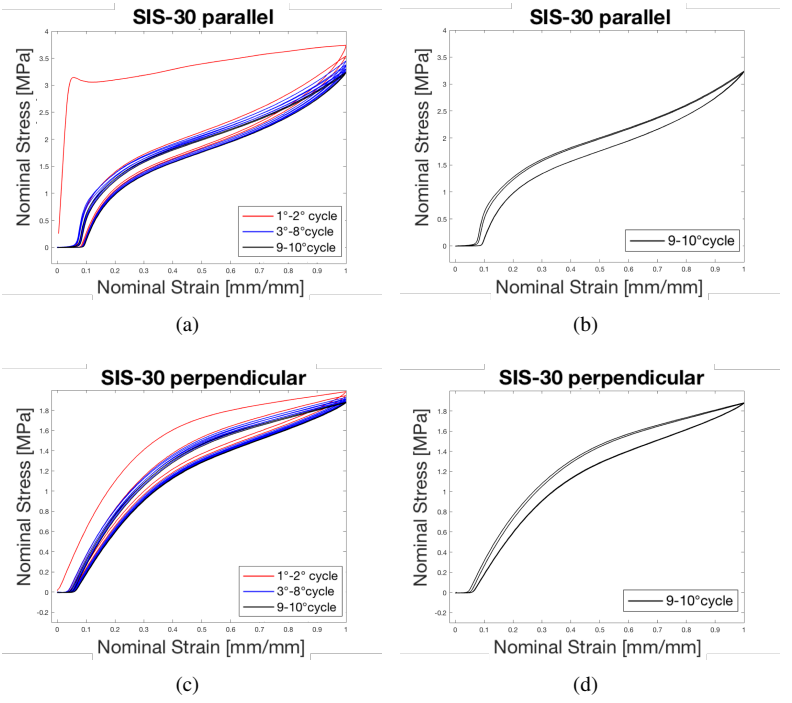

Figure 3.4 Behaviour of SIS-30 after 10 preconditioning cycles when tensile test are performed in the (a) perpendicular and (c) parallel micro-chains direction. The 9^{th} and 10^{th} cycles in both parallel and perpendicular direction are shown in (b) and (d), respectively, to better display the overlapping of the last two cycles

The chosen sample thickness is comparable to the leaflet thickness of PHVs design by different researcher (Section 2.6).
Table 3.2 shows the difference in the secant stiffness in both perpendicular and parallel direction at two different values of strain. Starting from the secant stiffness, the anisotropy degree was evaluated and reported in Table 3.3. The anisotropy is still present at both low and high strain values ($R_{0.2}$ and $R_{0.8}$ higher than 30%). SIS-30 and SEPS-22, even if only slightly, have a greater degree of anisotropy increasing the strain, while SI/BS-19 shows the opposite trend. While SIS-30 and SEPS-22 show similar anisotropy, the highest degree of anisotropy was found in the material with the lowest amount of styrene (SI/BS-19) with a value of $R_{0.2} = 61\%$ and $R_{0.8} = 58\%$.

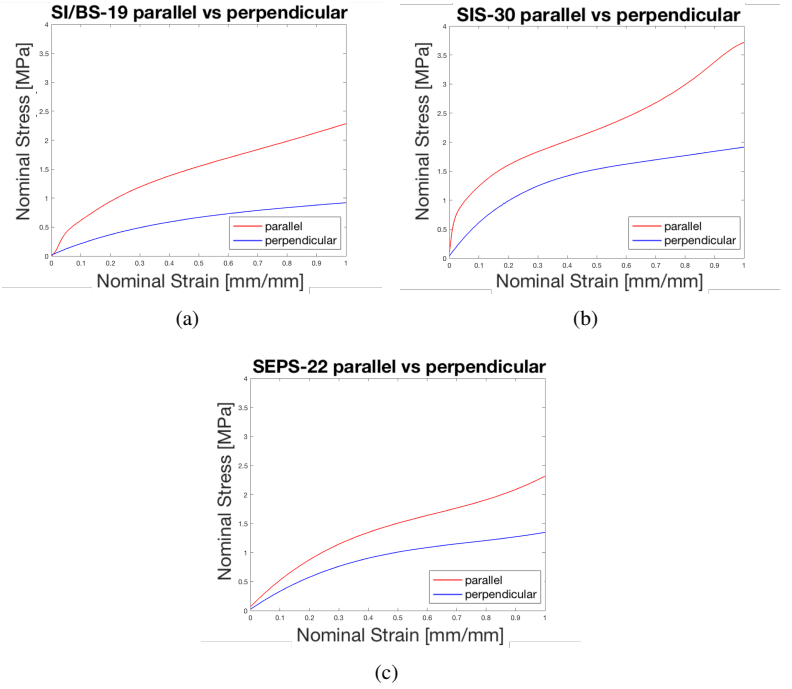

Figure 3.5 Anisotropy of (a) SI/BS-19, (b) SIS-30 and (c) SEPS-22: mean curve obtained from five experimental tensile test in direction parallel and perpendicular to the principal orientation direction according to the eq. 3.1.

Table 3.2 Secant stiffness in [MPa] at 20% and 80% of strain of the materials in both parallel ($\parallel$) and perpendicular ($\perp$) direction of micro-chain.

Stiffness [MPa]	$E_{20}^{\parallel}$	$E_{80}^{\parallel}$	$E_{20}^{\perp}$	$E_{80}^{\perp}$
SI/BS-19	4.77	2.48	1.86	1.04
SIS-30	8.00	3.73	5.09	2.20
SEPS-22	4.36	2.39	2.88	1.51

Concluding, it seems that the anisotropy degree is not dependent neither on the amount of styrene nor from the production technique.
Differences between parallel and perpendicular directions among the three ma-

Table 3.3 Increment in stiffness in the direction parallel to cylinders axis with respect to the transversal direction at 20% and 80% of strain of the materials

Materials	$R_{0.2}$	$R_{0.8}$
SI/BS-19	61%	58%
SIS-30	36%	41%
SEPS-22	34%	37%

terials are shown in Figure 3.6. In the parallel direction (Figure 3.6(a)), is clear how the behaviour is dependent from the styrene fraction: the higher is the fraction of styrene, the greater is the effort required to reach 100% of the strain, and, more important, it is independent from manufacturing. SEPS-22 and SI/BS-19 were produced by different manufacturing technique but, due to the fact that the styrene fraction is almost the same, the mechanical behaviour is the same. SEPS-22 and SI/BS-19 have the same stress at the maximum strain, 2.31 MPa and 2.28 MPa, respectively. The stress at the maximum strain for SIS-30 is equal to 3.71 MPa.
The same behaviour is also displayed in the perpendicular direction, even if the difference between SEPS-22 and SI/BS-19 is more sharp. SIS-30, SEPS-22 and SI/BS-19 reach the stress of 1.91 MPa, 1.35 MPa and 0.92 MPa at the maximum strain, respectively. These stress values are approximately half if compared to those obtained in the other direction.

3.3.2 Micro-Chain Orientation

Both SI/BS-19 and SIS-30, which were manufactured by compression moulding, exhibited cylindrical morphology, when styrene cylinders were distributed in an isoprene, butadiene or isobutylene soft matrix. Two arrangements of orientation with respect to stretching direction were considered as shown in Figure 3.3.
Figure 3.7 presents SAXS images for the examined block copolymers. The basal spacing of the domains was 27 nm for SI/BS-19 and 26 nm for SIS-30 (Stasiak et al., 2014b).
In Figure 3.8 X-ray images shows the results on the samples made by SEPS-22, which were obtained by injection moulding. The results show an interesting bi-modal orientation. The X-ray beam was perpendicular to the surface of the sample and it is possible to observe two directions of orientation; one vertical and one horizontal. In these samples, vertical peaks represent radial direction while horizontal peaks represent circumferential direction. The intensity of the

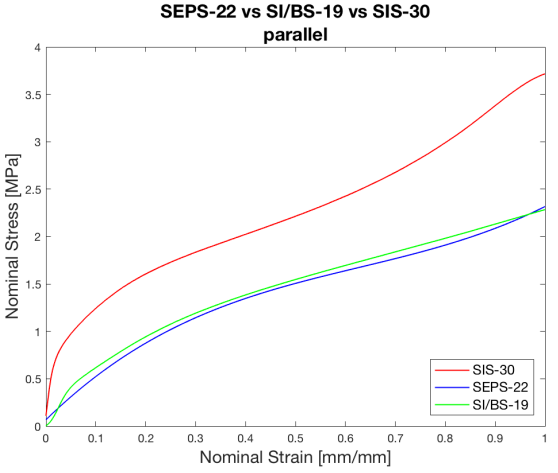

(a)

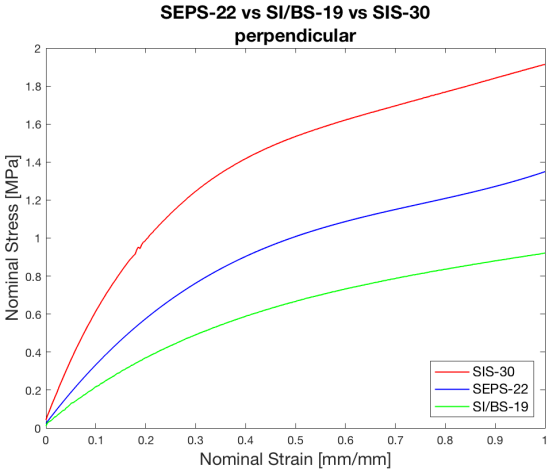

(b)

Figure 3.6 Comparison among SI/BS-19, SIS-30 and SEPS-22 in both tensile test direction: (a) parallel and (b) perpendicular to the principal orientation direction.

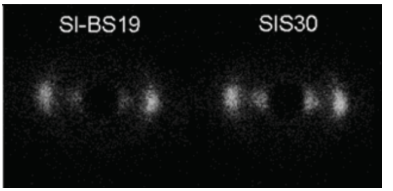

Figure 3.7 SAXS images of oriented block copolymers. Modified from Stasiak et al. (2014b).

vertical peaks are bigger than the horizontal ones, so, most micro chains are radially oriented. Figure 3.8(a) shows orientation of a sample injected at 180°C and 1 mm/s injection rate and annealed for 1 h at 150°C. Figure 3.8(b) shows orientation in a sample injected at the same conditions but quenched immediately after injection. It is possible to observe that samples shown in Figure 3.8(a) shows higher degree of orientation as we see the higher order peaks. Results in Figure 3.8(b) show only first order reflections, demonstrating that the sample is oriented, but less good than sample in Figure 3.8(a).

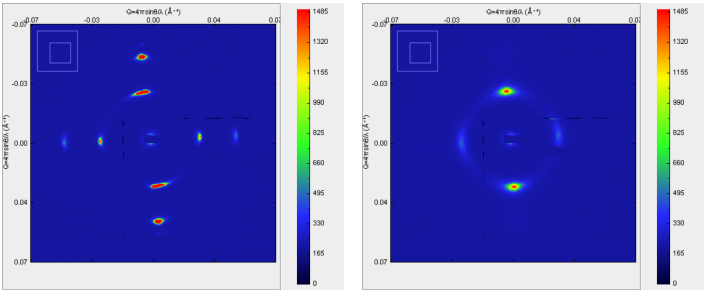

(a) (b)

Figure 3.8 X-ray images showing the bi-modal orientation on SEPS-22 sample annealed for 1h at 150°C (a) and quenched immediately after injection (b). Images and data are courtesy of Dr. Joanna Stasiak.

The samples were also scanned with the beam oriented in the same plane of the sample. The pattern is symmetric across the centre line of the sample, indicating that the bimodal orientation was layered independently by the annealing time (Figure 3.9).

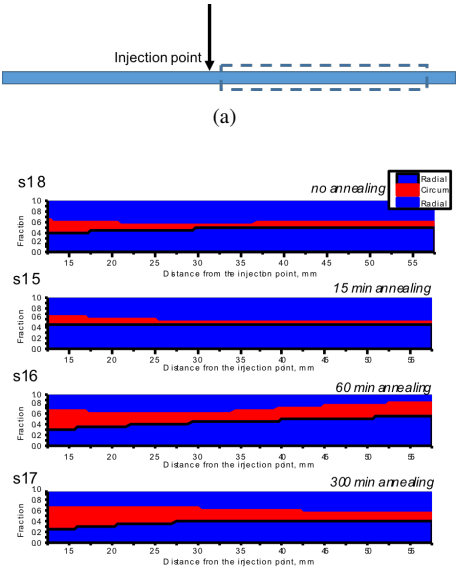

(b)

Figure 3.9 Investigated area: the X-rays beam are perpendicular to the cross-section of the disc (a). Results of the bimodal orientation through the thickness of the samples are shown (b). Images are courtesy of Dr. Joanna Stasiak.

3.4 Discussion

Mechanical properties of the thermoplastic elastomer depend on chemistry, microstructure and local conformation of the polymer chain. Two types of uniaxial tensile test were performed: *cyclic loading and unloading* and *quasi-static tensile* tests. The aim of the first test is the investigation of the hysteretic behaviour of the material during loading and unloading cycle, in order to identify the minimum number of preconditioning cycles. The results show that ten cycles of loading and unloading are enough in order to obtain a stable microstructure. The second test, aimed at identifying the stress-strain relationship of the selected materials. This data will be used both to obtain the parameter of the constitutive law that will be used in the computational model (cf. Section 4.3) and to choose the most suitable material for our purposes.
The mechanical response of natural aortic leaflet (cf. Section 2.2) is strongly

anisotropic with collagen fibres mainly oriented in circumferential direction, following principal direction of the the maximum solicitation.
The synthetic material to be used for the design of the biomorphic heart valve prosthesis should present anisotropic behaviour.
Both *cyclic loading and unloading* and *quasi-static tensile* tests show an high anisotropy degree in all the material. Specimens with styrene fibres oriented in the same direction of the applied force show both higher hysteresis area and stress in comparison to the sample tested perpendicular oriented.
Moreover both the stress at the maximum strain and the secant stiffness seem to be proportional to the styrene fraction. This effect is more evident in the parallel oriented samples, while the manufacturing technique would not seem to influence their behaviour.
In conclusion all the materials tested in this work show anisotropic mechanical properties, with tailorable microstructure tuning the styrene fraction. If it was possible to orient the chains of styrene in a suitable manner, these materials would be adequate for our purpose.
According to Stasiak et al. (2009) high-stress unidirectional shear flow in the channel die produce a well-oriented structure. Therefore, a cylindrical morphology inside the injection moulded samples was expected. Is was a surprise, on the other hand, to observe that the styrene micro-chain of the injection moulded samples did not orient solely in the direction of flow. As a matter of fact, a bimodal orientations was observed. We found anisotropic domains forming a layered structure exhibiting bi-directional orientation.
The same orientation was observed analysing the micro-chain orientations inside samples of SIS-30 obtained by injection moulded (Stasiak et al., 2014a). Thus, the layers structure exhibiting bi-directional orientation are function neither styrene fraction nor soft chain of the material but only of the manufacturing technique.
Secondly only injection moulding induced the bi-modal layered orientation, which we think is advantageous because is capable to mimic the orientation inside the natural leaflet. Compression moulding induced only unidirectional orientation.

Chapter 4

Abacus and Stent Design

This Chapter aims at showing the geometry of both the leaflet and stent of the new prosthetic heart valve. After a short introduction of the different geometry, the shape of the leaflet is shown. Two different designs are proposed for the stent geometry. Finally two different moulds are manufactured to obtain two devices characterised by the same shape of the leaflets but different stent geometry.

4.1 Introduction

THE aim of this work, as reported in **Chapter 1** is to develop an innovative aortic valve prosthesis completely made up of styrene based block copolymer. To this purpose both the material and the shape of the valve are fundamental.
As a matter of fact, the performance of artificial heart valves are closely governed by the fluid mechanics within these valves, which, in turn, is strongly related to the geometry, material and mechanism of the valve design.
Moreover, the shape not only of the leaflet, but also of the structure all around the leaflets, is fundamental to obtain acceptable performance both in the short and in the long term.
Polymeric heart valves have the great advantages of being able to assume, potentially, any form. Although several shapes have been taken into account, the trileaflet design, based on the shape of the natural aortic valve, is the most commonly used for polymeric heart valve design.
The native human aortic valve has hemispherical/cylindrical leaflets with variable thickness across the radial cross-section (Swanson and Clark, 1974).
Seven aortic homograft were studied by Lockie et al. (1993): the leaflet surface geometry was measured in the discharge state, and the leaflets were characterised by their radius of curvature and angle of inclination, using a cylindrical model. When the leaflets are opened a triangular orifice with low bending strains for a dilated root configuration were showed.
Different geometry were analysed in the last few years.
Jansen et al. (1991) developed a polyurethane heart valve prosthesis with minimum membrane stresses during performance. They achieved this result by designing almost flat leaflets in a medium opening position.
Leat and Fisher (1994) manufactured a prosthesis with a new curvature called "alpharabola". The radius of curvature increases from the centre of the leaflet at the free edge towards the base of the valve and perimeter of the leaflet (Figure 4.1).

In 1996, a new design was proposed by Mackay et al. (1996) in which the valve leaflet combined elliptical geometry in the radial direction and hyperbolic in the circumferential direction. The valve was entirely made by polyurethane with a very thin leaflet (approximately 0.1 mm thick).
Two alternative geometries were proposed by Jiang et al. (2004) to obtain a one-piece tricuspid artificial heart valve prototype to mimic the natural aortic valve: one with an hyperboloid of revolution about an axis and the second one with a revolution about an axis of an arc subtending (joining) two straight lines.

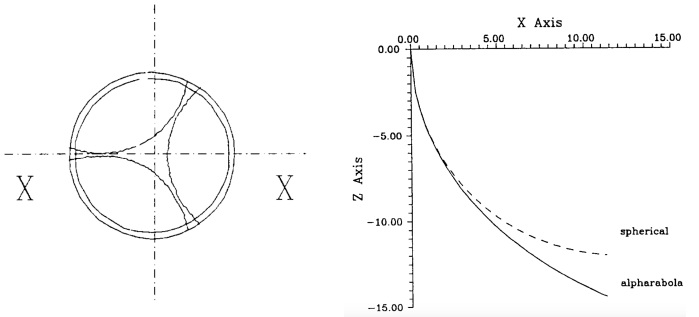

(a) (b)

Figure 4.1 Top view of the valve (a) and a section through the XZ plane at y=0 where the geometry of the "alpharabola" and of the spherical leaflets are compared. Modified from Leat and Fisher (1994)

Both symmetric and asymmetric leaflet valve were also considered (O'Connor et al., 2006).

An innovative procedure to develop a PHV model was proposed by Mohammadi and Mequanint (2011) using Bezier surface. Using this method, the boundaries of the surface can be fixed as the equation of the surface is designed in such a way that it passes directly through the control points defined as the boundary. To design the leaflet geometry, they first defined the position of the commissure and the free edges of the heart valve leaflet (boundary condition), after that they used a limited number of control points to produce the desired Bezier surface.

Rahmani et al. (2012) introduced an innovative concept of a low-profile semi-stented surgical polymeric aortic valve. This valve was created reducing the energy absorbed during the operating cycle and the leaflets were reinforced with a supportive medical-grade titanium wire frame (Figure 4.2). However, these efforts did not lead to a synthetic prosthesis suitable for implantation, because such valves still failed in long-term fatigue tests and in vivo experiments.

More recently Claiborne et al. (2013a) have modified their previously composite leaflet design (Claiborne et al., 2011) from cylindrical to hemispherical, created a variable thickness leaflet for optimised stress distribution and functionality.

Among all the prostheses designed, no one have come close to matching the healthy, native valve for durability and haemodynamics (Dasi et al., 2009) even

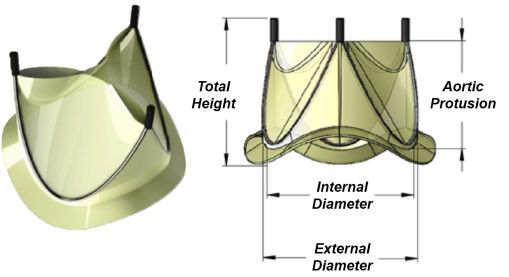

Figure 4.2 Representation of the polymeric valve proposed by Rahmani et al. (2012). Modified from Rahmani et al. (2012)

if some efforts seems to be promising (Claiborne et al., 2013a).
Starting from the different geometry studied in the past, and taking into account the geometry of the native aortic heart valve, a new geometry was developed.
The nomenclature used to refer to locations on prosthetic valves is displayed in Figure 4.3

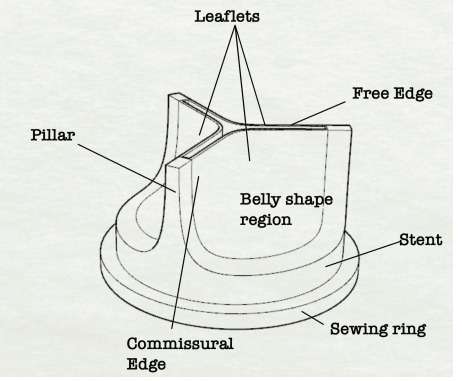

Figure 4.3 Sketch of prosthetic valve and nomenclature used to describe its different parts. The nodule of Arantius, where the collagen bundles are joined, is only present on the native valve.

4.2 The Leaflet

DIFFERENT requirements should be met to achieve efficient heart valve prosthesis. The device must fit well into the host anatomy, the leaflets should offer minimum resistance to the forward flow and open at a minimum systolic pressure drop, and finally the peaks of stress in all the valve components should be as low as possible during the entire cardiac cycle to ensure durability and minimal change to the geometric features (Ghanbari et al., 2009). Moreover the biomorphic PHV should guarantee appropriate coaptation of the leaflet in the closed position minimising the regurgitant volume. As reported in our work (De Gaetano et al., 2015a), a 3D model of the PHV leaflet was designed in our group by means of a Non-Uniform Rational B-Spline (NURBS) computer-aided design (CAD) software RHINOCEROS 5 (Rhinoceros, Robert McNeel and Associates, Seattle, WA).
In particular, NURBS surface admit parametric mapping, differentiation of the geometry and parametric scaling. These feature allow to create an automatic drawing procedure.
To obtain a circular, central orifice flow patterns that cause much less blood trauma (Leo et al., 2006) a trileaflet symmetric valve with constant leaflet thickness and identical material properties in each leaflet was assumed. Within the hypothesis of a circular orifice, the valve geometry can be parametrized by the *diameter (d)* of the orifice (internal diameter of the valve) and by the *heigh (h)*: the ratio $\alpha = h/d$ represents the aspect ratio of the device. The boundaries of the leaflet were obtained as a function of the aspect ration α and three parameter as a sequence of control points: *commissural edge*, *free edge* and *belly shape region* (Figure 4.3). Finally, to obtain a solid three-dimensional model of the valve, the *thickness (t)* of the leaflet has to be define. After setting all the parameter, the code automatically draws the leaflet shape (Figure 4.4). The leaflet shape consists of a central spherical region where the circular free edge is extended tangentially to connect the leaflet with the valve stent; the commissural edge is cut in a cylindrical shape (Figure 4.4).
The leaflet were design to obtain a valve with an internal diameter of 21 mm, the leaflet height at 10 mm, while the leaflet thickness was constant and equal to 0.3 mm.
The selection of the right thickness of the leaflet was obtained using the structural finite element model performed by Zaffora (2011). This model (Abaqus, SIMULIA, Dassault Systmes) was developed to analysed the mechanical behaviour of the valve of the leaflet thickness in the typical anatomical range 0.24-0.60 mm (*t24*=0.24 mm, *t30*=0.30 mm and *t60*=0.60 mm).

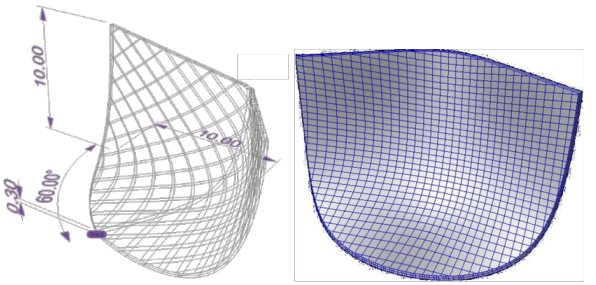

Figure 4.4 3D solid model of the leaflet

Each 3D solid model was discretized with about 3000 linear hexahedral elements.
The displacements of the commissural edge were avoided to simulate the presence of the valve stent. Uniform very high critical static pressure of 180 mmHg was applied (in quasi static loading condition) over the concave face of the leaflet to simulate the maximum diastolic pressure. The polymer mechanical behaviour was modelled by a particular hyperelastic Mooney-Rivlin constitutive law (Pandolfi and Vasta, 2012; Zaffora, 2011). The big advantage of using this model is the implementation of the styrene micro-chain orientation. Before testing the different thickness, the model was run to obtain the identification of the optimal orientation of the micro-chain to sustain the applied load with the minimum stress.
The model parameters were fitted to experimental data previously described (cf. Section 3.2.1). As reported in the work previously cited (De Gaetano et al., 2015a), the FE analyses were performed on t24, t30 and t60 thickness to calculate the stress distribution within the leaflet (Figure 4.5).
Under the diastolic load all the configurations show the higher stress near the junction between free edge and commissural region. While t24 shows high stress (2.1 MPa) and the highest contact area (104.4 mm^2), the model t60 presents no significant stress peaks but a reduced coaptation area (78.8 mm^2). Moreover, in the t60 model the thickness of the leaflet may limit opening and closing of the PHV. Model t30 (contact area = 95 mm^2) seems to be the best compromise among the analysed geometries.

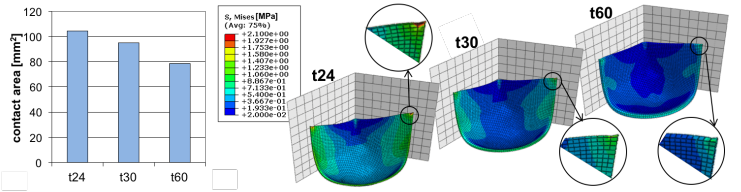

Figure 4.5 Computational outcomes of the coaptation area (on the left) and of the Von Mises stress (on the right) as a function of the leaflet thickness. Modified from De Gaetano et al. (2015a)

4.3 The Stent

Polymer can be moulded into a complete trileaflet prosthesis without the need of suturing individual leaflets. To obtain such a prosthesis, it is fundamental to design the structure all around the three leaflet, which will be referred to as *stent* from now on.

During surgery, the valve could be positioned mainly in two position: *intra-anular* (Figure 4.6(a)) and *supra-anular* (Figure 4.6(b)). In the first position the prosthesis replicates the position of the native valve while in the latter the stent and the sewing ring are contained into the sinus.

The design of stent, posts and sewing ring have an important role into define the positioning of the PHV, it makes no difference whether the performance could be different. At this purpose the International Standard ISO 5840:2015 that offers the guidelines for the test apparatus, design the dimension of surgical heart valve substitute sewing ring configuration and the minimum performance admitted in both case. As a matter of fact, the effective orifice area (EOA) and the regurgitation is given as a function of the tissue annulus diameter (TAD) (cf. **Chapter 6**).

The sewing ring of bioprosthetic and mechanical valves is typically made of Dacron®or Gore-tex®. It is well known that to avoid delamination at the interface between sewing ring and stent, it might be preferable to fabricate both components from the same material.

To manufacture a whole cardiac prosthesis from the same material it is necessary that this material can withstand the forces applied during the suturing of the valve.

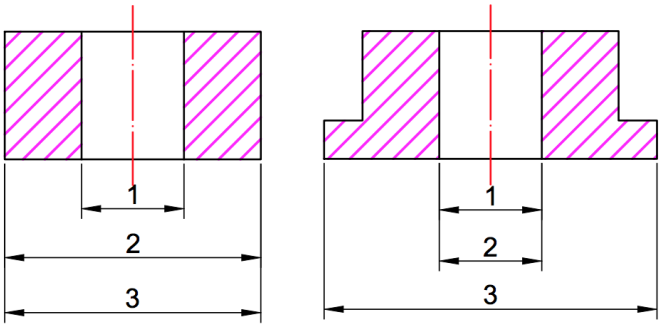

(a) (b)

Figure 4.6 Designation of dimensions of surgical heart valve substitution in two different sewing ring configurations: (a) intra-annular and (b) supra-annular. 1 - internal orifice area; 2 - tissue annulus diameter; 3 - external sewing ring diameter.

At this purpose, we sutured, (by using a commercially available thread TiCron, a non-absorbable braided polyester coated with silicone) samples of both SIS-30 and SI/BS-19 with styrene micro-chain parallel and perpendicular oriented (Stasiak et al., 2014b). The thickness of all the samples was 0.35 mm. Significant differences between the polymers were also observed in their tear-out behaviour. It has been shown that the deformation and tear out mechanisms are both functions of alignment direction. However, we proved that both SIS-30 and SI/BS-19 are suitable material for design and manufacture of sewing rings or stents for cardiac prosthesis.
All the studies reported in the Introduction of this Chapter were focused on the leaflet geometry and no one on the stent design.
Polymer leaflets clearly showed the maximum stresses near the intersection of the stent and the free edge of the leaflet (Figure 4.5); moreover the mechanical properties and geometrical shape of the stent/posts influences stress concentration on the leaflet. Therefore it is important to understand the interaction between leaflet and post, for this purpose a structural model of the whole PHV was designed.
A Finite element model was used to compare the peak leaflet stresses in the whole valve before and after the hydrodynamic tests. The displacement of the pillar were also investigated. The structural model of the valve, based on the model made by Zaffora (2011), were run by Dr. Serrani.

The polymer mechanical behaviour was modelled by an hyperelastic Mooney-Rivlin constitutive law using the non linear implicit finite element algorithm provided by ABAQUS. The parameters used to describe the materials, were base upon the mechanical properties of SIS-30, SI/BS-19 and SEPS-22 which were collected in **Chapter 3**. A quasi-static load condition was assumed until the pressure of 95 mmHg was reached.
Two different geometries have been proposed and compared: T4W1 (Figure 4.7(a)) and T5W10 (Figure 4.7(b)). Both designs have the same leaflet

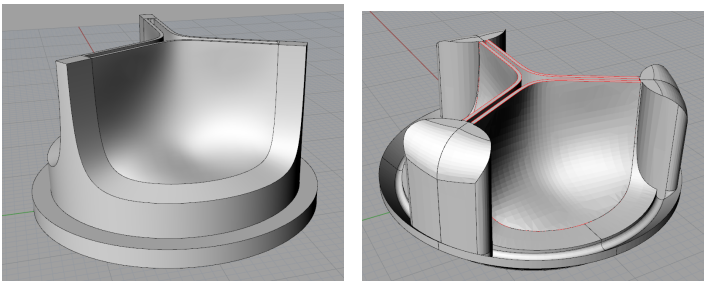

(a) (b)

Figure 4.7 3D rendering made with RHINOCERONS of the two proposed geometry: T4W1(a) and T5W10 (b).

geometry and shape. They differ in the design of the stent. T4W1 has a radial thickness of the pillar equal to 4 mm while the width is equal to 1 mm. The height of the polymeric sewing ring is equal to 2 mm while the polymeric stent has a variable height of between 3.5 and 4 mm; the total height of the valve is 18 mm. The TAD is equal to 21 mm while the external diameter is equal to 32 mm.
FEM analysis previously described was performed on this design taking into account three different materials, to observe how the mechanical properties can affect the behaviour of the valve.
A further design was also create in order to test how the geometry can affect the behaviour (stress and strain) of the leaflet using the same material (in this case SEPS-22 was chosen). As a matter of fact, in some preliminary tests using the same methods describe in **Chapter 6**, prototypes made by SI/BS-19 with T4W1 design, showed large bending of the pillar. To avoid this phenomenon, another design with much more strong pillar was created. T5W10 has a radial thickness of the semi circular pillar equal to 5 mm while the width is equal to 10 mm. Based on the suggestion given by Dr. Sukumaran Nair, (a cardiac

surgeon working at Cardiothoracic Services, Freeman Hospital, Newcastle, UK), we tried to reduce the total height of the PHV, keeping unaltered the profile of the leaflet. Following this criteria, a modified sewing ring was designed and the height of the stent was significantly reduced. The total height reached is only 14 mm. The T5W10 design with a TAD equal to 21 mm has an external diameter equal to 32 mm.

Results

Figure 4.8 shows the radial displacement of the posts applying the quasi-static load of 95 mmHg at the T4W1 design made from different material.

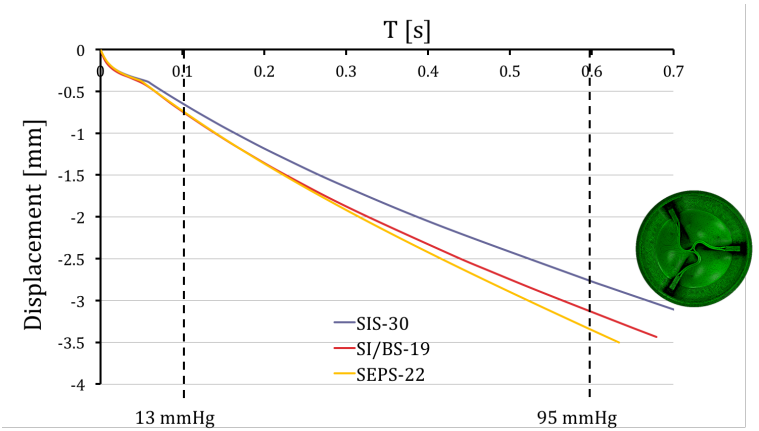

Figure 4.8 Computational outcomes of the radial displacement of the post and the deformed configuration at the maximum load of 95 mmHg for the SIS-30, SI/BS-19 and SEPS-22. Modelling and images are courtesy of Dr. Marta Serrani.

As expected, the polymer with the highest fraction of styrene shows the lowest displacement while SI/BS-19 and SEPS-22, particularly at low pressures, show a similar behaviour. At the maximum load of 95 mmHg, T4W1 configuration modelled with SIS-30 has the minimal radial displacement of the post equal to 2.6 mm, while the same configuration modelled with SI/BS-19 and SEPS-22 show the maximal radial displacement equal to 3.2 mm and 3.4 mm, respectively.
To understand the influence of the designs on the stress of the leaflet, the same

analysis was performed using the same hyperelastic Mooney-Rivlin constitutive law parameters of the SEPS-22 material in both T4W1 and T5W10.
Figure 4.9 shows the displacement between the two designs while Figure 4.10 and Figure 4.11 show the deformed configuration and the stress map of the leaflet for T5W10 and T4W1, respectively. The difference of the displacement between the two design is much larger than the difference of the displacement among the three materials. Passing from the T5W10 geometry to the T4W1, in addition to vary the intensity of stress, also changes its position.

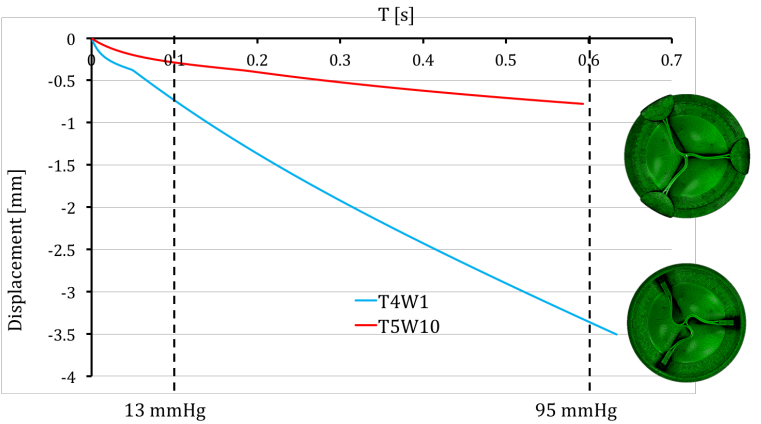

Figure 4.9 Computational outcomes of the radial displacement of the post and the deformed configuration at the maximum load of 95 mmHg in the two configuration for the SEPS-22. Modelling and images are courtesy of Dr. Marta Serrani.

In Figure 4.10 it is possible to observed that the maximum stress ($\sigma_{max} = 0.62MPa$) for T5W10 geometry is located between the post and the free edge, while for the T4W1 geometry (Figure 4.11), the maximum stress is double ($\sigma_{max} = 1.15MPa$) and it is located at bottom between the leaflet and the stent/post.
By changing the material properties, the results are similar. The maximum strain for the T4W1 geometry using SI/BS-19 is located at the bottom at the same position previously described, while the maximum strain for the T4W1 geometry using the same material, is located between the post and the free edge. The maximum logarithmic strain ($\varepsilon_{log_{MAX}} = ln(1+\varepsilon)$) is equal to 41%, a very high value (Figure 4.12). As well as switching from T4W1 to T5W10 geometry the stress is halved, likewise the the $\varepsilon_{log_{MAX}}$ is halved (Figure 4.13).

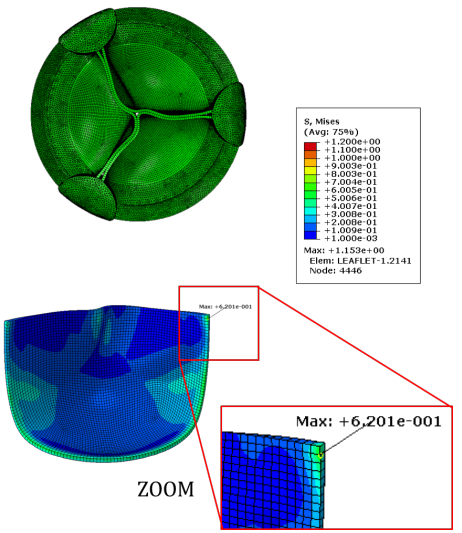

Figure 4.10 Deformed configuration (top) and Von Mises stress (bottom) at the maximum load for T5W10 geometry using SEPS-22. Modelling and images are courtesy of Dr. Marta Serrani.

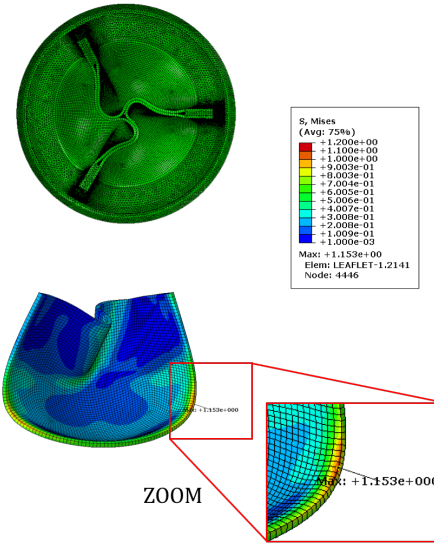

Figure 4.11 Deformed configuration (top) and Von Mises stress (bottom) at the maximum load for T4W1 geometry using SEPS-22. Modelling and images are courtesy of Dr. Marta Serrani.

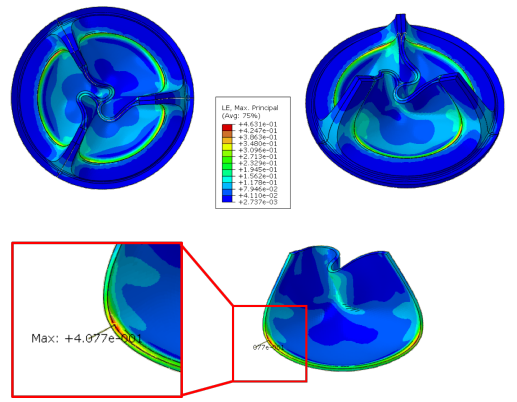

Figure 4.12 Deformed configuration (top) and Maximum logarithmic strain (bottom) at the maximum load for T4W1 geometry using SI/BS-19. Modelling and images are courtesy of Dr. Marta Serrani.

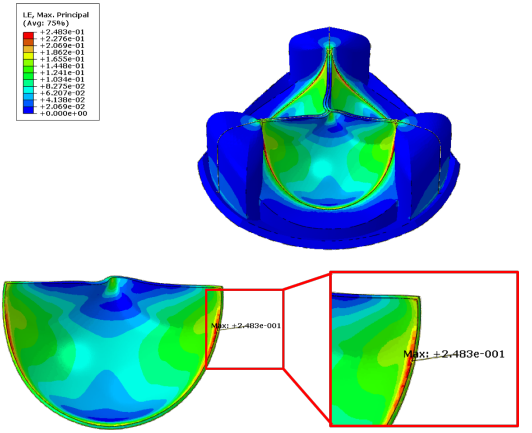

Figure 4.13 Deformed configuration (top) and Maximum logarithmic strain (bottom) at the maximum load for T5W10 geometry using SI/BS-19. Modelling and images are courtesy of Dr. Marta Serrani.

4.4 Mould and Fabrication technique

The Valve performance is dependent of the valve design, material and manufacturing. From the computational analysis showed in the previous section, it is clear how the stent design much more influence the maximum stress and their location if compared to the influence of the material.
Injection moulding and compression moulding technique could significantly modify the real prototypes. For this reason prototypes with both manufacturing processes were produced.
16 prototypes were manufactured by compression moulding technique with T4W1 geometry, 8 made from SIS-30 and the other 8 from SI/BS19. In this manner it would be possible to study the influence of the styrene fraction. Based on the mechanical properties investigated in **Chapter 3**, SEPS-22 demonstrate low mechanical properties if compared at SIS-30. For that reason 8 prototypes made from SEPS-22 were manufactured by injection moulding technique with T5W10 geometry. As a matter of fact this geometry shows the lowest displacement of the pillar.
As previously reported both the moulds and the valves were manufactured in Cambridge. In addition to the geometry described above, another important feature is to integrate all components into a one piece construction. Normally, in-

deed, the valve stents are fabricated separately from the leaflet. A cavity mould is a good way to forming the leaflet, stent and sewing ring simultaneously as a single unit rather than combining components, as is the case with conventional manufacturing process of the biomorphic valves. The moulds were designed using a CAD software RHINOCEROS 5 (Rhinoceros, Robert McNeel and Associates, Seattle, WA) and were fabricated using both computerised numerically controlled (CNC) machining methods and spark erosion.
In detail, the mould used to manufacture PHVs by compression moulding (Figure 4.14) was manufactured in aluminium by spark erosion (Cambridge Reactor Design Ltd., Cambridgeshire, UK), based on the 3-dimensional geometry of the T4W1 design.
On the other hand, how reported in Brubert (2015), the male part of the injection moulding mould (Figure 4.15(b)) was CNC machined from stainless steel, and the female part (Figure 4.15(c)) spark eroded (Cambridge Reactor Design Ltd., Cambridgeshire, UK) based on the 3-dimensional geometry of the T5W10 design.

Figure 4.14 Mould used to manufacture PHVs by compression moulding

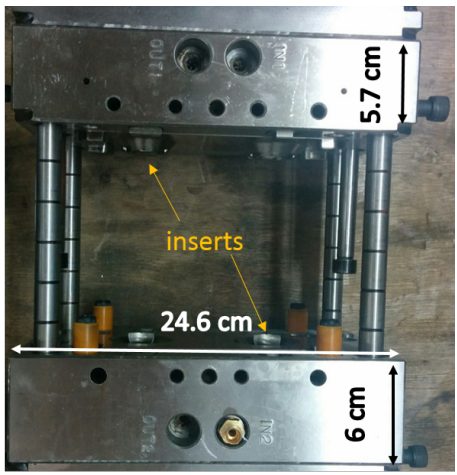

(a)

(b)

(c)

Figure 4.15 Mould used to manufacture PHVs by injection moulding (a). A detailed picture of the male (b) and female (b) inserts are reported.

Chapter 5

Computational investigation of the micro-chain orientation

In this chapter the description of the investigation of the micro domains orientation within the PHV leaflets is given. Specifically, a computational fluid dynamic model was used to design the best injection mould to achieve as much as possible a circumferential orientation of the polymeric chains. The numerical model was initially validated on a simplified geometry and the real micro-chain orientation of the leaflets was assessed and compared to the results obtained by the numerical model.

5.1 Introduction

THE styrene block polymers can be processed through compression moulding or injection moulding techniques that allow controlling the alignment of the polystyrene micro chains.
Compression moulding was successfully used to produce heart valve prosthesis (Claiborne et al., 2013a) and it is relatively easy to reproduce different temperature conditions but it is hard to control the flow field within the cavity and ensure complete filling of complex parts. On the contrary, as reported in **Chapter 3**, injection moulding has the capability to made a bi-modal orientation: skin layers distributed radially from the injection point and the core layer oriented perpendicular to the two outers layer. The injection moulding mass flow rate and location point of the injector used during this manufacturing technique could modify the micro-chain orientation. Hence, the effects of this parameters were investigated by using a numerical model.
The cooling time is another parameter that could have a big role in the orientation on the styrene micro-chain (Wang et al., 2013; Zhao et al., 2015) but at this step it was not considered.
Polystyrene micro-chain in thin films can be oriented perpendicularly and in parallel to the fluid flow. When the temperature of the polymer is between the *melting temperature* (T_m) and *order-disorder transition temperature* (T_{ODT}) the micro-domain can be moved and deformed using mechanical force field (Brubert, 2015).
It is already known that anisotropic particles align parallel to the flow direction. When flowing through narrowed channel sections, one expects the increased flow rate improves the parallel alignment. Using microfocus synchrotron X-ray scattering and polarised optical microscopy Trebbin et al. (2013) showed, on the contrary, that anisotropic colloidal particles align perpendicular to the flow direction after passing a narrow channel section (Figure 5.1). Anisotropic colloidal particles possess large axial ratios, and their thickness can be adjusted over a wide range from 5 to 50 nm by tailoring the polymer molecular weight, just as styrene BCPs.

Injection moulding has the potential to achieve this perpendicular orientation. As a matter of fact, using an injection moulder (Figure 5.2) the solid polymer is compacted and screw in the barrel. Once melted, it advances along the heated barrel and then polymer passes through the sprue bushing, along a runner or runners and through a gate into the cavity.

The cavity was vented through the sewing rings and injection was continued until a steady flow through the vents developed. After injection, the tool was

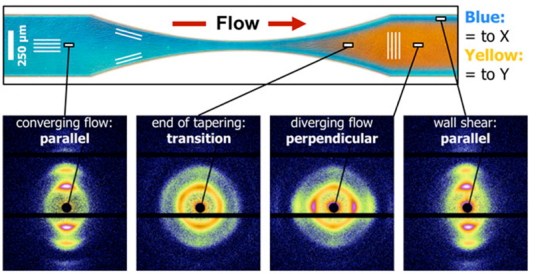

Figure 5.1 Narrowed micro channel section with measured SAXS patterns along the centre line, showing the surprising perpendicular orientation of the cylindrical micelles after passing through the channel tapering. (Scale bars: 100). Modified from Trebbin et al. (2013)

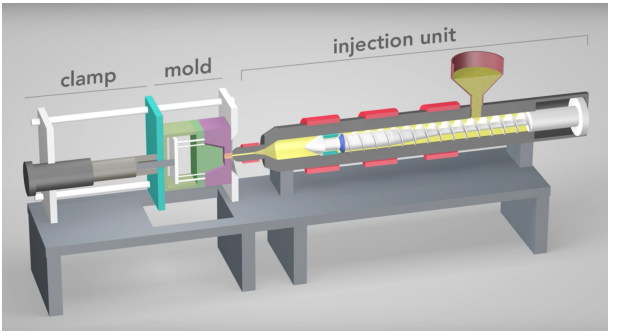

Figure 5.2 Computer graphics of an injection moulder. It is made by three main part: the injection unit, the mould and the clamp. Inside the mould the prototypes were manufactured.

removed from the injection moulder and cooled by direct contact with running water. The tool is left at temperate for 2 h over which time the polymer relaxes. To pass from the sprue bushing through a gate into the cavity is similar to go through a narrow channel section and for that reason it would be possible observe a perpendicular orientation at the flow direction.
In this chapter, the orientation behaviour of the cylindrical styrene micro-chains when flowing through injection channels into the leaflet of the valve was investigated.

5.2 Computational model for the determination of the orientation of the polymeric micro chains

The flows occurring during the injection moulding process is complex and will usually involve some combination of planar Couette flow, planar elongational flow, and biaxial/uniaxial stretching flow (Matin et al., 2000). The anisotropic orientation of styrene block co-polymers' polymeric chains is determined by *shear* and *extensional* flow. In fluid mechanics, the term shear flow refers to a type of fluid flow which is caused by forces, where adjacent layers of fluid move parallel to each other with different speeds. Couette flow is the simplest example of shear flow. On the other hand, the extensional flow is typically observed along the centreline of contractions when viscous flow pass through. *Shear rate* and *extensional rate* are the rate at which a progressive shearing and elongation deformation are applied to some material, respectively. Shear rate and extensional rate, are defined by the following equation:

$$\dot{\gamma} = \nabla_y v_x \tag{5.1}$$

$$\dot{\varepsilon} = -\nabla_y v_y \tag{5.2}$$

The shear vector γ (Equation (5.3)) and the stretch vector ε (Equation (5.4)) show the directions along which shear flow and extensional flow align the polymeric chains.

$$\boldsymbol{\gamma} = \begin{pmatrix} \dfrac{\partial u}{\partial x} \\ \dfrac{\partial v}{\partial y} \\ \dfrac{\partial w}{\partial z} \end{pmatrix} \tag{5.3}$$

$$\boldsymbol{\varepsilon} = \begin{pmatrix} \dfrac{\partial u}{\partial y} + \dfrac{\partial u}{\partial z} \\ \dfrac{\partial v}{\partial x} + \dfrac{\partial v}{\partial z} \\ \dfrac{\partial w}{\partial x} + \dfrac{\partial w}{\partial y} \end{pmatrix} \tag{5.4}$$

In complex geometry, many flows may result in non-orthogonal and non-planar stretch and shear vectors, but stretch and shear can even co-aligned, and promote the orientation of the micro domains in the same direction. Thus, below

a critical angle, the direction vector of the micro-chain will be an average of the stretch and shear vectors. Instead, above that threshold angle, the stretch and shear vectors are not co-aligned and the dominant mechanism can be determined by comparing the magnitudes of the vectors.
The angle between shear and stretch vectors can be defined by the scalar product of this two vectors (Equation (5.5)):

$$\Theta_v = \boldsymbol{\gamma} \cdot \boldsymbol{\varepsilon} \tag{5.5}$$

If Θ_v is bigger than a critical value, stretch vector and shear vector are not aligned and it is necessary understand which of the two mechanisms is predominant. To understand this, the modulus of the two vector was compared.

$$\psi_v = \frac{|\boldsymbol{\gamma}|}{|\boldsymbol{\varepsilon}|} \tag{5.6}$$

The ratio of the Equation (5.6) can be compared with a threshold value, which is used to discriminate which zones of the domain show dominant shear flow or have prevailing extensional flow.
The micro-chains orientation vector ($\boldsymbol{\Theta_v}$) in the styrene block copolymer was obtained by the following equation:

$$\boldsymbol{\Theta_v} = \frac{\boldsymbol{\varepsilon}}{|\boldsymbol{\varepsilon}|} \qquad \text{if} \quad \psi_v \leqslant \psi_{vc} \tag{5.7}$$

$$\boldsymbol{\Theta_v} = \frac{\boldsymbol{\gamma}}{|\boldsymbol{\gamma}|} \qquad \text{if} \quad \psi_v \geqslant \psi_{vc} \tag{5.8}$$

where ψ_{vc} is the critical threshold that allows to discriminate the domain areas where the *extensional flow* is prevalent on the *shear flow* and vice versa. The fibres are assumed to be inertia-less, which is a reasonable assumption in a creeping flow.
The critical threshold depends on the material proprieties. ψ_{vc} was varied as long as the output of the numerical model was exactly matched with the experimental data. Regarding the poly-(Styrene-Ethylene-Propylene-Styrene) containing 22 wt% styrene (SEPS-22), those information were evaluated from Small Angle X-ray Scattering Analysis (SAXS) performed on a thin membrane (55 mm x 50 mm, thickness 0.5 mm) of the copolymer made by injection moulding (Figure 5.3). Before to explain how compare experimental information with numerical data, a rheology characterisation of the polymer (Section 5.2.1) was performed and the mathematical model (Section 5.2.2) was described.

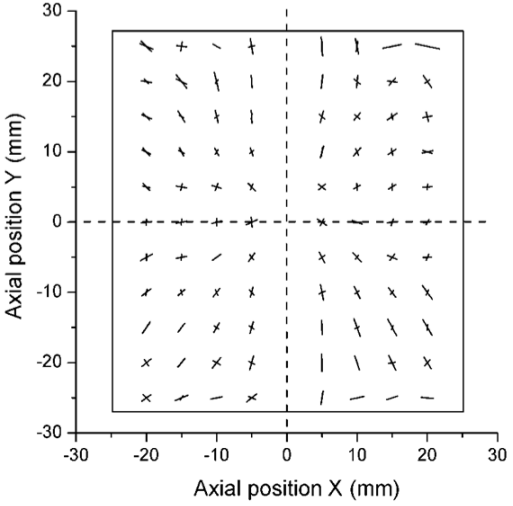

Figure 5.3 Small Angle X-ray Scattering analysis (SAXS) of the polymeric membrane produced by injection moulding of SEPS-22 used for the validation of the computational model. The direction of the vectors indicates the orientation of the styrene micro-chain and their length is proportional to the degree of orientation.

5.2.1 Polymer Rheology

Experimental test to asses the rheology behaviour of molten poly-(Styrene-Ethylene-Propylene-Styrene) containing 22 wt% styrene at 150°C was performed at the University of Cambridge by the Prof. Moggdrige's group. Experimental data (Figure 5.4) show the relationship on the one hand between apparent viscosity (*non-Newtonian viscosity*) and shear rate and on the other between stress and shear rate. Experimental data of the relationship between apparent viscosity and shear rate were taken into account before the sample break and was used to understand which model implemented in the commercial software Fluent®(ANSYS, Inc., Canonsburg, PA, USA), best fits the experimental data. According to the ANSYS FLUENT User's Guide, even if in many non-Newtonian fluids the shear stress - viscosity relationship can be modelled by the *Power law model*, the model chosen to best fit the experimental data was the *Carreau Model*, which is the most suitable to describe this kind of styrene based copolymers.

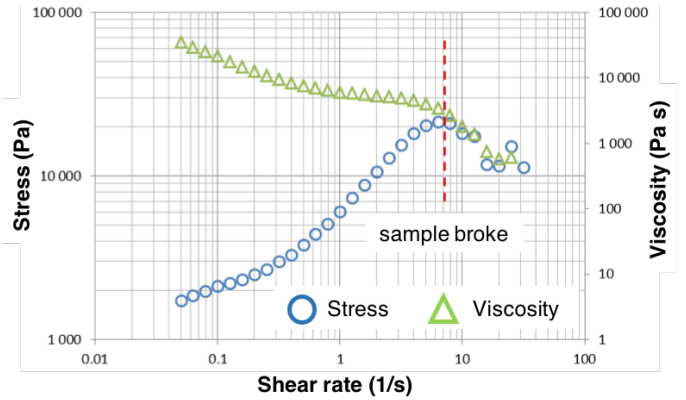

Figure 5.4 Experimental data of and stress depending of the shear stress obtained from molten SEPS-22 at 150°C.

In the *Carreau Model* the apparent viscosity was defined by Equation (5.9):

$$\eta = \eta_{\infty} + (\eta_{\infty} - \eta_0) \cdot (1 + \dot{\gamma}^2 \cdot \lambda^2)^{\frac{n-1}{2}} \tag{5.9}$$

where η_{∞} and η_0 are minimum and maximum apparent viscosity obtained when the shear rate to approach to infinity and zero, respectively; λ is the relaxation time (in seconds) and n is the power law index; which were set as shown in Table 5.1.

Table 5.1 Carreau model parameters used to best fit experimental data of molten SEPS-22 at 150°C

Parameter	Value	Unit
η_{∞}	4234.91	Pa $\cdot s$
η_0	70346.28	Pa $\cdot s$
λ	38.614	s
n	0	-

Figure 5.5 shows the comparison of raw apparent viscosity data with the predicted apparent viscosity using a Carreau model.

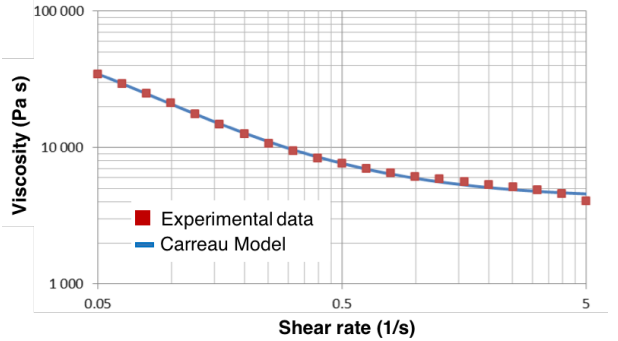

(a)

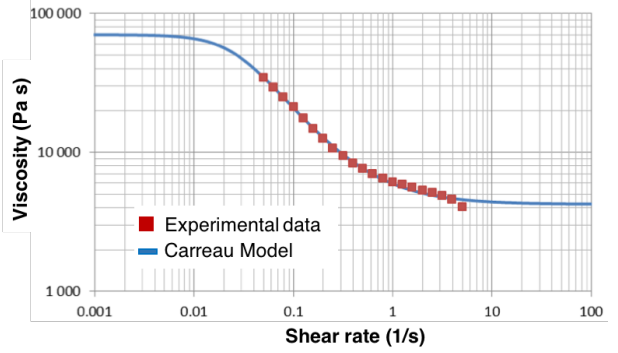

(b)

Figure 5.5 Experimental data (red) and predicted data (blue) in the interval of experimental data (a) and in a bigger range (b).

5.2.2 Fluid-dynamic Model

In this analysis incompressibility, constant density and no wall slip condition are assumed:

$$\frac{\partial \rho}{\partial t} + \nabla \cdot (\rho \mathbf{v}) = 0 \tag{5.10}$$

$$\nabla \cdot \mathbf{v} = 0 \tag{5.11}$$

where $\mathbf{v}$ is the velocity vector and ρ is the density.
Conservation of momentum in an inertial (non-accelerating) reference frame is

described by Equation (5.12)

$$\frac{\partial}{\partial t}(\rho \cdot \mathbf{v}) + \nabla \mathbf{v} \cdot (\rho \mathbf{v} \cdot \mathbf{v}) = -\nabla p + \nabla \cdot (\boldsymbol{\tau}) + \rho \mathbf{g} + \mathbf{F} \tag{5.12}$$

where p is the static pressure, $\boldsymbol{\tau}$ is the stress tensor (described below), and $\rho \mathbf{g}$ and $\mathbf{F}$ are the gravitational body force and external body forces, respectively. The stress tensor $\boldsymbol{\tau}$ is given by

$$\boldsymbol{\tau} = \boldsymbol{\eta} \cdot \mathbf{D} \tag{5.13}$$

where $\boldsymbol{\eta}$ is the fourth order viscosity tensor while D is the rate of deformation tensor given by

$$\mathbf{D} = \begin{bmatrix} \dfrac{\partial u}{\partial x} & \dfrac{1}{2}\left(\dfrac{\partial u}{\partial y} + \dfrac{\partial v}{\partial x}\right) & \dfrac{1}{2}\left(\dfrac{\partial u}{\partial z} + \dfrac{\partial w}{\partial x}\right) \\ \dfrac{1}{2}\left(\dfrac{\partial u}{\partial y} + \dfrac{\partial v}{\partial x}\right) & \dfrac{\partial v}{\partial y} & \dfrac{1}{2}\left(\dfrac{\partial v}{\partial z} + \dfrac{\partial w}{\partial z}\right) \\ \dfrac{1}{2}\left(\dfrac{\partial u}{\partial z} + \dfrac{\partial w}{\partial x}\right) & \dfrac{1}{2}\left(\dfrac{\partial v}{\partial z} + \dfrac{\partial w}{\partial y}\right) & \dfrac{\partial w}{\partial z} \end{bmatrix} \tag{5.14}$$

where u, v and w are the velocity in the x, y and z direction, respectively. In general, the viscosity tensor $\boldsymbol{\eta}$, it will be function of the fluid strain but the viscosity parametrical model implemented in Fluent®, describes the viscosity of a *non-Newtonian fluid*, as SEPS-22 is, introducing the apparent viscosity as function of the *shear rate* $\dot{\gamma}$, a scalar defined below:

$$\dot{\gamma} = \sqrt{2tr(\mathbf{D}^2)} \tag{5.15}$$

The apparent viscosity of the fluid (η), modelled by the parametric model described earlier in function of the shear rate (Equation (5.9)), admits to simplify the constitutive relationship of a non-Newtonian in the following way:

$$\boldsymbol{\tau} = \eta(\dot{\gamma}) \cdot \mathbf{D} \tag{5.16}$$

The fluid dynamic simulations were performed using the *3D double precision* in stationary flow, neglecting the gravitational acceleration and considering laminar flow due to the slow injection moulding flow rate. However, the Reynolds numbers in the different section of the considered geometry confirm that the flow is laminar. Moreover, due to the fact that both the polymer and the mould are at the same temperature, isothermal conditions are assumed. This is an approximation because the mould temperature is generally lower than the polymer melt.

5.2.3 Simulation of injection moulding between two parallel plates

The orientation of the polymer chains obtained from the computational model and determined by experimental techniques must be compared in order to obtain the threshold value ψ_{vc}. Due to the geometry symmetry, a quarter of the thin membrane (55 mm x 50 mm, thickness 0.5 mm) with the central injection point was duplicated. The sensitivity analysis was performed and a mesh with 437000 hexahedral elements was used. 40 elements along the thickness of the parallel plate (Figure 5.6(d)) were used to well investigate the micro-chain orientation.

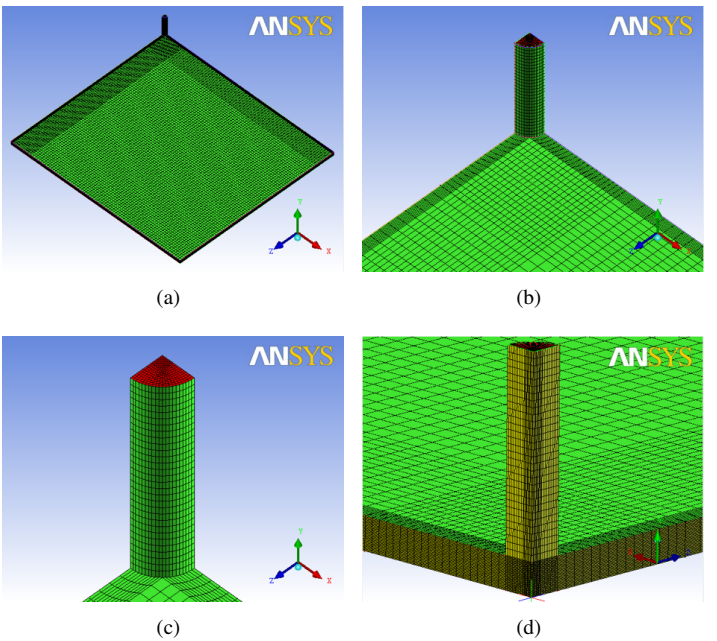

Figure 5.6 Hexahedrical mesh of the whole considered domain (a). It is possible observe the major element density in the middle (b) and in the injector(c). Moreover, It was shown the axial thickening of the mesh between the two parallel plates (d).

Therefore, fluid dynamics simulations reproducing the experimental procedure performed during the manufacturing of the thin membrane were performed. The rheology of SEPS-22 at 150°C was described by the *Carreau Model* in

Section 5.2.1. The steady fluid dynamic simulations were carried out using the commercial software Fluent®(ANSYS, Inc., Canonsburg, PA, USA) with hexahedral elements mesh. The *Pressure-Based Steady solver* and the SIMPLE *Pressure-Velocity Coupling* method were used. The chosen under-relaxation factors were the Fluent default settings (0.3 for the pressure and 0.7 for the momentum). Finally, the residuals values considered for the simulations convergence were equal to $1 \cdot 10^{-6}$ for the continuity equation and $1 \cdot 10^{-5}$ for the velocity equation in the x, y and z direction. The imposed boundary conditions are:

- *Mass flow inlet* on the top of the injection moulder;
- *Outflow* on the lateral wall of the mould;
- *Wall* at the internal surface of the two parallel plates;
- *Symmetry* on the lateral boundary;
- *Interior* on the whole fluid domain.

The post-processing of the simulation results to determine the micro-chain orientation was implemented in Matlab®(The MathWorks Inc., Natick, MA, USA) following these steps:

1. selection of the points on the mould wall where experimental data are available and where the numerical model is used to evaluate the average orientation direction;
2. creation, for every point selected on the XY plane (Figure 5.7(a)), 41 points place on a line perpendicular to the parallel plates surfaces (Figure 5.7(b));
3. evaluation of the micro-chain orientation vector for each point created within the polymeric membrane thickness (Figure 5.7(c));
4. for each point selected on the XY plane, all the vector with the same orientation (Θ_v lower than critical value), were collected in one *vector of micro-chain direction*. The length of this vector is proportional to the number of the vector aligned in the same direction (Figure 5.7(d));
5. finally, the X and Y components of the average orientation vectors are extracted in order to calculate the orientation angle referred to the x-axis and the fraction of the polymeric chains oriented in the considered direction.

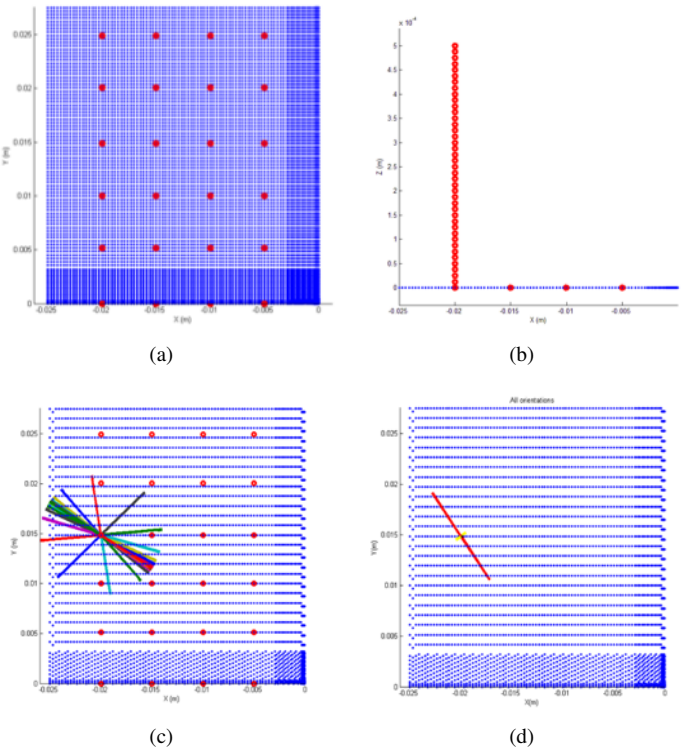

Figure 5.7 Post-processing procedure: (a) selection of the points on the mould wall (marked in red) where the numerical model is used to evaluate the average orientation directions; (b) example samples perpendicular to the mould walls where the orientation vector is evaluated at different sample thickness (41 samples along the z-axis, X=-20mm Y=15mm); (c) projection on the XY Plane of all the orientation vectors evaluated in the sample points created in the mould thickness (on the same XY location); (d) projection on the XY plane of the average orientations vectors of the styrene micro-chains (the direction of the vectors indicates the orientation of the micro-chain while their length is proportional to the degree of orientation).

The comparison between the orientation evaluated using the computational model and the orientation known experimentally was possible. For the comparison, Θ_{vc} was chosen constant with a value of 10 degree, and the threshold ψ_{vc} was hypothesised equal to four different values (10, 30, 50, 100). Comparing computational result and experimental data the threshold was chosen.

This threshold value led to the minimisation of the difference between computational and experimental orientations. The difference in the volume fraction of the chains oriented in the prescribed direction was evaluated accordingly. Specifically, the threshold value equal to 30 led to the best superimposition between experimental and computational data (Figure 5.8).

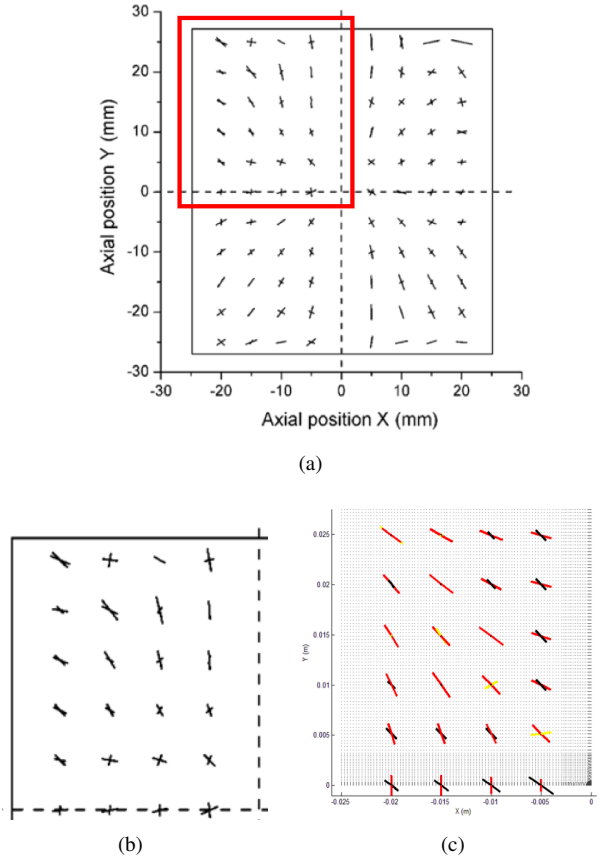

Figure 5.8 Small Angle X-ray Scattering (SAXS) analysis of the whole membrane (a). A quarter of a membrane is highlighted (b) and the experimental orientation was compared with the micro-chain orientation obtained setting a $\psi_{vc} = 30$ (c). Direction and length of the computational micro-chain orientation vectors are very close to the vector obtained by SAXS analysis, denoting a good choice of the critical threshold.

5.2.4 Orientation of the polymer chains in the leaflets of the modelled biomorphic heart valve prostheses

Once determined the threshold ψ_{vc}, that allows the model to predict the orientation of the polymer chains, the same critical value was used to predict the micro-chain orientation inside the leaflet of the valve.
Specifically, different configurations have been modelled (Figure 5.9) with different *Inlets* and *Outlets* position in order to determine which configuration leads to a predominantly circumferential orientation of the polymer chains. While the dimension of the outlets are always the same, the inlets configuration are different both in position and in cross section area.
Even if the real injection points have a circular section, in this model it was decided to simply the injectors geometry with squared section to have continuity with the mesh of the leaflets to avoid singularity.

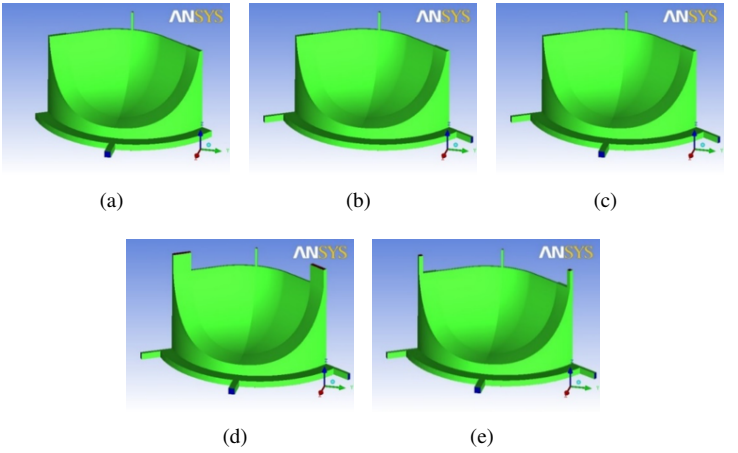

Figure 5.9 Fluid domains with different *Inlet* and *Outlet* locations. The central injector of each configuration is a channel with square cross section (side 0,3 mm, length 3 mm) located in the middle of the leaflet free edge; the *Outlets* are located in different points of the stent and are channels with square cross section (side 1 mm, length 3 mm). The shown configurations are: (a) 1 *Inlet* 1 *Outlet* (central location); (b) 1 *Inlet* 2 *Outlets* (on the sides); (c) 1 *Inlet* 3 *Outlets* (1 in central location, 2 on the sides); (d) 3 *Inlets* 2 large (conducts on the sides with cross section of 2.9 mm x 1.1 mm, length 3 mm) 3 *Outlets* (1 in central location, 2 on the sides); (e) 3 *Inlets* 2 Small (conducts on the sides with cross section of 1.45 mm x 1.1 mm, length 3 mm) 3 *Outlets* (1 in central location, 2 on the sides).

The central injection inlet has a square section of side 0.3 mm in all the configuration while the lateral ones are different: in the configuration *3 Inlet 2 Large* the lateral rectangular sections are 2.9 mm x 1.1 mm while in the configuration *3 Inlet 2 Small* he lateral rectangular sections are 1.45 mm x 1.1 mm. The outlets have a square section of side 1 mm in all the configuration.
Due to the valve symmetry only a third of the valve was taken into account. After carrying out a sensitivity analysis, 747200 hexahedral elements mesh (quality factor equal to 0.833) with 40 elements in the thickness of the leaflet was created.
The steady fluid dynamic simulations were carried out using the same settings described previously (cf. Section 5.2.3).
The imposed boundary conditions are:

- *Mass flow inlet* on the top of the injection inlets (Figure 5.10(a));
- *Outflow* on the lateral surface of the outlets (Figure 5.10(b));
- *Wall* at the internal surface of the valve (Figure 5.10);
- *Symmetry* on the lateral boundary (Figure 5.10(c));
- *Interior* on the whole fluid domain.

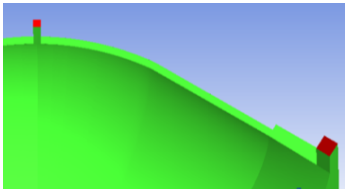

(a)

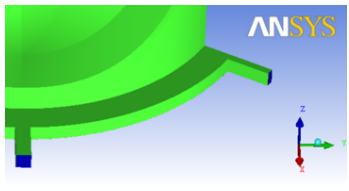

(b)

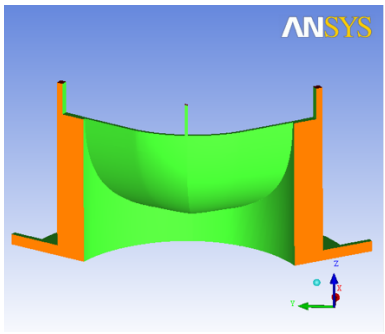

(c)

Figure 5.10 Boundary conditions given for the configuration *3 Inlet 2 Small 3 Outlet*. The inlets are shown in red (a), the outlets in blue (b). The symmetry planes are coloured by orange (c) while the mould wall are in green.

5.3 Results

5.3.1 Outlets' position effect

The analysis of the configurations characterised by only one inlet in central position and mass flow rate equal to $5.3 \cdot 10^{-6} \frac{kg}{s}$ led to the conclusion that the position of the outlets had no significant effects on the fluid dynamics and the chains orientation in the leaflet, while significantly modified the flow in the valve annulus (Figure 5.11).

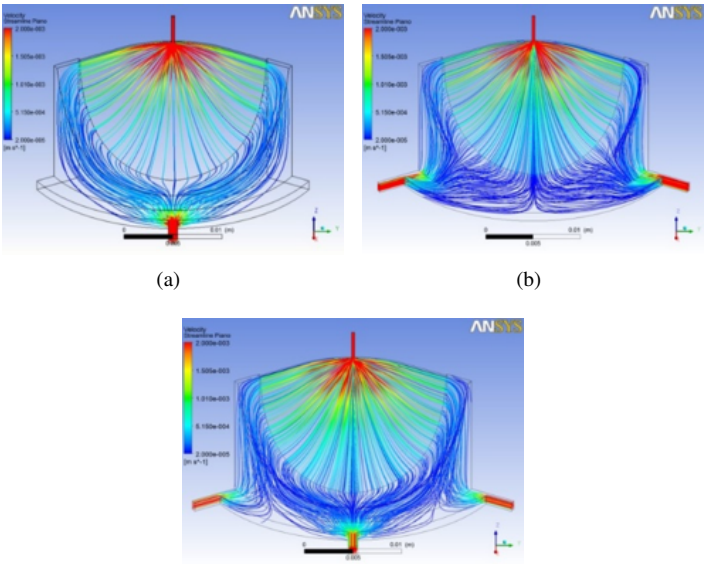

(a) (b)

(c)

Figure 5.11 Streamlines in different configurations all characterised by only 1 Inlet, 1 Outlet (central location) (a), 2 Outlets (on the sides) (b) and 3 Outlets (1 in central location, 2 on the sides) (c). The colour scale ranges from 0.02 mm/s (blue) to 2 mm/s (red).

The differences in the polymeric chains orientation in the leaflets among the different configurations resulted negligible and for that reason the results obtained in the configuration 1 Inlet 1 Outlet, shown in Figure 5.12 and Figure 5.13, are representative also of cases not reported. In each configuration, the orientation of the polystyrene micro domains was mainly perpendicular to the direction of

the flow. Only in the middle of the leaflet the micro-domain are oriented in the same direction of the flow. Moreover, the analysis of the results highlights that the *extensional flow* was the dominating mechanism of polystyrene micro domains even near the walls (Figure 5.13).
No significant differences in the orientation of the polymeric micro domains were observed comparing the different configurations. Furthermore, even if the phenomena that leads the polymer chains orientation is the same, differences in the orientation directions were seen among the points located near the mould walls and the ones in the middle of the leaflet thickness.
In the first case (Figure 5.13(a)), almost all the polymer chains were perpendicular to the flow direction, only the ones close to the leaflet symmetry plane align themselves to the direction shown by the normalised velocity vector.

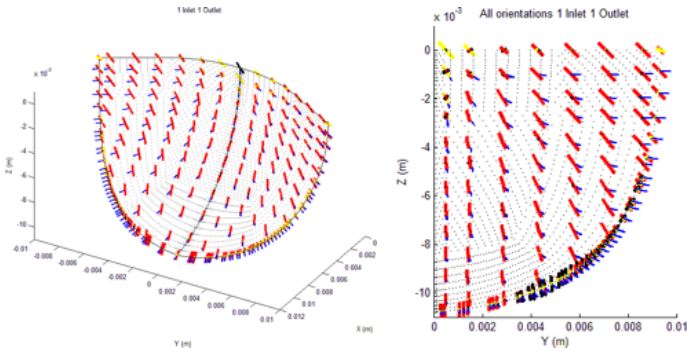

(a) (b)

Figure 5.12 Typical orientations of the polymer chains predicted by the model for the configurations characterised by a single inlet located in the middle of the leaflet free edge. Results are shown for the configuration 1 Inlet 1 Outlet: (a) 3D view of the entire leaflet and (b) 2D view of one half of the leaflet. The red line are the first direction, the black ones the second and the yellow one the third. The blue vector is the normalised velocity vector.

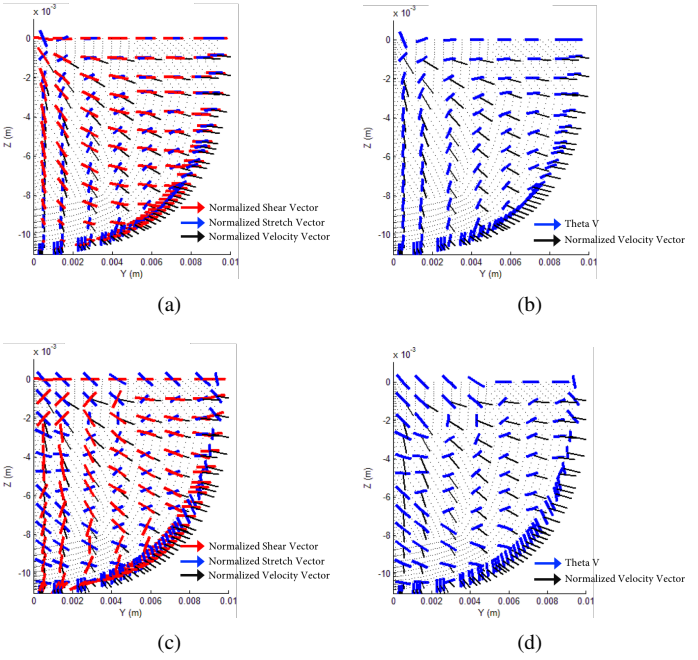

Figure 5.13 Two-dimensional view of the results of one half of the leaflet referred to the configuration 1 Inlet 1 Outlet: (a, c) normalised *shear vectors* (blue), normalised *stretch vectors* (red) and (b, d) *orientation vectors* Θ_v of points located 30 from the mould walls (a, b) and in the middle of the leaflet thickness (c, d).

Instead, in the middle of the leaflet thickness (Figure 5.13(c)) the orientation of the polyester micro domains perpendicular to the flow was more evident and characterised all the chains, particularly near the leaflet symmetry plane where the observed difference relative to the walls was maximum. The normalised shear vectors were mainly oriented along the flow direction, even if there was not a whole superimposition.

5.3.2 Inlet's position effect

In order to further optimise the mould and enhance the stent filling the configurations with different injectors located in the sides of the mould have been analysed. The simulation results confirm that these changes let us reach this goal without significantly altering the flow in the leaflet (Figure 5.14).
No significant effects on the polymer chains orientation along the leaflet were

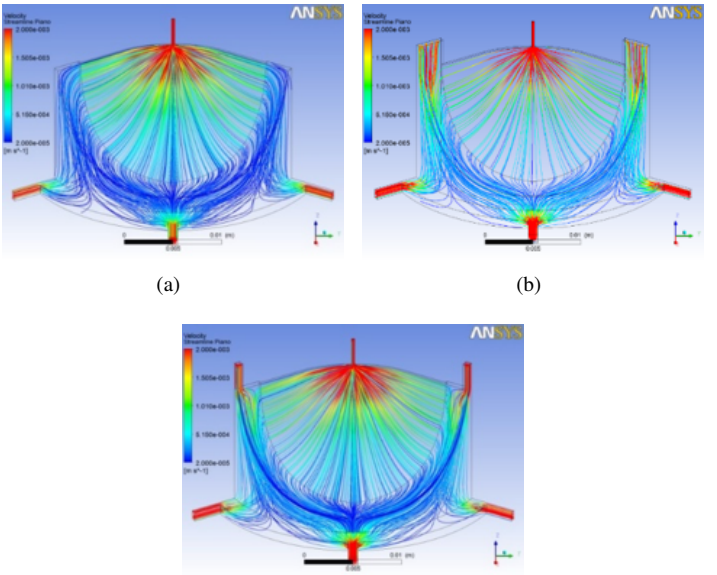

(a) (b)

(c)

Figure 5.14 Streamlines in different configuration with different injector location, but the same outlets: (a) 1 Inlet 3 Outlets; (b) 3 Inlets 2 Large 3 Outlets; (c) 3 Inlets 2 Small 3 Outlets. The colour scale ranges from 0.02 mm/s (blue) to 2 mm/s (red).

obtained adding the injectors on the side of the mould. Comparing the three configurations with the same outlets but different injection points, the differences observed in the micro-chains orientation were negligible (polymer chains were still perpendicular to the direction of the flow) and located only near the lateral injection points. Along the thickness, the same observations can be made.As observed in the configuration characterised by a single inlet and several outlets, at the centre of the leaflet and near the wall the polymeric micro-

chain are aligned in the same direction of the velocity vector; while in the middle of the leaflet thickness all the micro-chain were oriented perpendicularly to the flow field. The results obtained in the configuration *3 Inlets 2 Small 3 Outlets* are shown in Figure 5.15 and Figure 5.16, considering these representative also for the cases not reported.

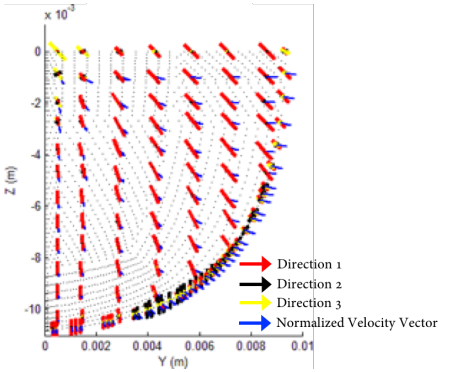

Figure 5.15 Typical orientations of the polymer chains predicted by the computational model for the configurations with the same outlets, but different injection locations. A 2D view of one half of the leaflet is shown for the configuration 3 Inlets 2 Small 3 Outlets.

Experimental micro-chains orientation inside the polymerical leaflet (Figure 5.17), was compared with the numerical model results. The leaflet was dissected from the valve and mounted on a frame perpendicular to the X-ray passing throughout the sample. SAXS was used to asses the spatial distribution of polystyrene cylinders across the valve leaflet. As described in **Chapter 3** for SEPS-22, SIS-30 and SI/BS-19 samples materials, SAXS was performed on beamline I22 at Diamond Light Source, Harwell Science and Innovation Campus, UK.
The peak integration method previously described, was used to assess orientation.
According to the predicted orientation, the SAXS map displayed in Figure 5.17 has a high degree of biaxial orientation. However, a dominance of horizontal orientation is still evident in the belly region of the leaflet.
However, their exact orientation is not always correct, nor is their fraction.

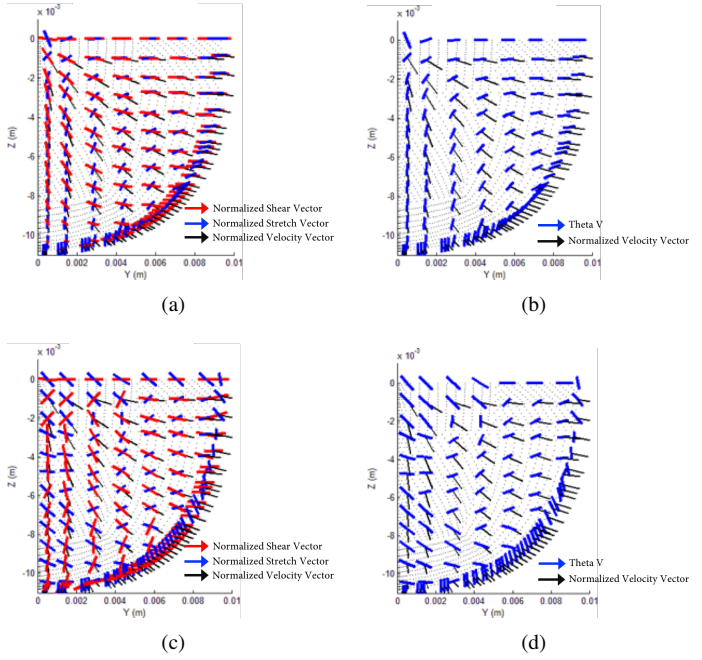

Figure 5.16 Two-dimensional view of the results of one half of the leaflet referred to the configuration 3 Inlet 2 Small 3 Outlet: (a, c) normalised *shear vectors* (blue), normalised *stretch vectors* (red) and (b, d) *orientation vectors* Θ_v of points located 30 m from the mould walls (a, b) and in the middle of the leaflet thickness (c, d).

5.3.3 Mass flow rate effect

The analysis performed on different configurations allowed to highlight how the orientation of the polymer chains achieved in the leaflets is not affected by inlet and outlet locations tested. Therefore, it is possible to focus the mould's design to optimise the distribution of the polymer in the stent. Among the analysed configurations, the one that shows the best performance is the 3 Inlets 2 Small 3 Outlets. Keeping constant this configuration, different mass flow rates were considered (ten times higher and ten times lower than the standard case) to highlight the effects on the orientation of the polymer chains along the leaflet (Figure 5.18). The different mass flow rates were negligible on the orientation of the polymer chains within the leaflet. The unchanged results after an increase

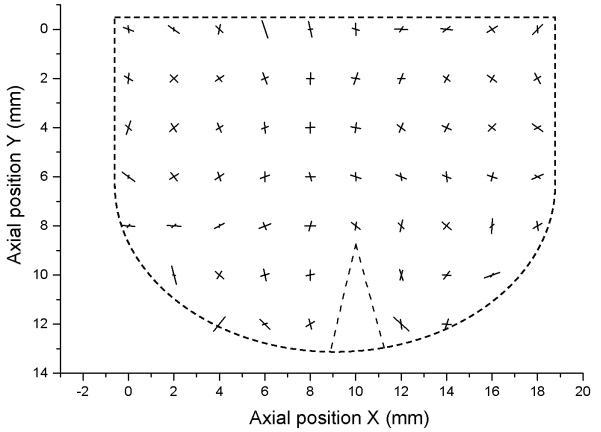

Figure 5.17 Picture of a leaflet with vector graphs presenting orientation map in particular points of the leaflets, based on X-ray measurements. Two crossing lines are visible in most cases, indicating orientations in two directions. The length of the vector is proportional to the volume fraction of the radial and circumferential orientation. There is a kind of a triangle in the bottom of the leaflet, which results from cutting the leaflet in order to flatten it for the X-ray measurements.

of the mass flow rate showed that the extensional flow still drives the polymer chains orientation (as an example in Figure 5.19 are shown the results obtained with a flow rate equal to $5.3 \cdot 10^{-7} \frac{Kg}{s}$). Similarly, a decrease of the mass flow rate leads only to a slight increase of the chains arranged in the direction perpendicular to the flow. Higher flow rates promote orientation in the direction of flow, and thus at lower flow rates it may be possible to produce more circumferential orientation. The results along the sample thickness highlight that the influence of different mass flow rates was lower near the mould walls, while was higher in the middle of the leaflet thickness. In these points, a decrease of the inlets mass flow rate enhanced the extensional flow: the orientation of the polyester micro domains perpendicular to the flow was more noticeable, especially near the leaflet symmetry plane.

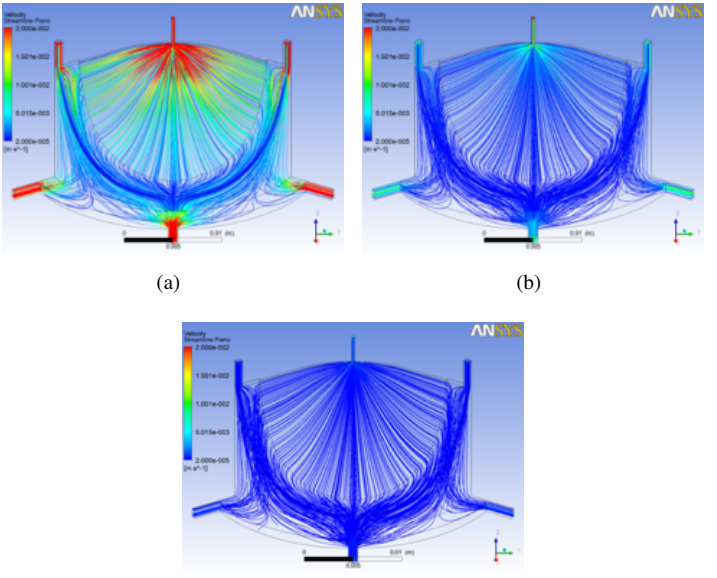

(a) (b)

(c)

Figure 5.18 Streamlines of the configuration 3 Inlet 2 Small 3 Outlet with mass flow rate equal to (a) $5.3 \cdot 10^{-5} \frac{Kg}{s}$; (b) $5.3 \cdot 10^{-6} \frac{Kg}{s}$; (c) $5.3 \cdot 10^{-7} \frac{Kg}{s}$. The colour scale ranges from 0.02 mm/s (blue) to 20 mm/s (red).

5.4 Conclusion

The comparison of the different configurations showed that the polymer chains of the considered Styrenic Block Copolymer aligned themselves perpendicular to the flow direction, without obtaining the perfectly desired circumferential orientation needed to further improve the performance of the prosthetic valve. Slight variations were observed among the configurations with different Inlets and Outlets and so in order to optimise the entire mould, configurations with different injection points' location can be selected without affecting the micro domain alignment in the PHV leaflets. Different mass flow rates showed a micro domains orientation always in the direction perpendicular to the flow. Therefore, the higher mass flow rate can be employed to speed up the PHVs manufacturing, without affecting the anisotropy obtained in the leaflet. However, most of the time to prepare a new prototypes is used during the cooling

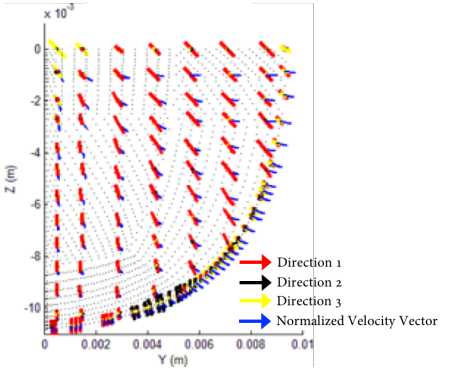

Figure 5.19 Average orientation vectors provided by the computational model for the configuration 3 Inlets 2 Small and 1 Outlet with mass flow rate equal to $5.3 \cdot 10^{-7} \frac{Kg}{s}$, a 2D view of one half of the leaflet.

phase, then increasing the injection flow rate does not entail a big advantage. Furthermore, in order to improve the anisotropy of the valve leaflets and get closer to a circumferential arrangement of the polymer chains, further injection points that can produce streamlines in the desired directions should be tested, considering that the SEPS-22 micro domains align themselves perpendicular to the flow. In summary, near to the free edge the orientation is in all the different layout horizontal, and parallel to the free edge. Brubert (2015) analysed different configuration in a similar way and observed that the configuration without an injector located in the middle of the free edge of the leaflet, is the only one that does not show this horizontal distribution. For that reason that configuration was not taken into account.

The orientation showed in both model and prototype leaflet is similar to the natural leaflet, which is shown in Figure 2.8 and by Rock et al. (2014). Moreover, in both numerical and experimental results, the polymers fibre approximate to arcs as in the natural leaflet.

All the configuration analysed promote biaxial orientation of the polymeric fibres in the leaflet with the core oriented in a proper way. The fibre orientation into the stent was neglected.

Both the configuration with three inlets and the other configurations with one centred inlet show a changing of the flow direction between the leaflet and the pillar. Where three inlet are present the changing of flow direction, referred to the *weld line*, are more close to the leaflet compared to the other configuration. The weld line may be a source of flaws from which cracks could grow. For

that reason the configuration *3 Inlet 2 Small 3 Outlet*, was preferred because the small lateral injection point admits a better mould filling moving the *weld line* more closed to the stent posts. In the end, given that SEPS-22 is anisotropic, it is likely that the viscosity is also anisotropic. For that reason, maybe, the model is unlikely to provide an accurate description of the flow.

Chapter 6

Experimental Tests

In this Chapter, the experimental campaign performed on the manufactured prototypes is reported. First hydrodynamics testing are performed to assess if performance met the requirements of the ISO 5840:2015 Standard. Then the flow fields through the prototypes are investigated using the 2D and 3D particle image velocimetry. Finally, durability testing were conducted.

6.1 Introduction

THE in vitro fluid-dynamic testing are fundamental steps in the evaluation of performance for a prosthetic heart valve. The ISO 5840:2015 and FDA standards suggest both the method and the specifications for testing equipment, thereby providing the minimum device performance requirements that a PHVs shall meet.
The ISO 5840:2015 also covers important hydrodynamic and durability characteristic of heart valve substitutes. However, it is important to underline that the ISO 5840-series does not specify exact test methods for hydrodynamic and durability testing, but offers guidelines for the test apparatus.
The test benches developed in this work were designed and built up following the ISO 5840:2015 guidelines.
To well characterise the behaviour of the prosthetic device, three kinds of tests were performed:

- Hydrodynamic testing;
- Flow visualisation test;
- Durability testing.

Hydrodynamic testing were performed on all the manufactured prototypes while the flow visualisation test and mainly durability testing were performed on the prosthetic heart valves that showed the best hydrodynamic performances. A total of 24 new PHVs prototypes were manufactured by both compression and injection moulding technique from the three different commercially available styrene block copolymers previously described (cf. Chapter 3). Three groups of valves were investigated, each one comprising 8 valves:

- Group A: valves manufactured from poly(styrene-b-isoprene/butadiene-b-styrene) block copolymers with 19% percentage by mass (wt) polystyrene fraction (SI/BS-19).
- Group B: valves manufactured from poly(styrene-b-isoprene-b-styrene) block copolymers with 30% wt polystyrene fraction (SIS-30);
- Group C: valves manufactured from poly(styrene-ethylene-propylene-styrene) block copolymers with 22% wt polystyrene fraction (SEPS-22).

Prototypes belonging to both Group A and B, were obtained by compression moulding, hot pressing at 150°C cuboids (approximately 0.5 cm^3) of the block copolymer initially located at the commissural of each of the three leaflets of the valve. SI/BS-19 and SIS-30 prototypes have the same geometric profile and dimensions (Figure 6.1) as previously described (Chapter 3).
SEPS-22 prototypes, belonging to Group C, were obtained by injection moulding, and as described in Chapter 5, they differ from Group A and B prototypes in stent structure, while have the same leaflet shape and dimension (Figure 6.2).

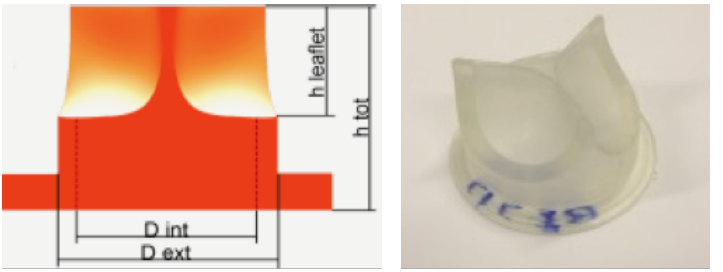

(a) (b)

Figure 6.1 (A) sketch and (B) picture of a compression melted prototype. The dimensions are: h leaflet = 10.7 ÷10.9 mm; h tot = 21 mm; D int = 21 mm; D ext = 28 mm; Tissue Annulus Diameter (TAD) = 21 mm; thickness leaflet = 0.36 ÷ 0.42 mm.

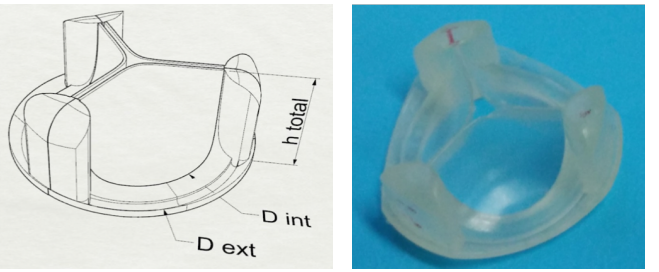

(a) (b)

Figure 6.2 Sketch (A) and picture (B) of the PHV belonging to the Group C. The dimension are: h total = 14 mm, D int = 21 mm, D ext = 32 mm, Tissue Annulus Diameter = 21 mm, thickness leaflet = 0.29 ÷ 0.33 mm and height leaflet = 11 mm

6.2 Hydrodynamics Tests

Hydrodynamic tests are designed to give information on the fluid mechanical performance of the PHVs and to provide indicators of valve performances. According to the Standards, these tests should be performed on at least three surgical prototypes of each size and on at least one reference valve of each size. At this step, only one size (TAD = 21 mm) was taken into account and a biological valve (3000 PERIMOUNT Magna, Edwards Lifesciences), the PHV with the best performances in the short term period, was used as the reference valve. Moreover, also a tilting disc mechanical valve currently on the market (Omniscience tilting disk) was investigated.
Two typologies of tests were carried out: *steady* and *pulsatile* tests. The first set is divided into *steady forward-flow testing* and *steady back-flow testing* to measure the pressure drops at constant flow rate and the regurgitant volume at constant back-pressure, respectively. On the other and, performing *pulsatile tests* it is possible obtain time dependent pressure drops measurements and regurgitant volume at the same time.
Minimum performance requirements for prosthetic valves are provided by ISO 5840:2015 (Table 6.1) only for pulsatile test at given test conditions. This requirements are given as a function of valve size. The minimum performance requirements are based on values in the scientific literature while no minimum performances are given about the steady tests. As a matter of fact, it is very difficult to obtain published data on the PHVs performance in steady condition. Continuous flow is usually studied by using particle image velocimetry, neglecting pressure drops and regurgitant volume (Hutchison et al., 2011).

Table 6.1 Minimum device performance requirements for aortic heart valve prosthesis prescribed by ISO 5840:2015. The minimum performance requirements correspond to the following pulsatile-flow condition: beat rate = 70 cycle/minute, simulated cardiac output = 5 l/min, and systolic duration = 35% at normotensive conditions.

Parameter	Valve size (mm)			
	17	19	21	23
EOA (cm^2) larger than or equal to	0.70	0.85	1.05	1.25
Total Regurgitant Fraction (% of forward flow volume) less than or equal to	10	10	10	10

Continuous and pulsatile flow tests were performed using saline solution at

room temperature (22°C) with specific gravity of $1.005\ \frac{g}{ml}$ and viscosity of $1.0\ cP$. Pulsatile tests were performed at the body temperature (37°C) to asses if there are any effects due to the temperature on the PHVs behavior.
No variation in the viscosity and density of the test fluid were observed moving from 22°C to 37°C. Each pulsatile test was performed at least for 15 consecutive cycles at each test condition. SPSS Statistical version 21 (IBM®) was used to perform statistical tests. All data are reported in the *Results* section as mean $\pm$ standard deviation (SD). Independent-sample *t-test* and *Anova test* was used to determine statistically significant differences among the groups. Significance level for the test was chosen at $p < 0.01$.
First, Group A and Group B prototypes results were compared to assess how the styrene fraction could influence the hydrodynamic behaviour, and then the result between Group A and Group C were compared to observe the influence due to the stent geometry.

6.2.1 Continuous Forward Flow Tests

Methods

The experimental set-up by which valves are tested in a continuous flow system is shown in Figure 6.3 and it is made up of:

- a housing unit designed according to the guidelines of the ISO 5840 standard which describes the need to fix the valves in the circuit;
- a reservoir at the free surface;
- a centrifugal pump with magnetic drive BIO-MEDICUS-550 BIOCONSOLE®(Medtronic, Minneapolis, USA).

The valves were tested at flow rates from 0 to 10 l/min in increments of 0.5 l/min, the flow rate was measured by using a transit-time ultrasound flowmeter (HT110 series, Transonic Systems). Transvalvular pressure drop was measured 3 times for each valve by a pressure transducer (140PC pressure sensors, Honeywell) to verify the repeatability of the test.
At the end of each test the data were recorded for the analysis of pressure drops across each valve and to compare the behaviour of different prototypes. According to ISO 5840:2015 Standard, pressure was measured one diameter upstream (35 mm) and three diameters downstream (105 mm) the valve plane in order to allow the flow to be fully developed.
Frontal pictures from the observation point (Figure 6.3) were taken each 1 l/min.

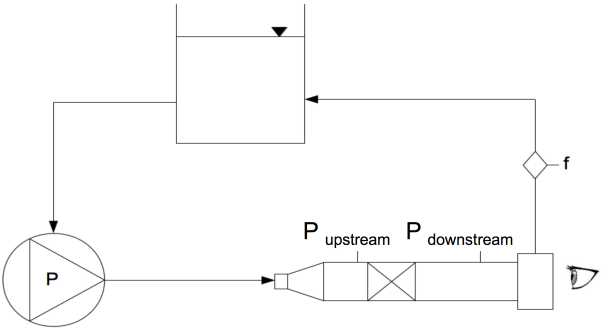

(a)

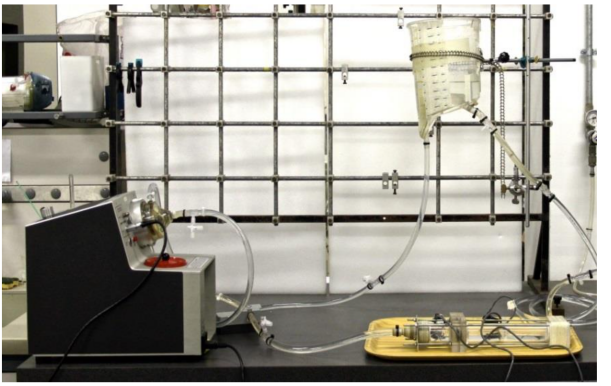

(b)

Figure 6.3 Outline (a) and picture (b) of the experimental set up for continuous flow tests. On the diagram are shown the locations of upstream and downstream pressure measurements, the flow rate measurement location and the observation point from which pictures of the valve opening at each flow rate were taken.

Results

As we described in De Gaetano et al. (2015b), Group A showed a statistically lower ($p = 3.2 \cdot 10^{-4}$) mean transvalvular pressure drop ($8.36 \pm 1.33\ mmHg$) than Group B ($15.26 \pm 1.87\ mmHg$) at the maximum flow rate (10 L/min) while Group C showed, at the maximum flow rate, a mean transvalvular pressure drop equal to $9.35 \pm 1.53\ mmHg$.
All these data were summarise in Table 6.2. Even if Group C show low pressure drops, no significant statistical difference were found between Group A and C. It's important to remind that Group A and Group C have the lowest amount of styrene fraction, 19% and 22%, respectively.

Table 6.2 Transvalvular pressure drop among the 8 valves of each group at the maximum flow rate (10 L/min). The pressure drop of one biological and one mechanical prosthesis used as reference valves are also shown. The mean transvalvular pressure drop of both Group A and Group B are statistically different (p¡0.01) as well as between Group A and C (p¡0.01). On the other hand, no statistically difference in pressure drops were found between Group A and C (p¿0.05).

Group	ΔP_{max} [mmHg]
A	8.36 ± 1.33
B	15.26 ± 1.87
C	9.35 ± 1.25
Biological	1.53 ± 0.21
Mechanical	3.03 ± 0.40

Even if the pressure drops of both Group A and Group C is half of the pressure drops measured in valves of Group C (Figure 6.4), it is still four times greater than the pressure drops measured on the biological valve.
The tested mechanical valve shows pressure drops of about 3 mmHg. It is a very low value not unexpected as it is related to the type of test: performing continuous forward flow tests, the inertia effects of the leaflet (the main factor of the pressure drops in mechanical valves) it is not taken into account. Figure 6.5 shows the leaflet behaviour during the opening at different flow rate. The behaviour among the valves belonging to the same group is similar. While the behaviour between the compression moulded valve is the same, a different movement of the leaflet of the Group C prototypes was observed.

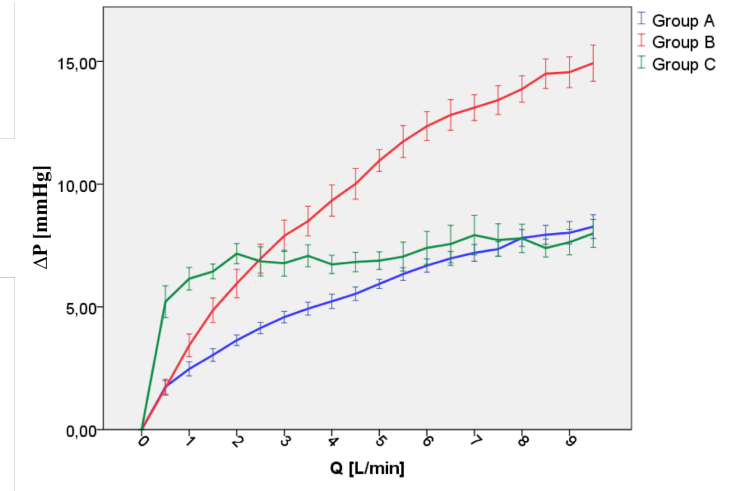

Figure 6.4 Results of continuous forward flow test: comparison of transvalvular pressure drops among the three groups of valve (data are reported as mean among 8 valve $\pm$ SD).

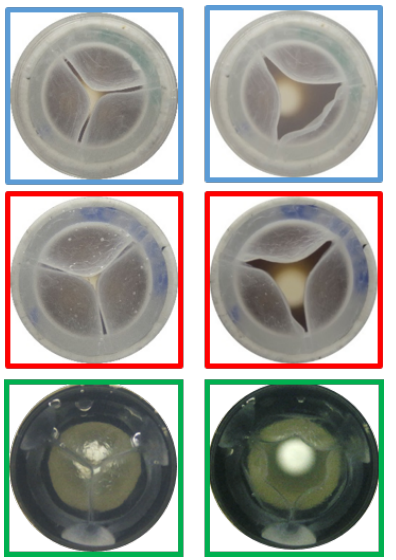

Figure 6.5 Picture of 3 prototypes (top blue outlined valve from Group A; middle red outlined valve from Group B and bottom green outlined from Group C) at two different flow rate (0 L/min on the left and 10 L/min on the right).

The pressure drops for the three groups are summarised in Figure 6.4. By averaging the values of the pressure drops among of the different prototypes belonging to each group, it is possible observe an increase of the pressure drops increasing the flow rate. This is not always true, as it is possible to observe by analysing the charts of the pressure drops of the single valves (Figure 6.6).
Some prototypes show a reduction in pressure drops, at increasing flow rates because one or more leaflets, suddenly change curvature, providing a larger flow passage section. For that reason the maximum pressure drop was not always displayed at the maximum flow rate.

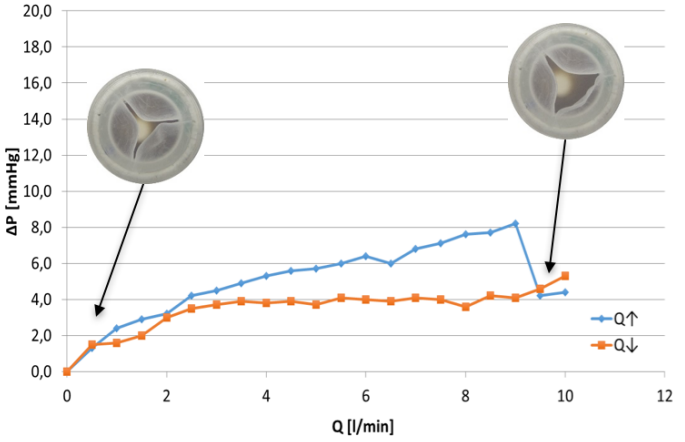

(a)

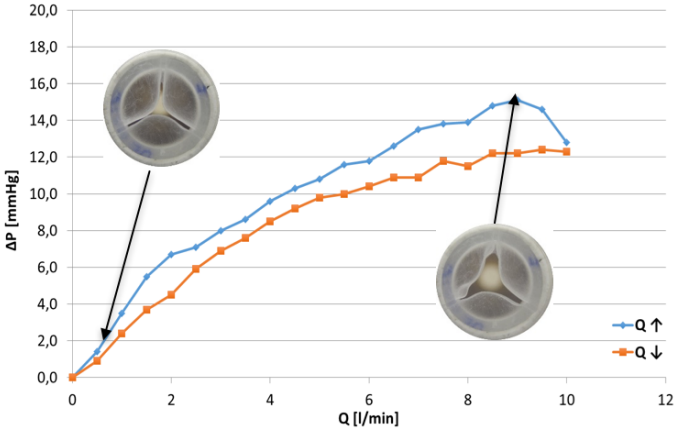

(b)

Figure 6.6 Results of continuous forward flow test: transvalvular pressure drops of valve belonging to Group A (a) and of valve belonging to Group B (b). The blu tracing shows an increasing flow rate while the orange indicated a decreasing flow rate.

6.2.2 Assessment in continuous back flow conditions

Method

The experimental setup for the regurgitation test contains the following elements:

- a housing for the valve (as used in the continuous flow tests);
- a reservoir at the free surface to provide a constant pressure upstream the valve;
- a pressurized reservoir connected to the pressure line using a modular pressure regulator to vary the backpressure acting on the valve;

During testing the pressure regulator was set to provide backpressure ranging from 30 mmHg to 140 mmHg. The pressure was increased by 5 mmHg for each test. Between two consecutive measurements, backpressure was set to zero mmHg to allow the valve to recover its initial configuration. Pressure measurements were performed by pressure transducer (140PC pressure sensors, Honeywell).
The regurgitant rate at each back pressure was measured by using a transit-time ultrasound flowmeter (HT110 series, Transonic Systems). Regurgitation rate at each backpressure was determined and from this the average regurgitation rate for each valve at all backpressures was found.

Results

As in the continuous flow test in which the valves with lower percentage of styrene showed better performance, also the mean regurgitation displayed by Group A ($175.3 \pm 19\ mL/min$) was lower than Group B ($264 \pm 26\ mL/min$), but the difference is statistically insignificant ($p = 0.077$). The small differences in regurgitation between the two groups with the same geometry, may be ascribed to the different leakage area which forms during the valve closing phase (Figure 6.7). The valve belonging to Group C show the lowest regurgitation if compared to the other two groups (Figure 6.8).
Moreover, the valves made by injection moulding show a very low regurgitation (Group C), comparable to the regurgitation of the biological tested valve. The difference between injection moulded and compression moulded prototypes are in both cases statistically significant ($p < 3 \cdot 10^{-5}$). The mechanical valve, as expected, has a very high static regurgitation (Table 6.3).

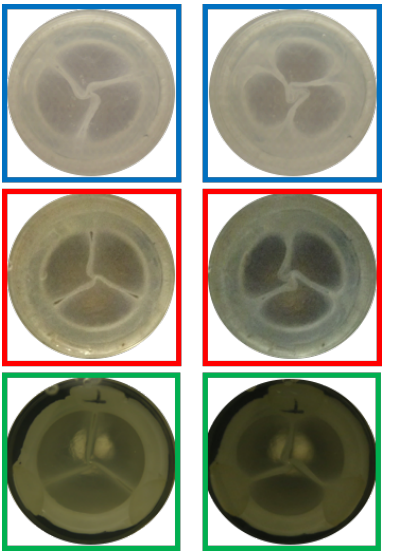

Figure 6.7 Picture of 3 prototypes (top blue outlined valve from Group A; middle red outlined valve from Group B and bottom green outlined from Group C) at two different backpressure (40 mmHg on the left and 130 mmHg on the right).

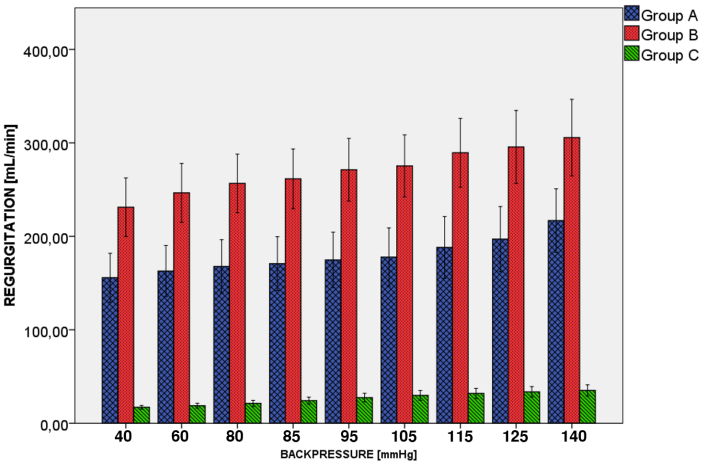

Figure 6.8 Results of continuous back flow test: comparison of regurgitation among the three groups of valve (data are reported as mean among 8 valve $\pm$ SD).

Table 6.3 Mean transvalvular regurgitation among the 8 valves of each group. The transvalvular regurgitation of one biological and one mechanical prosthesis used as reference valves are also shown.

Group	$Q_{backflow}\ mean$ [mL/min]
A	175.33 ± 19.21
B	263.97 ± 26.90
C	26.88 ± 12.08
Biological	32.58 ± 28.79
Mechanical	568.09 ± 231.72

6.2.3 Pulsatile flow test condition

In vitro pulsatile evaluation of an aortic valve requires the replication of the systemic circulation, including the left atrium, left ventricle, and the large and small arteries. The left ventricle pumps oxygenated blood into the systemic arteries, which progressively decrease in size as they branch. The large arteries offer low resistance to flow, and can be considered as compliant elements, whereas pressure drops across the small arteries are high, defining them as resistance elements. Blood is routed back to the left ventricle through the left atrium, which acts as a reservoir for the system. As a result, the systemic circulation can be represented by a reservoir (left atrium), a pump (left ventricle), compliance elements (aortic and systemic compliance), and a resistance element (peripheral resistance). A system composed of these elements and capable of reproducing physiological flow characteristics is referred to as a "Pulse Duplicator". A pulse duplicator is required to have a valve chamber with relevant dimensions, thereby replicating the haemodynamic characteristics across the valve. The system must be capable of producing pressure and flow waveforms that approximate a range of physiological conditions from rest to exercise (Figure 6.9) arranging resistance and compliance elements.

Parameter	**General condition**			
Surrounding medium	Human heart/Human blood			
Temperature	34 °C to 42 °C			
Heart rate	30 bpm to 200 bpm			
Cardiac output	3 L/min to 15 L/min			
Forward flow volume	25 mL to 100 mL			
Blood pressures and resultant pressure loads by patient condition	Arterial peak systolic pressure mmHg	Arterial end diastolic pressure mmHg	Peak differential pressure across closed valve[a]	
			Aortic ΔP_A mmHg	Mitral ΔP_M mmHg
Normotensive	120	80	100	120
Hypotensive	60	40	50	60
Hypertensive				
Mild	140 to 159	90 to 99	115 to 129	140 to 159
Moderate	160 to 179	100 to 109	130 to 144	160 to 179
Severe	180 to 209	110 to 119	145 to 164	180 to 209
Very Severe	≥210	≥120	≥165	≥210

[a] Peak differential pressure across closed aortic valve estimated clinically using the following relationship:

— $\Delta P_A \approx$ pressure associated with dicrotic notch assuming LV pressure is zero ≈ Arterial End Diastolic Pressure + 1/2(Arterial Peak Systolic Pressure – Arterial End Diastolic Pressure).

— Peak differential pressure across closed mitral valve estimated to be equivalent to Arterial Peak Systolic Pressure.

Figure 6.9 Heart valve substitute operational environment for left side of heart - Adult population. Modified from ISO Standard 5840:2015

Pressure and flow measurements are the primary determinants of valve performance, and hydrodynamic performance is evaluated with respect to the following parameters:

- *Stroke volume*: volume of blood pumped by a ventricle in one contraction;

- *Regurgitant Volume*: volume of fluid that flows through a heart valve substitute in the reverse direction during one cycle and is the sum of *closing volume* and *leakage volume*;

- *Closing volume*: portion of regurgitant volume that is associated with the dynamics of valve closure during a single cycle (Figure 6.10);

- *Leakage volume*: portion of regurgitant volume which is associated with leakage during the closed phase of a valve in a single cycle (Figure 6.10);

- *Cardiac output* (CO): stroke volume times heart rate;

- *Mean systolic pressure difference* (MSPD): time-averaged arithmetic mean value of the pressure difference (ventricle pressure and aortic pressure) across a valve during the positive differential pressure period of the cycle (Figure 6.11);

- *Back pressure* (BP): differential pressure applied across the valve during the closed phase.

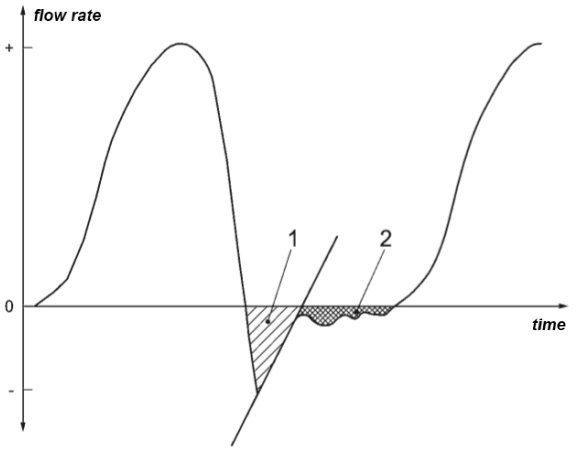

Figure 6.10 Schematic representation of flow waveform and regurgitant volumes (closing -1- and leakage volume -2-) for one cycle. Modified from ISO Standard 5840:2015

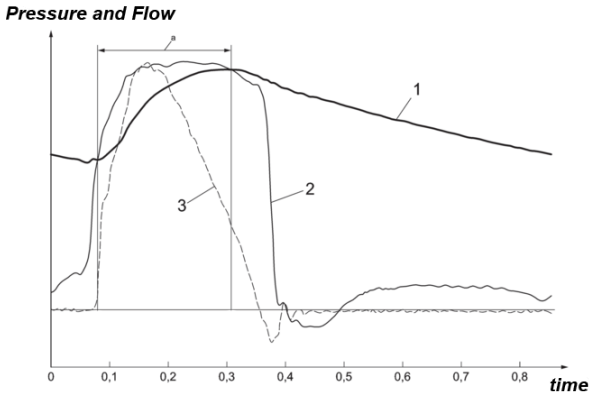

Figure 6.11 Schematic representation of the positive pressure period of an aortic forward flow interval. In the schema are reported the aortic pressure (1), the left ventricle pressure (2), the aortic flow rate (3) and the positive pressure range (a). Modified from ISO Standard 5840:2015

Since the mid-seventies, several test benches were designed and built (Bellhouse, 1972; Cornhill, 1977; Gabbay et al., 1978). Cornhill (1977) was one of the first to demonstrate the possibility of obtaining *in vitro* physiological aortic pressure and flow curves, therefore, his study became an important reference point from which almost all of the following work have been inspired. In 1986, Fisher et al. (1986) designed the first test bench capable to test PHVs in both aortic e mitral position.
Subsequently, many test benches were developed with the ability to better and better represents pressure and flow waveforms in both pathological and physiological conditions.
In the last few year, several test benches have been put on the market: ViVitro Labs Inc. (455 Boleskine Rd, Victoria, BC V8Z 1E7, Canada), BCD Laboratories (4060 Youngfield St, Wheat Ridge CO 80033 USA) and Dynatek Labs Inc (105 East 4th Street Galena, MO 65656) are the most important manufacturers of commercial test benches.
The ViVitro Pulse Duplicator is the in vitro cardiovascular hydrodynamic testing system most widely used in the world to assess the performance of prosthetic heart valves under simulated cardiac conditions.
However an *ad-hoc* pulse duplicator was developed in our laboratory to allow a better control of all the parameters that come into play (value and number of resistances and compliance, geometry of the conduit where the PHVs are placed). Moreover this test bench was conceived to allow us to perform a wide range of tests (e.g. *quasi* real-time fatigue test).
Even if ISO 5840:2015 Standard provides guidelines to design the test bench and perform the pulsatile tests, a direct comparison of the performances of valves tested on different pulse duplicator systems is not simple due to the high variability in the layout of these test benches. A complete hydrodynamic characterisation of a reference valve commercially available is therefore fundamental.

Method

Starting from a previous work (Lanzarone et al., 2009), a new pulse duplicator was designed and built up to perform pulsatile flow tests (Figure 6.12). It consists of the following elements:

- volumetric pumping system;
- ventricular chamber;
- aortic valve housing;

- Resistance-Compliance-Resistance (RCR) analogue to replicate the compliance and resistance (aortic and peripheral) of the cardiovascular system (systemic impedance simulator);

- reservoir simulating the left atrium;

- mitral valve housing (the same used for testing of continuous flow).

The pumping system is software controlled to allow the user to provide different flow rate waveforms. The pumping system is made of a working fluid (the liquid flowing through the heart system) and a service fluid (contained in the piston) separated by a membrane. The pump acts by supplying energy to the service fluid which deforms the membrane positioned within the next section of the system. The movement of the membrane pumps the test fluid within the circuit.
The Swanson and Clark waveform (Equation (6.1)) was used to replicate systolic flow rate.

$$\begin{cases} q_a = 0, & \text{if} \quad 0 < t < T_d \\ q_a = Q_a \cdot \left(0.924 \cdot \sin\left(\dfrac{\pi t}{T_s}\right) + \right. & \\ \quad \left. + 0.23 \sin\left(\dfrac{2\pi t}{T_s}\right) + 0.092 \sin\left(\dfrac{3\pi t}{T_s}\right), \right. & \text{if} \quad T_d < t < T_c \end{cases} \tag{6.1}$$

where t is the time, T_s is the systolic time (obtained by the Katz and Feil (1923) formulation), T_d is the diastolic time and T_c, the whole cycle time is the sum of T_d and T_s. Q_a is the peak value of the flow rate and it is described by the Equation (6.2):

$$Q_a = 1.65 \cdot Q_f \cdot \frac{T_c}{T_s} \tag{6.2}$$

where Q_f is the mean flow rate (CO) at the operating frequency.
On the other hand, a modified Talukder and Reul flow rate waveform was used to reproduce the diastolic flow rate.

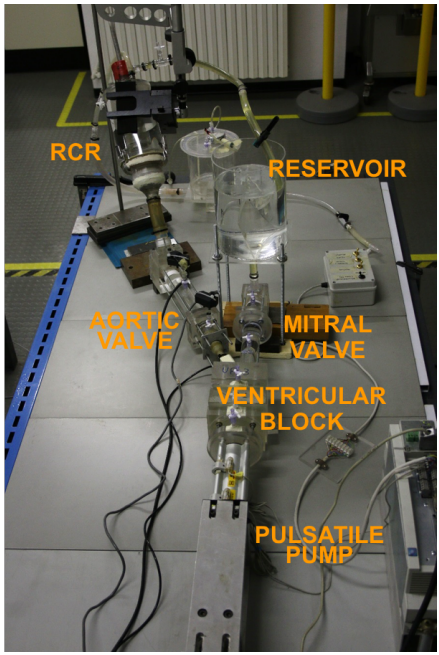

(a)

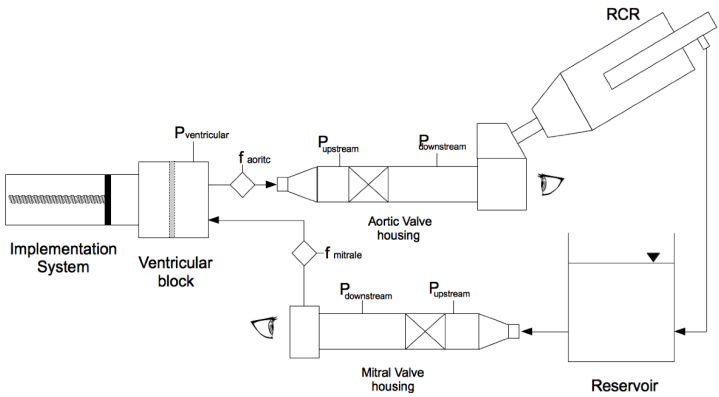

(b)

Figure 6.12 (Picture (a) and schematic (b) of the experimental set-up used for the pulsatile flow tests. Shown on the diagram are the locations of upstream and downstream pressure measurements, the flow rate measurement location and the observation point from which pictures of the valve opening were taken.

The ventricular chamber allows the simulation of both physiological and pathological stroke volume. The ventricular chamber and the pumping system are divided by a thin silicon membrane (thickness = 0.3 mm). In this way the piston can be isolated and filled with distilled water to prevent damage to the mechanical system, while the other elements of the pulse duplicator can be filled with different fluids (e.g., blood or fluids simulating the blood rheological properties) if required.
The aortic and the mitral valve housing are the same used for the continuous flow test and are connected with straight tubes to the systemic impedance simulator and to the ventricular element, respectively. Furthermore, this set up allows the direct visual observation of both valves during all the cycle time.
In compliance with the UNI EN ISO 5840:2015 Standard, this pulse duplicator allows to reproduce the physiological pressure and flow waveform (Figure 6.13).

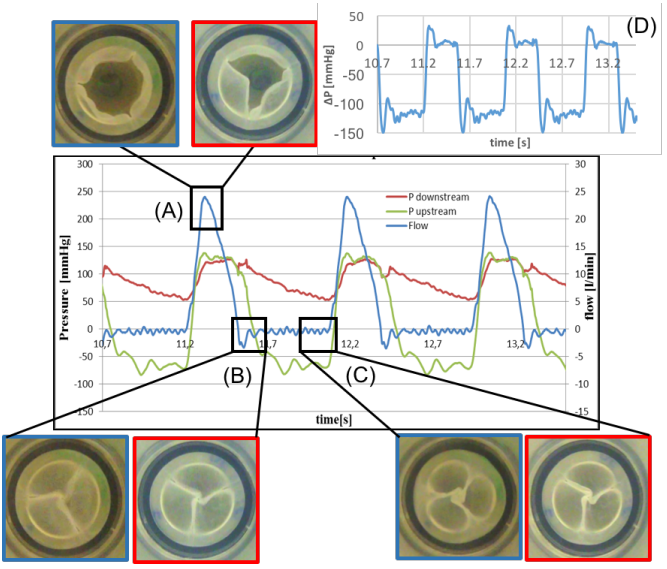

Figure 6.13 Pressure and flow courses of a generic PHV tested in this work. The pictures show the behavior of the two group of valve (blu line Group A and red line Group B) at different cycle time: (A) peak systolic flow, (B) early diastole and (C) end of diastole. Transvalvular pressure course of a generic PHV (D) is shown.

The valves were subjected to different flow rates and pressures as required by the ISO 5840:2015 Standard. The pressure difference across each valve was measured at a constant frequency (70 bpm) and variable flow rate (2 l/min, 3.5 l/min, 5 l/min, 7 l/min). The regurgitation was determined by testing each valve at a mean flow rate of 5 l/min at three different heart rates (45 bpm, 70 bpm, 120 bpm). At each heart rate three back pressure values were tested (80 mmHg, 120 mmHg, 160 mmHg). All the test conditions are summarised in Figure 6.14. All the instrumentation is the same used to perform continuous forward flow test.

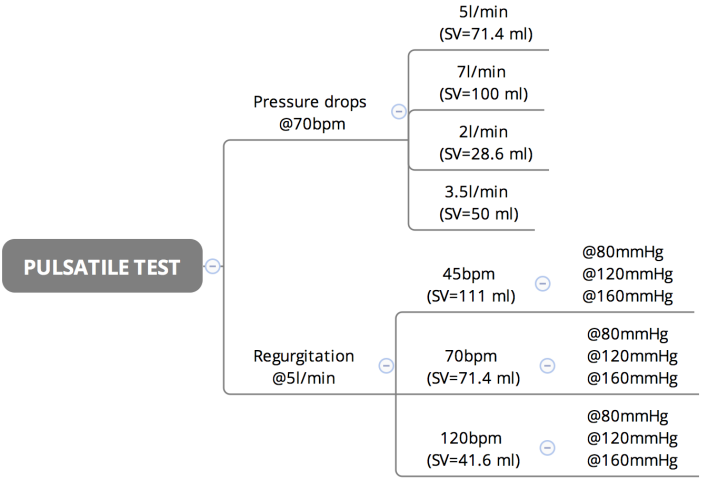

Figure 6.14 Schematization of all the pulsatile tests suggest by ISO Standard 5840:2015

Simultaneous measurements were recorded by using transit-time ultrasound flowmeter and pressure transducer located 35 mm upstream and 105 mm downstream from the aortic valve plane. Trans-valvular pressure drops, regurgitation (RG), regurgitant fraction (RF) mean systolic pressure difference and effective orifice area (EOA) were calculated for each valve. Equation (6.3) was used to calculated MSPD

$$MSPD = \frac{\sum_{i=1}^{n} \Delta P_i}{n} \tag{6.3}$$

where ΔP_i is the pressure difference across the valve in mmHg and n is the number of samples during the systolic phase.
Equation (6.4) from ISO 5840:2015 was used to calculate EOA

$$EOA = \frac{Q_{RMS}}{51.6 \cdot \sqrt{\frac{\Delta P}{\rho}}} \tag{6.4}$$

where ΔP is the pressure difference in mmHg, ρ is the density of the test fluid in grams per cubic centimetre, and Q_{RMS} is the root mean square of forward flow in millilitres per second given by Equation (6.5):

$$Q_{RMS} = \sqrt{\frac{\int_{t_1}^{t_2} Q(t)^2 \, dt}{t_2 - t_1}} \tag{6.5}$$

where $Q(t)$ is the instantaneous flow at time t while t_1 and t_2 are time at start and end of forward flow, respectively.
Regurgitation is given by Equation (6.6):

$$RG = \int_{t_3}^{t_4} Q(t) \, dt \tag{6.6}$$

where t_3 and t_4 are time at start and end of backward flow, respectively. RF% is calculated by Equation (6.7)

$$RF\% = \frac{RG}{SV} \cdot 100 \tag{6.7}$$

Results

All the 24 tested prototypes exceeded the minimum performance requirements set by the ISO 5840:2015 Standard in both EOA (Figure 6.15(a)) and regurgitant volume(Figure 6.15(b)): all the PHVs showed an $EOA > 1 \; cm^2$ and a $regurgitant \; volume < 10\%$ of the stroke volume (71.4 mL). The minimum performance requirement correspond to the following pulsatile flow condition: heart rate = 70 cycles/min, simulated CO = 5 L/min, SV = 71.4 mL, mean aortic pressure = 100 mmHg, and systolic duration = 35%.

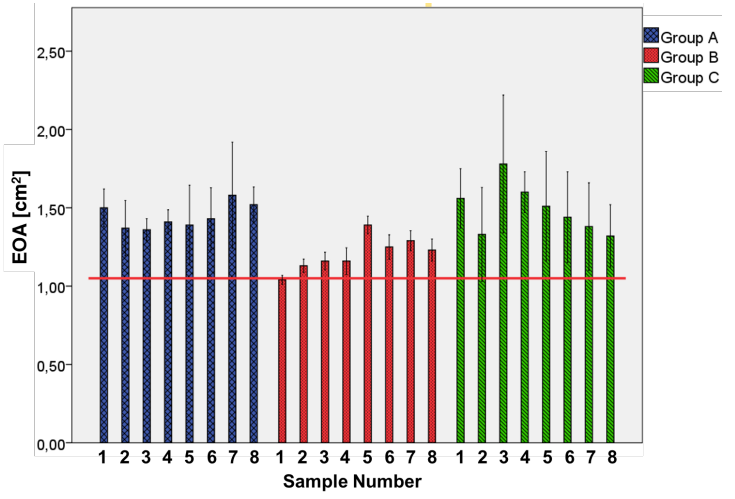

(a)

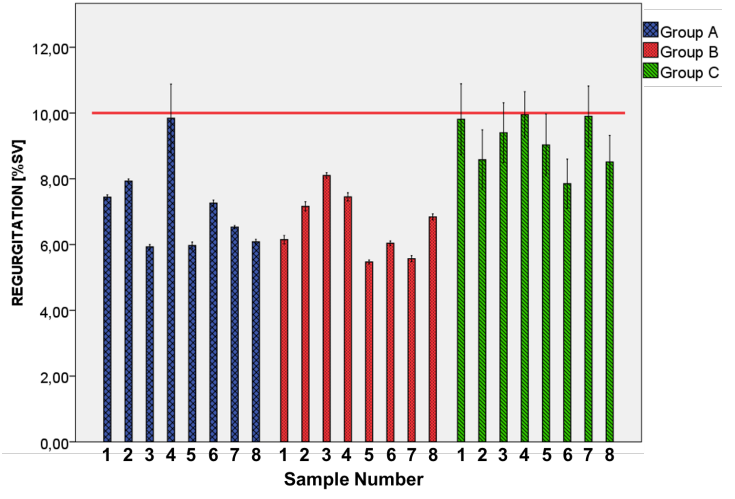

(b)

Figure 6.15 EOA (a) and regurgitation (b) for the three groups of valves, during physiological pulsatile test condition: heart rate = 70 cycles/min, simulated CO = 5 L/min, SV = 71.4 mL, mean aortic pressure = 100 mmHg, and systolic duration = 35%. The horizontal lines indicate the ISO 5840:2015 specifications for the same pulsatile flow condition.

Group A showed statistically higher EOA ($1.45 \pm 0.21\ cm^2$) than Group B ($1.21 \pm 0.12\ cm^2$)($p = 2.29 \cdot 10^{-4}$). The injection moulded prototypes (Group C) show the highest EOA values ($1.49 \pm 0.16\ cm^2$) and the difference in the EOA performance is not statistically different if compared to Group A ($p = 0.65$) while on the contrary it is statistically different if compared to Group C ($p = 4.75 \cdot 10^{-3}$).
Mean regurgitation volume was comparable between the three groups ($7.13 \pm 1.33\%$ of Group A vs $6.60 \pm 0.94\%$ of Group B vs $9.04 \pm 0.78\%$ of Group C). Even thought the regurgitation of Group A is higher than the regurgitation of the Group B, the differences between these two groups are not statistically significant. The prototypes belonging to Group C show the highest regurgitation (9.04 ± 0.78 % of SV), and this difference is statistically significant ($p = 1.34 \cdot 10^{-4}$ if compared to Group A and $p = 1.99 \cdot 10^{-4}$ if compared to Group B).
All these data are summarised in Table 6.4.

Table 6.4 Mean regurgitation volume (% of the SV), mean systolic pressure difference (MSPD) and effective orifice area (EOA) among the 8 prototypes of the three groups and the two reference valve.

Group	Regurgitation $[\%SV]$	MSPD $[mmHg]$	EOA $[cm^2]$
A	7.13 ± 1.33	12.20 ± 1.41	1.45 ± 0.08
B	6.60 ± 0.94	17.09 ± 3.39	1.21 ± 0.11
C	9.13 ± 0.78	8.94 ± 1.30	1.49 ± 0.16
Biological	4.62 ± 0.33	7.06 ± 0.20	1.64 ± 0.91
Mechanical	22.04 ± 1.94	15.28 ± 2.96	1.55 ± 0.11

The performed pulsatile tests showed that the MSPD recorded in Group A was statistically lower ($12.20 \pm 1.41\ mmHg$) than in Group B ($17.09 \pm 3.39\ mmHg$)($p < 0.0019$) according to the EOA results. As the matter of fact, MSPD and EOA are directly proportional quantities.
The effect of temperature among all the groups was also investigated. All the prototypes were kept four hours in water at 37°C before being tested at the same temperature. No differences were observed in performing these tests for all the compression moulded prototypes, both in continuous and in pulsatile flow conditions.

On the other hand, prototypes belonging to Group C show different effect orifice area if tested at 22°C ($1.49 \pm 0.16\ cm^2$) or at 37°C ($1.65 \pm 0.16\ cm^2$) even if without statistical significance ($p = 0.03$).

6.2.4 Discussion

Steady state and pulsatile hydrodynamic tests were performed to acquire information and indicators on the fluid mechanical behaviour of prototypes manufactured both by injection and compression moulding with different styrene fraction. The results from continuous and pulsatile flow tests demonstrated that the transvalvular pressure drop is related to the stiffness of the polymer (cf. Section 3.3.2), which increases with polystyrene mass percentage in the material (Figure 6.4 and Figure 6.15(a)).
Differences between Group A and Group B for EOA and mean transvalvular pressure drops are statistically significant as demonstrated by independent-sample *t-test*. Also the Group C and the Group B show statistically significant difference for EOA, mean transvalvular pressure drop, and regurgitation. Group A and Group C, the groups with a similar amount of styrene fraction, show the same behaviour in term of both EOA and regurgitation. The movement of the leaflets of the this two groups of valve, on the contrary, seems very different (Figure 6.7 and Figure 6.5).
The effect of the styrene fraction is evident between Group A and B. As a matter of fact, keeping all the other conditions constant (i.e. geometry, fabrication technique etc.) a higher material stiffness is responsible for a smaller leaflet deformation during the systolic phase, and consequently for a reduced valve opening. This result can be ascribed to the reduced leaflet deformation obtained during the systolic phase in the valve belonging to Group B; as a matter of fact, the higher polystyrene weight fraction characterising the polymer in these valves induces stiffer leaflet behaviour thus resulting in a smaller valve opening. The prototypes made by injection moulding (Group C) showed good opening and closing performances mimicking the behaviour of natural heart valves.
The regurgitation of the valve belonging to the Group C during the continuous test is lower (almost ten time lower) if compared to the other two groups. Conversely the regurgitation of the Group C, obtained during pulsatile tests, is the highest. Even if the regurgitation is below the threshold suggested by the Standard (10% of SV), it is still quite high compared to the regurgitation obtained in continuous tests. The cause of this difference is due to inertial effects. During the continuous back flow test, a low backpressure is enough to close very well the valve, leaving only a small hole in the centre (Figure 6.7).

Analysing the slow-motion video captured during the pulsatile tests, it was observed that the valves belonging to Group C presented a sort of "bouncing" of the pillar during the diastolic phase. As soon as a backpressure is imposed, the valve tends to close, initially. After that, the return force exerted by the side posts tends to reopen a little bit the valve, only to close again because the backpressure further increases, causing this rebound phenomenon.
However, all the 24 prototypes meet the minimum requirements specified in the ISO 5840:2015 Standard, both in terms of regurgitation and EOA (Figure 6.15), demonstrating their effectiveness.
The better performances in opening during systolic phase displayed by the valves belonging to Group A and C, suggest that block copolymers having lower than 30% styrene fraction should be chosen for PHV manufacturing.
The fluid dynamic behaviour displayed by the three groups of polymeric valves were compared (Table 6.5) with one biological and one mechanical prosthetic heart valve currently on the market with the same tissue annulus diameter.
Both EOA and regurgitation of the tissue heart valve, the gold standard in term of fluid dynamic behaviour, is comparable with the data obtained from prototypes.
Biological heart valve shows the best performance in term of total regurgitation volume and EOA ($(4.62 \pm 0.33)\%$ and $(1.64 \pm 0.91) cm^2$, respectively). On the other hand, the mechanical heart valve shows the worst performance in term of regurgitation while the EOA is comparable with the other valve (both polymeric and biological).
The results of this comparison show that the hydrodynamic behaviour of polymeric prototypes may make them a valid alternative to the valve prostheses currently available on the market. Among the three groups, the injection moulded prototypes show the best compromise between EOA and regurgitation.
The pulsatile results, in particular the regurgitation results indicates that, even though the leaflet geometry is the same, the size of the lateral posts and the method of production affect more valve performance than the percentage of styrene.

Table 6.5 Summary of the results in both continuous and pulsatile flow.

Group	Continuous flow		Pulsatile flow		
	ΔP_{max} [mmHg]	$Q_{backflow}\ mean$ [mL/min]	Regurgitation $[\%SV]$	MSPD $[mmHg]$	EOA $[cm^2]$
A	175.33 ± 19.21	8.36 ± 1.33	7.13 ± 1.33	12.20 ± 1.41	1.45 ± 0.08
B	263.97 ± 26.90	15.26 ± 1.87	6.60 ± 0.94	17.09 ± 3.39	1.21 ± 0.11
C	26.88 ± 12.08	9.35 ± 1.25	9.13 ± 0.78	8.94 ± 1.30	1.49 ± 0.16
Biological	32.58 ± 28.79	1.53 ± 0.21	4.62 ± 0.33	7.06 ± 0.20	1.64 ± 0.91
Mechanical	568.09 ± 231.72	3.03 ± 0.40	22.04 ± 1.94	15.28 ± 2.96	1.55 ± 0.11

6.3 Flow visualisation: Particle Image Velocimetry

To design heart valve prosthesis combining the benefits of both biological valves and the durability of the mechanical valves it is necessary to obtain a detailed understanding of the fluid mechanics of the prosthetic valve, that is shear stress, flow separation, stagnation regions and vortex are fundamental factor to determine the valves performance.
Also the ISO 5840:2015 Standard suggests to assess the flow field, velocity and shear, in the immediate vicinity of the surgical heart valve substitute, including within the valve housing mechanism. The suggested techniques are laser Doppler velocimetry (LDV), particle image velocimetry (PIV) and computational fluid dynamics (CFD); any further details as test protocol or minimum performance requirements are not provided.
To compare the performance of the valve prototypes manufactured in this project, also in these fluid dynamic test two valves currently on the market were characterised: one biological and one mechanical prosthetic valve.
Two kinds of tests were performed: two dimensional particle image velocimetry (2D-PIV) and tomographic particle image velocimetry (Tomo-PIV). While the former is a simple tool to investigate the flow and the velocity profile along one plane, the latter is a robust and accurate technique to investigate three-dimensional flows.
First a 2D-PIV was performed on a small groups of prototypes for discriminating the valves displaying the worst performance. Eventually, the valve with the best performance was analysed by tomo-PIV.

6.3.1 Method

Two dimensional PIV

The experimental set-up (Figure 6.16) used for the continuous flow test with PIV was composed of a volumetric pump (0.75 hp, Lowara SGM7, Direct Industry), a free surface reservoir, a valve housing replicating the Valsalva sinus dimensions, a Ng:Yag pulsed laser generator (Twins Ultra, Quantel, France) and a camera (PCO SensiCam, Germany). Neutrally buoyant silver-coated seed particles ($\phi = 10\mu m$) were placed inside the liquid used in the system which is a mixture of glycerol and water in a 43% v/v ratio at 22°C ($\mu = 0.003\ Pa \cdot s;\ \rho = 1060 \frac{kg}{m^3}$).

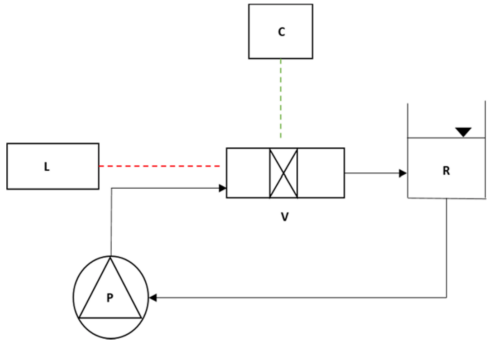

(a)

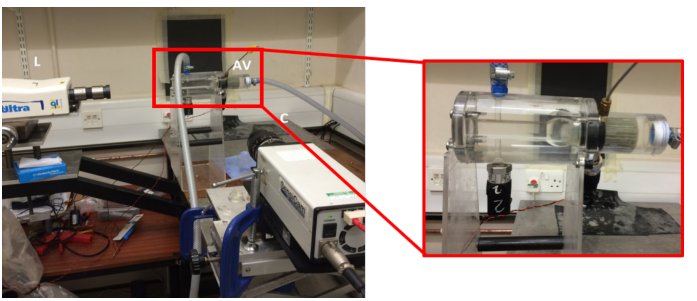

(b)

Figure 6.16 Sketch (a) and picture (b) of the experimental set-up used for the PIV tests. Shown on the diagram are the centrifugal pump (P), the laser (L), the recording camera (C) and the valve housing mimicking the Valsalva sinus dimension obtained following the guidelines of the American Heart Association (AHA). Downstream the valve a free surface reservoir is present. In the picture, on the right it is possible to observe a zoom of the valve housing.

The valve housing (Figure 6.17) was built specifically trying to reproduce the physiological anatomic site of the aortic valve. The data used for the sizing come from the papers published by the American Heart Association (AHA): the aortic sinus has a diameter of 34 mm in its largest point , while the diameter of the downstream pipe is 22 mm.

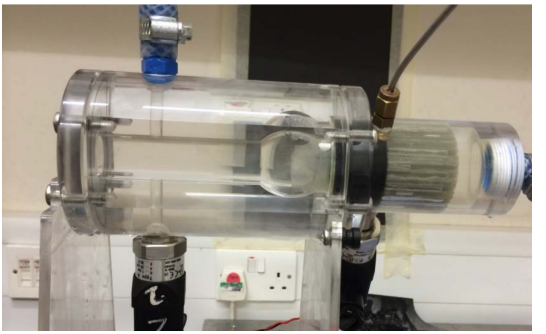

Figure 6.17 Picture of the valve housing mimicking the Valsalva sinus dimension obtained following the guidelines of the American Heart Association (AHA). Upstream the Valsalva sinus a flow straightener was used to maintain the flow as laminar as possible.

The housing is made by polymethyl methacrylate (Perspex®) and is composed of two specular elements. The external lateral side of the housing has been flattened to prevent optical distortions due to the index of refraction of the Perspex®.
As required by ISO 5840 the pressure drop was measured using two pressure sensors (Wika, tipe A-10, Germany), placed one diameter upstream and three diameters downstream the valvular plane.
The valves were subjected to four steady flow rates: 5 l/min, 10 l/min, 15 l/min and 20 l/min. Twenty image pairs were taken for each valve at each flow rate.
Two prototypes belonging to each one of the three groups, for a total of 6 valves, have been tested. The selected prototypes showed the best performance in the pulsatile tests. At the end, the images were analysed with VidPIV software (version 4.6) and then processed with Tecplot software (version 360 ex).

Tomo-PIV

At the ARTORG Center for Biomedical Engineering Research of the University of Bern, the tomographic PIV tests were performed using the same setup described by (Hasler et al., 2016).
The setup for the tomo-PIV experiment is shown in Figure 6.18.

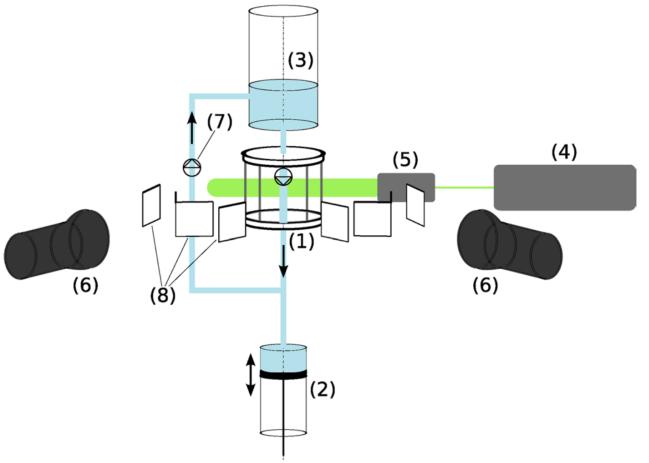

(a)

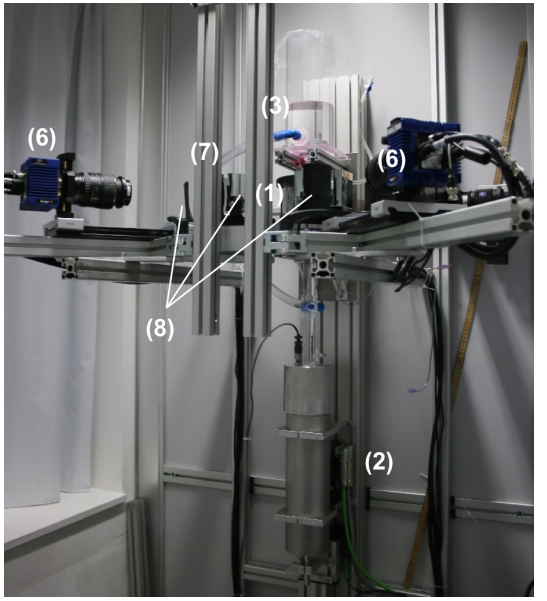

(b)

Figure 6.18 Schematics (a) and picture (b) of the experimental setup: valve housing containing a silicone phantom of the aorta and the valve prosthesis to test (1); piston pump (2); free surface reservoir (3); Nd:YAG laser (4); beam expander (5); CCD cameras (6) with mirrors (8) and a unidirectional valve in the feedback tube (7). Modified from Hasler et al. (2016).

This test bench consists of several elements: the valve housing (1) holds the prosthetic heart valve which is firmly inserted in a transparent silicone model (phantom) of the aortic root (Figure 6.19). The material which is used to model the aortic root is optically transparent for the purpose of image recording and illumination.The used silicone (ELASTOSIL 601, Wacker Silicones, Germany), has very good transparency properties and a refraction index of $1.40 \div 1.41$.
The valve housing is integrated in a pulsatile flow loop which is driven by a computer-controlled piston pump. The neutrally buoyant silver-coated seed particles were placed inside the liquid used in the system which is a mixture of glycerol and water in a 30% v/v ratio at 22°C ($\rho = 1140 \frac{kg}{m^3}$ and $\mu = 9 \cdot 10^{-3} Pa \cdot s$). Viscosity is very high (two times higher than blood viscosity) but it is necessary for obtaining the same refraction index between the silicon model of the aortic root and the fluid used.
The fluorescent particles (PMMA-RhB-FRAK/SA29 with $\phi = 20 - 50 \mu m$), have an emissivity wave length at $584nm$ and absorbance at $560nm$. Upon illumination of the valve housing with a laser (Figure 6.18(4)), these particles emit light at a slightly higher wave length which is captured from different angles by CCD cameras (Figure 6.18(6)). The system was synchronised using the phase of the piston pump as the trigger signal. The two-dimensional particle images were combined by tomographic algorithms to reconstruct a three-dimensional representation of the particle cloud. Particle image cross-correlation was then applied to two particle clouds subsequently captured within a short time interval. In this way obtaining three-dimensional velocity fields is possible.

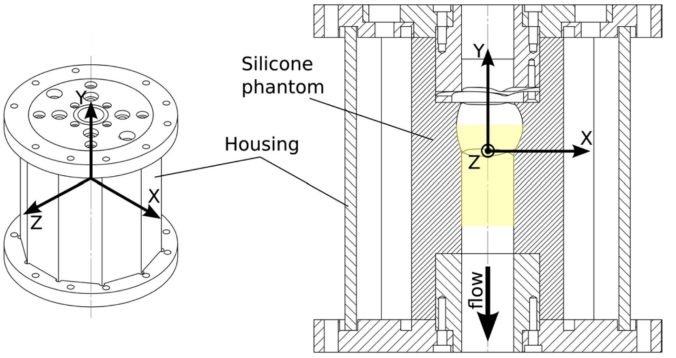

(a)

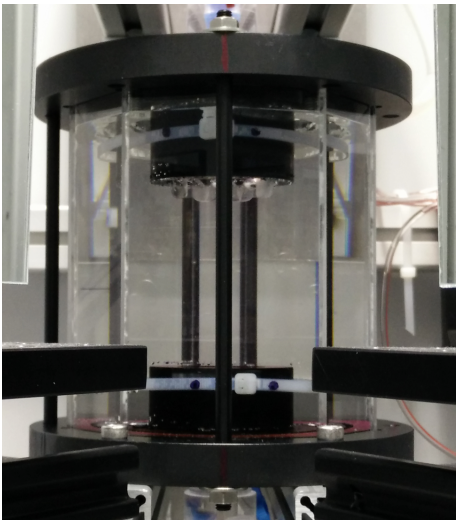

(b)

Figure 6.19 Technical drawing (a) (3D view left, sectional view right) and picture (b) of the aortic housing with the ten-edge polygonal housing for the silicone. Yellow shading indicates measurement volume. Modified from Hasler et al. (2016).

The used camera are two 8 Mpixel 12 bit CCD Digital Camera (Imager LX, LaVision, Göttingen, Germany) with an aspect ratio of 4:3 and prime lenses with a focal length of f = 100 mm, and a maximum aperture of F2.8 (Kenko Tok-

ina, Tokyo, Japan). With the dual-view modality, each of the four recorded image had a resolution of 1656×2488 pixels and the maximum frame rate was 3.1 Hz which limited the possibilities for time-resolved measurements. A double-pulse Nd:YAG laser (Nano L PIV, Litron Lasers, Rugby, England) emitting at 532 nm wave length with a power of 235 mJ/pulse was used.
For the flow measurements, the FlowMaster Tomographic PIV system (LaVision, Göttingen, Germany) was used while for all computational tasks, the software package DaVis (LaVision, Göttingen, Germany) was used (Hasler et al., 2016).
After camera calibration, the tests were performed on one SEPS-22 valve.
A valve belonging to Group C was chosen due to the better hydrodynamic and 2D-PIV results showed (cf. Section 6.2.3 and Section 6.3.2).
For pulsatile flow measurements, the pump was operated in a sinusoidal mode with a period of T = 1 s (60 beats per minute) according to Equation (6.8):

$$\overline{u}(t) = \overline{u}_{max} \cdot \sin\left(\frac{2\pi t}{T}\right) \tag{6.8}$$

with the maximum bulk velocity $\overline{u}_{max} = 0.5m/s$. By multiplying Equation (6.8) for the cylinder bore of the pump, the flow rate equation was obtained. By integrating this new equation over the first half of the period, yielding a physiological stroke volume of 72 ml, the maximum bulk velocity $\overline{u}_{max} = 0.5m/s$ is obtained. In reality, the flow profile (over time) during systole is steeper and shorter than a sine and the maximum bulk velocities lies around 1 m/s (Schmidt and Thews 2007).The resulting flow rate through the valves corresponded approximately to a cardiac output of 4.3 l/min.
Using this setting in the piston frequency and flow rate, it was possible to compare the data obtained with the prototypes tested in this work with a Carpentier Edwards Model 2625 Aortic valve (Edwards Lifesciences, Irvine,USA) tested by Hasler et al. (2016) using the same apparatus and the same pulsatile flow.

6.3.2 Results

Two dimensional (2D) PIV

The fluid dynamic velocity field of the PHVs are compared with a tissue valve (3000 PERIMOUNT Magna, Edwards Lifesciences) and a mechanical valve (Omniscience tilting disk) with the same TAD, currently on the market. All the data are summarized in Table 6.6.
Prototypes belonging to the same groups showed very close velocity field. For this reason, results of only one prototype per group are shown.

Table 6.6 The table shows the maximum velocity peak and the diameter of central orifice jet of the Tissue and Mechanical valve at the flow rates of 5 l/min and 20 l/min. Range of velocity peak among the PHVs are reported.

Flow rate $\left[\frac{L}{min}\right]$	Valves	Velocity peak $[m/s]$	Diameter of central orifice jet $[mm]$
5	Tissue	0.14	22.89
	Mechanical	0.16	8.82
	PHVs	0.16 - 0.24	10.82 - 17.39
20	Tissue	1.15	27.54
	Mechanical	1.14	12.75
	PHVs	0.85 - 1.25	17.68 - 29.86

Figure 6.20, Figure 6.21 and Figure 6.22 show the velocity field at the four chosen velocity. The behaviour of the biological and mechanical valve which were tested are shown in Figure 6.23.

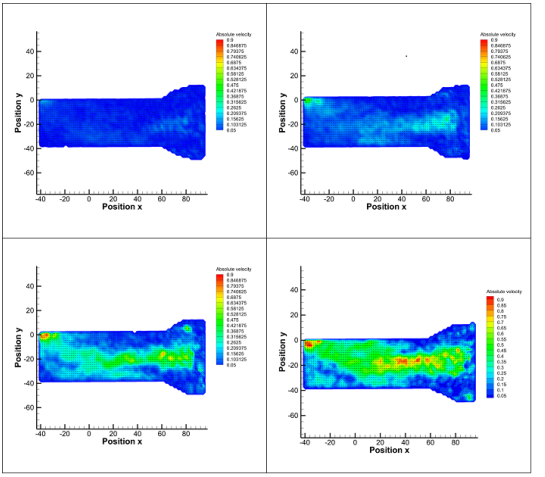

Figure 6.20 Flow velocity field at four flow rate: 5 L/min (top left), 10 L/min (top right), 15 L/min (bottom left) and 20 L/min (bottom right) of the best SIBS-19 valve belonging to group A.

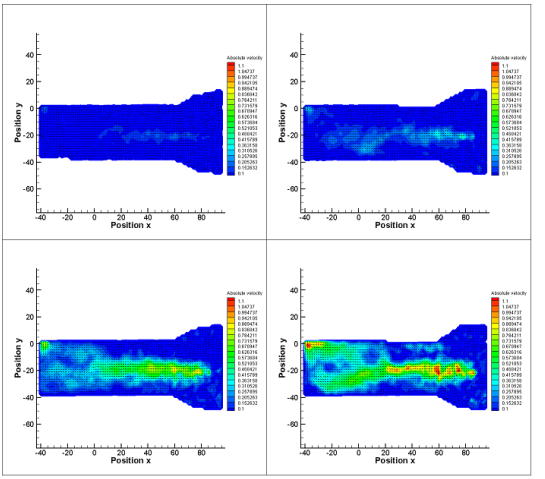

Figure 6.21 Flow velocity field at four flow rate: 5 L/min (top left), 10 L/min (top right), 15 L/min (bottom left) and 20 L/min (bottom right) of the best SIS-30 valve belonging to group B.

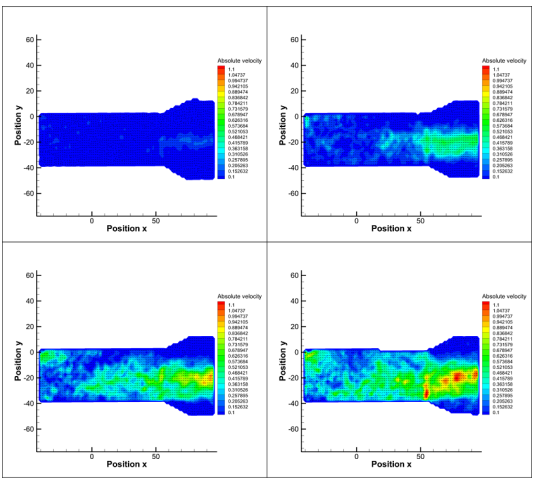

Figure 6.22 Flow velocity field at four flow rate: 5 L/min (top left), 10 L/min (top right), 15 L/min (bottom left) and 20 L/min (bottom right) of the best SEPS-22 valve belonging to group C.

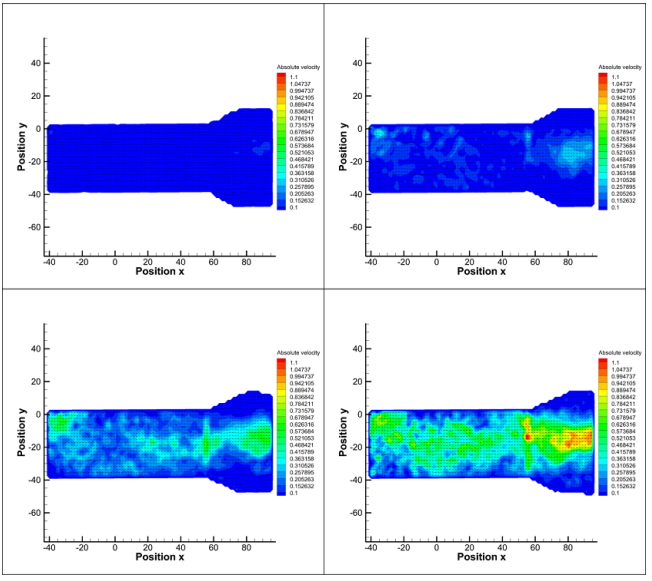

(a)

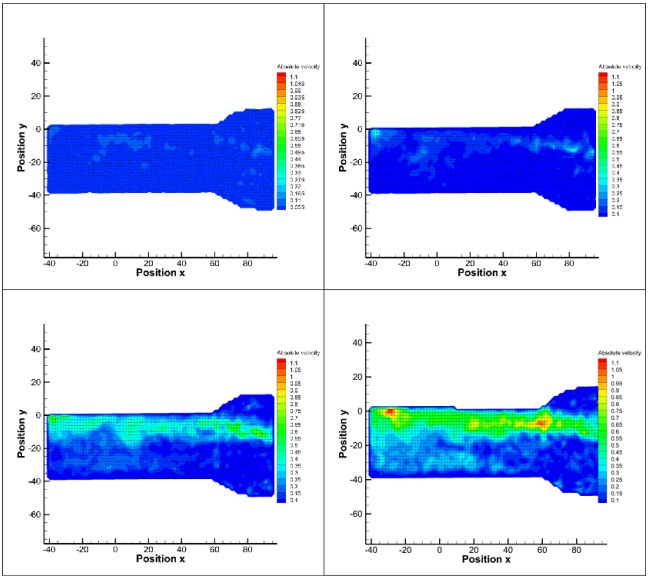

(b)

Figure 6.23 Flow velocity field at four flow rate: 5 L/min (top left), 10 L/min (top right), 15 L/min (bottom left) and 20 L/min (bottom right) of the Biological valve (a) and Mechanical one (b).

Figure 6.24 shows the profile of the PHVs and the biological valve at the flow rate of 5 L/min. The flow induced by both the PHVs and the tissue valve was characterised by a strong central orifice jet. Specifically the velocity profile distribution in the presence of PHVs showed a central orifice jet flow with recirculation areas symmetrically located near the aortic wall of the Valsalva sinus. However, PHVs were found to generate higher vortex than the tissue valve due to their more constricted flow orifices. The same observation was made at the flow rate of 20 l/min (Figure 6.25).

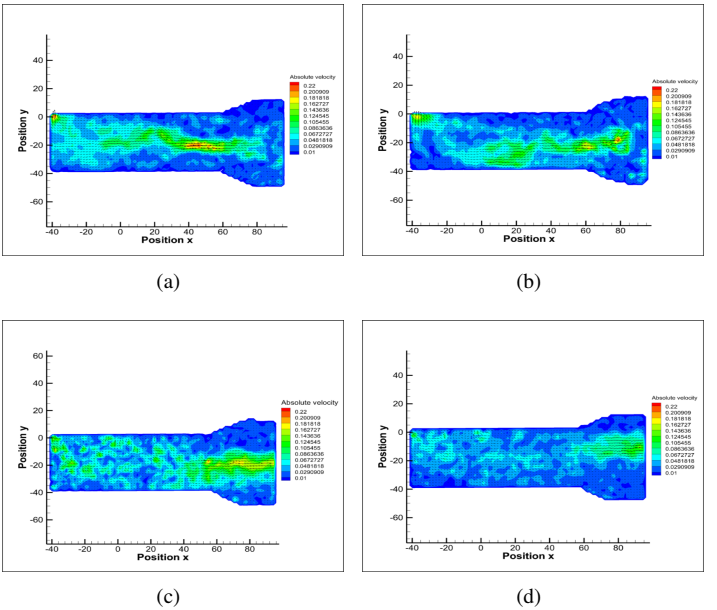

Figure 6.24 Flow velocity field at 5 L/min in a prototypes belonging Group A (a), Group B (b) Group C (c) and Biological one (d).

The biological valve shows velocity peak of 0.14 m/s and the diameter of the central orifice jet is larger than the central orifice jet of the PHVs tested. The prototypes with the maximum velocity belongs to the Group B (0.24 m/s). The prototypes showing a large central orifice area, on the contrary, belong to Group C. These prototypes show a velocity peaks higher than the velocity peaks of the biological one (0.18 m/s vs 0.14 m/s) but the two central orifice jets are comparable.

The velocity peak observed in the upper left of the conduit is due to the presence of the outlet pipe which is connect to the free surface reservoir.

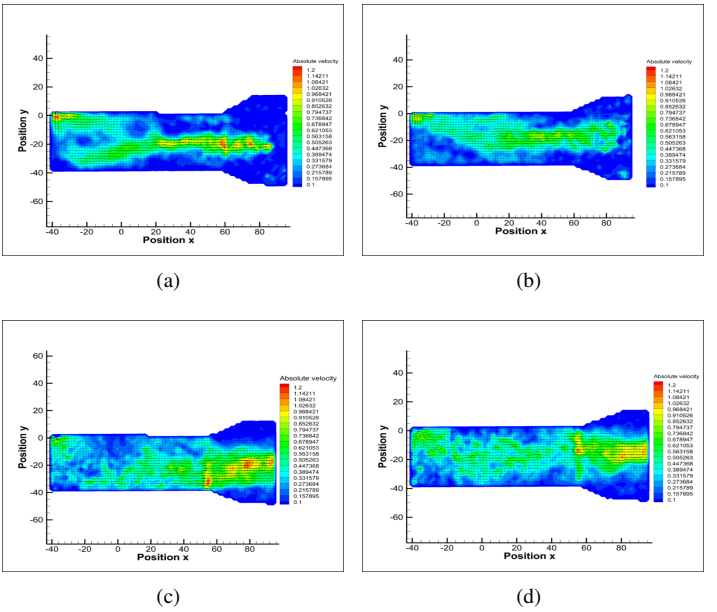

Figure 6.25 Flow velocity field at 20 L/min in a prototypes belonging Group A (a), Group B (b) Group C (c) and Biological one (d).

At the steady flow rate of 20 L/ min, the biological valve reaches the maximum velocity peak of 1.15 m/s and the fluid in the aortic sinus presents a larger central orifice jet compared to those of the other valves. One valve belonging to group C, in addition to reaching the highest velocity peak value (1.25 m/s) is the only one showing a central orifice area jet larger than the jet showed by the biological valve. Also the valves belonging to Group A show a good fluid dynamic behaviour, while the prototypes of the Group C show turbulence in the aortic sinus and do not present a developed profile flow downstream the valvular plane.
Even at 20 L/min the velocity peaks observed in the upper left of the conduit are due to the presence of the outlet pipe, which is connected to the free surface reservoir.

Tomo-PIV

The Tomo-PIV allows to reconstruct the three-dimensional fluid-dynamic profile of the flow through the cardiac prosthesis (Figure 6.26). This technique is very interesting because allows to observe at different time how the fluid passes through the device. Moreover, it is possible to assess the velocity peak in different planes using one single acquisition.

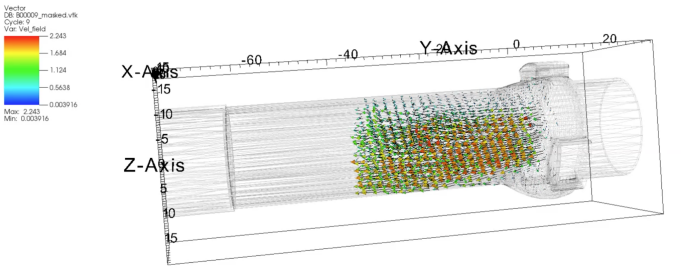

Figure 6.26 3D velocity field (arrow)

Figure 6.27 shows the velocity field (arrow) and velocity magnitude in the XZ-plane at two different Y position: 1 mm (Figure 6.27(c)) and 15 mm (Figure 6.27(b)) downstream the valve, while Figure 6.28 shows the velocity field (arrow) and velocity magnitude in the YZ-plane. The velocity peak at the t=0.36 s (peak of pulsatile flow) is equal to 2.8 m/s. It is possible to observe how the force induced by the fluid is not sufficient to open all the three leaflets, for that reason the velocity field of the Section 1 show in Figure 6.27(c) presents that form.

This section allows appreciating the central orifice jet, that is very similar to the one showed by Hasler et al. (2016) when testing a bioprosthesis currently on the market.

The velocity peak observed in the bioprosthetic heart valve is slightly above 2 m/s, the 30% lower than the velocity peak in the prosthesis developed in this work.

To summarise, Figure 6.29 shows the velocity field over time in a single cycle. It is interesting to note that both Hasler et al. (2016) and Leo et al. (2005) (who tested different polymeric heart valve prototypes) observed a three-lobe configuration of the central orifice jet.

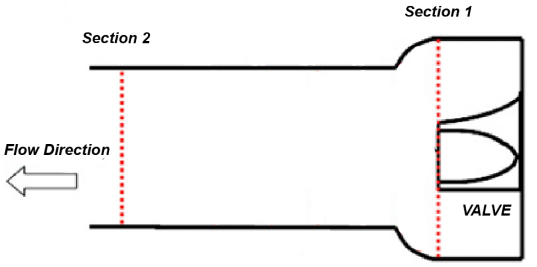

(a)

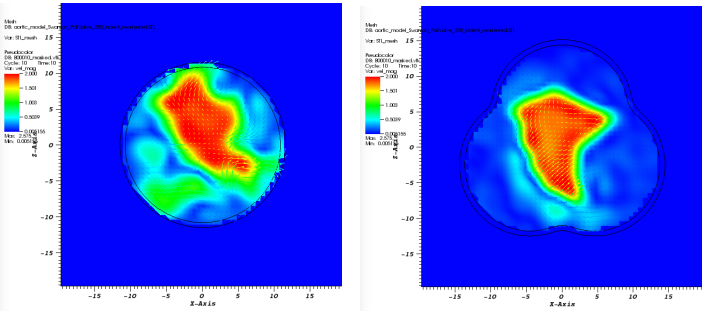

(b) (c)

Figure 6.27 Data acquired along two measurement planes downstream of the valve at two different locations shown in (a): at the valvular plane (b) and 15 mm downstream the valve (c) at the peak of pulsatile flow (t=0.36s).

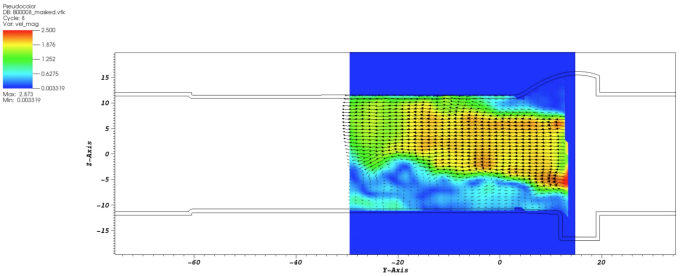

Figure 6.28 Velocity field (arrow) and velocity magnitude in the YZ-plane at the peak of pulsatile flow (t=0.36s).

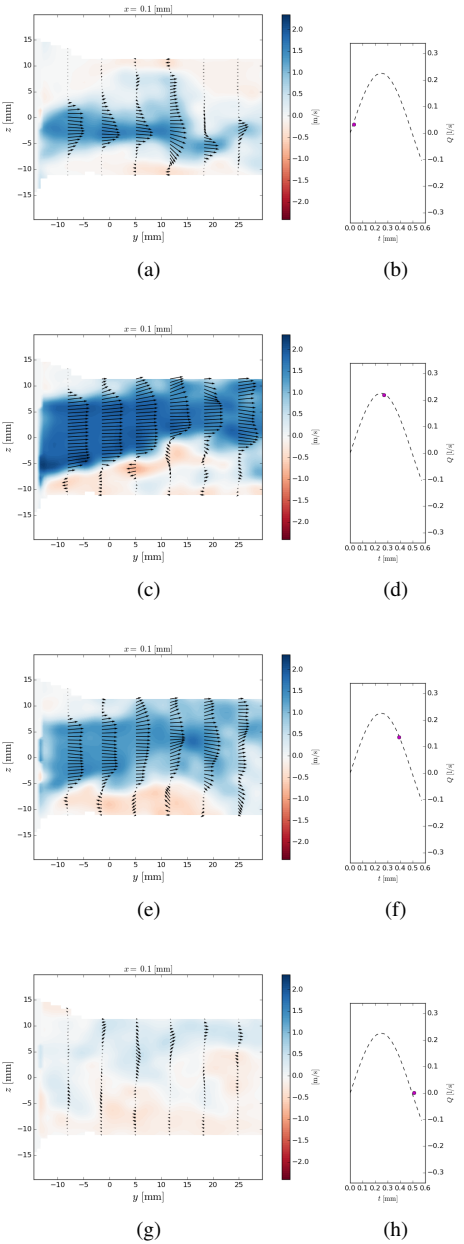

Figure 6.29 Flow field in the central YZ-plane (left) and corresponding flow rate (right) at different time: t=0.05 s (a and b), t=0.30 s (c and d), t=0.40 s (e and f) and t=0.50 s (g and h)

While in the work of Hasler et al. (2016) this three-lobe configuration, called star-like jet, has the three lobes pointing into the sinus portion, in Leo et al. (2005) the three-lobe of this star pointed toward the commissures.
However, this phenomenon has not been clearly noticed in the valves which were analysed in this work. As a matter of fact Figure 6.30 shows a sort of "three-lobe" profile but, due to the fact that the valve does not completely open, this shape can also be a false result.
Among the "three-lobe" there are three regions that show some recirculation of flow even during the systolic phase. During diastole, a central vortex was observed (Figure 6.31) while smaller lateral vortex are present.

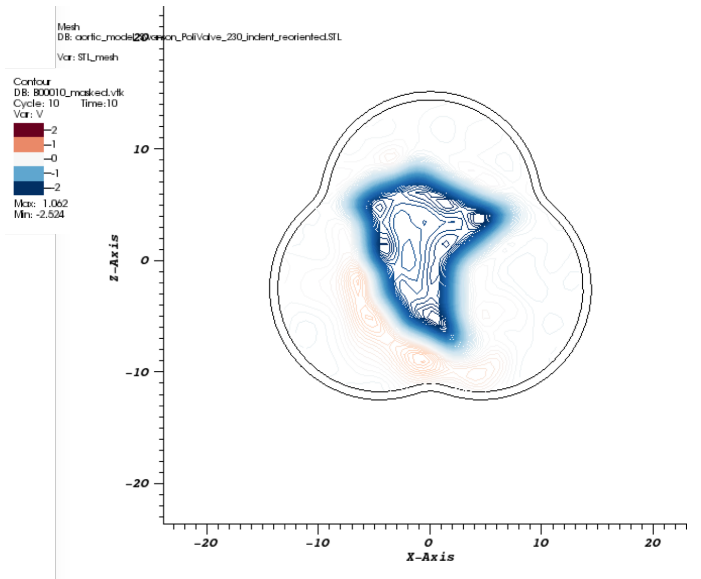

Figure 6.30 Velocity in the y direction in cross section at the valvular plane. Solid lines indicates $U_y = 0\ m/s$ (t=0.36s).

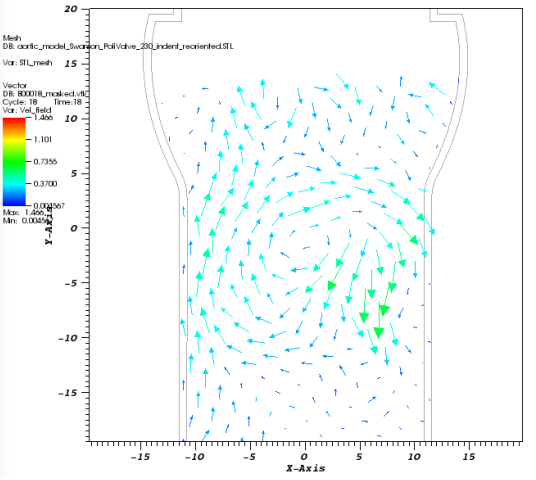

Figure 6.31 Velocity in the YZ-plane at the end of systolic phase $(t = 0.9s)$.

6.3.3 Discussion

Even at low continuous flow rate, the flow induced by the biological valve and the valve belonging to the Group A and C are characterized by a strong central orifice jet (Figure 6.24). The velocity profile distribution in PHVs showed a central orifice jet flow with recirculation area symmetrically located near the aortic wall of the Valsalva sinus. However, PHVs generate larger vortexes than the tissue valve due to their more constricted flow orifice. The same effects are present at 20 L/min (Figure 6.25) but the prototypes with the low amount of styrene, present a higher central orifice area jet, which is comparable to the one of the biological valve.

As reported in the pulsatile test results, there is a relationship between styrene fraction and cross section areas available for the fluid to pass through the valve. In the pulsatile test we refer to the EOA while in the PIV test the index that well explain this behaviour is the central orifice jet.

Both PHVs and tissue valves exhibit vortex flow in the sinus region generally less than 0.02 m/s at the flow rate of 5 l/min while at 20 l/min all the valves tested valves show vortex flow in the same region less than 0.2 m/s.

On the other side, Tomo-PIV allows to have a full fluid dynamic characterisation of the valve both in time and space. However to display the full dynamic behaviour of the instantaneous velocity field, higher acquisition frequency have

to be performed.
It would be interesting to better analyse the flow field at different pulsatile flow rate to understand if the star-like jet is always present. Since the prototype does not fully open, it is possible to observe how the flow is not completely centred but shifted upwards. This results in a lower cross section area and therefore and in the higher speed. If the valve was able to open completely, as can be observed at higher flow (20 L/min), probably the speed would reduce significantly as observed in the 2D PIV.
Based on the results obtained both by hydrodynamic testing and flow visualisation tests the prototypes made by injection moulding seem to be the ideal candidate to investigate the long term performance. As explained in the Section 6.4, therefore, the fatigue tests will only be conducted on this type of valves.

6.4 Valve fatigue testing

A successful prosthesis is characterised by both good short term fluid dynamic performance and lifelong durability. To make sure of the effective number of cycle that the prototypes could sustain, fatigue test are necessary.
The fatigue failure of a polymer is complicated by its viscoelastic properties: the Maxwell model (Figure 6.32) using a spring and damper in series can explain this behaviour.

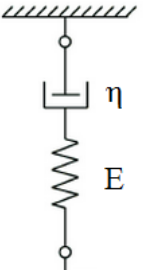

Figure 6.32 Maxwell model represented the viscoelastic properties of a polymeric material: where E is the elastic modulus and η is the material coefficient of viscosity.

By applying a force, the deformation presents both an elastic and viscous response:

$$\varepsilon = \varepsilon_{el} + \varepsilon_{visc} \tag{6.9}$$

where ε is the total strain, ε_{el} is the strain in the spring and ε_{visc} is the strain in

the damper. The same happens for the deformation speed:

$$\dot{\varepsilon} = \dot{\varepsilon}_{el} + \dot{\varepsilon}_{vis} \tag{6.10}$$

where $\dot{\varepsilon}$ is the total strain rate, $\dot{\varepsilon}_{el}$ is the strain rate in the spring and $\dot{\varepsilon}_{vis}$ is the strain rate in the dumper.
Combining Equation 6.9 and Equation 6.10 with the Hooke and Newton law, we obtain:

$$\dot{\varepsilon} = \frac{\dot{\sigma}}{E} + \frac{\sigma}{\eta} \tag{6.11}$$

where $\dot{\sigma}$ is the stress rate, E is the elastic modulus, σ the applied stress and η the viscosity. Keeping constant the strain rate, the stress shows an exponential behaviour, characterised by a relaxation time which it is a direct consequence of the thermal movement of molecules.
Moreover, if a sinusoidal stress is taken into account:

$$\sigma = \sigma_0 sin(\omega t) \tag{6.12}$$

where ω is the frequency, the strain (that is time-dependent) will be:

$$\varepsilon(t) = \sigma_0[(\frac{1}{E})\sin(\omega t) - (\frac{1}{\omega\eta})\cos(\omega t)] + c \tag{6.13}$$

where the strain amplitude is strictly dependent of the frequency.
Applying a sinusoidal cyclic loading to a polymeric material, it is observed the phase shifting between the applied stress and strain which increases or decreases depending on the nature of the material that could be more viscous or more elastic, respectively. This phase shift means that, during each stress cycle, the material dissipates energy in the form of heat due to hysteresis phenomena: local increase in temperature may bring the polymer to exceed the glass transition temperature, thus causing a local softening (thermal fatigue failure). It is evident that, the working frequency and temperature play an important role in the fatigue behaviour of a polymer (Reul and Potthast, 2000).
The ISO 5840:2015 Standard prescribes that rigid valve must survive 400 million cycles, while flexible prosthesis must survive 200 million cycles, equivalent to approximately 11 and 5.4 years, respectively, assuming a physiological heart rate of 70 bpm. The ISO 5840:2015 Standard does not suggest any test frequency, but says that: “Where the test frequency may influence the results of durability tests, e.g. where components are manufactured from viscoelastic materials, *real time testing* should be considered.” Real time testing should be performed at the maximum beat rates of 200 bpm while accelerated fatigue test

could reach whatever frequency, usually from 5 to 30 Hz, equal to 300 and 1800 bpm respectively.
It is possible, therefore, to reduce the time for fatigue testing by increasing the frequency but, as previously described, frequency could influence the test. Viscoelastic materials should not be tested above the frequency at which they undergo a β or glass transition. Dynamic mechanical analysis of BCP samples were performed in Cambridge by Dr. Brubert (Brubert, 2015). He found not only a large transition in the dumping factor at 80 Hz, but also a smaller, β transition at 20 Hz (Figure 6.33).
Performing accelerated fatigue test below the β transition frequency of this material, makes the failure of the prototypes independently from the test frequency.

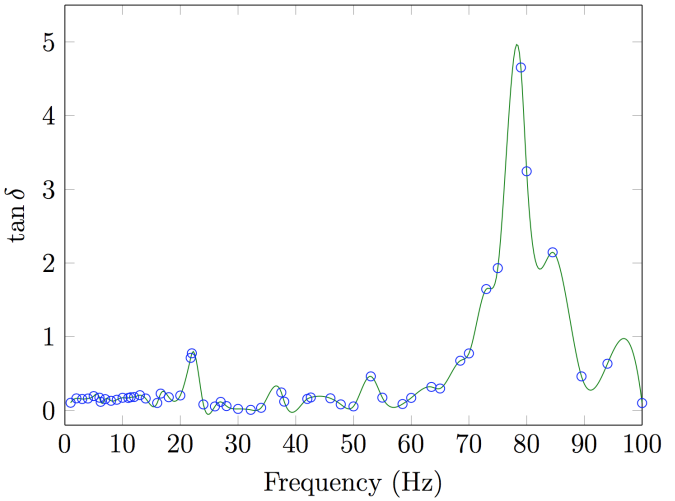

Figure 6.33 Dynamic mechanical frequency sweep of SIBS material at 0.1% strain. A spline is used to fit the data. Note the peak in the damping factor, $\delta = \frac{viscous\ modulus}{elastic\ modulus}$, indicates a glass transition occurring at 80 Hz. The peak seen at 20 Hz corresponds to a smaller β transition. Modified from Brubert (2015).

6.4.1 Method

The prototypes belonging to Group A, B and C have been subjected to different tests and have been subjected to over-stress. For that reason new prototypes were manufactured and tested.
Moreover, the prototypes belonging to Group C showed the best hydrodynamic results and a flow field similar to the flow field of the biological valve. For that reason new prototypes made by injection moulding of SEPS-22 were fabricated.
A total of 21 PHVs were manufactured: 9 valves were identical to those belonging to Group C, while the other 12 prototypes differed from the previous 9 in the size of the tissue annulus diameter (TAD=23 mm).
For the selected valves, both quasi-real durability test and accelerated fatigue test were performed following the Standard requirement.
The tests were performed under normotensive condition (Figure 6.9), with a peak differential pressure across the closed valve equal to 100 mmHg. The defined differential pressure across the closed valve was maintained for at least 5% of each cycle (10% during diastole).
Two different test benches were used to perform the two types of durability test. In order to perform quasi-real time durability test, the test bench used for the pulsatile test was modified. The systemic impedance simulator (RCR block) was removed and an *ad hoc* lower resistance was designed and 3D printed. The length of all the tube was reduced to minimise the inertial effects. The test were performed at frequencies of 200 bpm with a low SV (25 ml) to obtain a cardiac output of $5\frac{L}{min}$. In these tests a sinusoidal curve was implemented in the pulse duplicator, obtaining a sinusoidal pressure variation at the valve.
This test bench was duplicated and was sent at the Cambridge University to doubling the test at the same time.
Two units of the Bose®DuraPulse™ (Figure 6.34) were used to perform accelerated test at the University of Cambridge. On this commercial test bench, four valves could be tested at the same time and each sample is independently controlled, no matter how many are running. Removal or adjustment of one sample does not affect other samples. Using the Bose®DuraPulse™ it is only possible to choose the test frequency and the backpressure. With this commercial test bench it is not possible to perform quasi-real fatigue tests, because to obtain a back pressure of at least 100 mmHg a frequency of at least 10Hz is required. The selected frequency to perform accelerate fatigue tests is 20 Hz, however, the same frequency at which the β transition had been observed.
Testing was performed using distilled water, without takin into account calcification effects.

Figure 6.34 The Bose® DuraPulse™ used to perform accelerated fatigue test.

While some minor damage is expected on valve after completing durability testing, failures are characterised by functional impairment due to excessive structural damage. In this work, an excessive regurgitation correlated to an abrupt decrease in backpressure is the primary index of valve failure.
The valves were inspected every 5 million cycles even though the backpressure was constant at 100 mmHg to look for holes, tears, gross delamination, fracture or fraying that could then propagate and cause the fail of the prosthesis.
Prior to perform the fatigue tests the valve were examined: the thickness of the leaflet were measured and optical observations have been performed using a confocal Laser Scanning Microscope (Olympus LEXT OLS4100).
Micro computed tomography (micro-CT) is performed on two prototypes with different TAD. The micro- CT is x-ray non-destructive imaging technique able to really represents 3D microscopy. A micro-focus x-ray source illuminates the object and a planar x-ray detector collects magnified projection images. Based on hundreds of angular views acquired while the object rotates, a computer synthesises a stack of virtual cross section slices through the object. SkyScan 1172 scanner was used. The geometry reconstruction was performed with Mimics™ software (version 17.0, Materialise, Leuven, Belgium).

6.4.2 Results

All the valve manufactured by injection moulding showed a defect on the top of the free edge Figure 6.35.
These defects are due to the manufacturing technique. The injector locator is directly in contact with the male of the mould, and when the injection moulding is over, an air bubble is left (Figure 6.36).

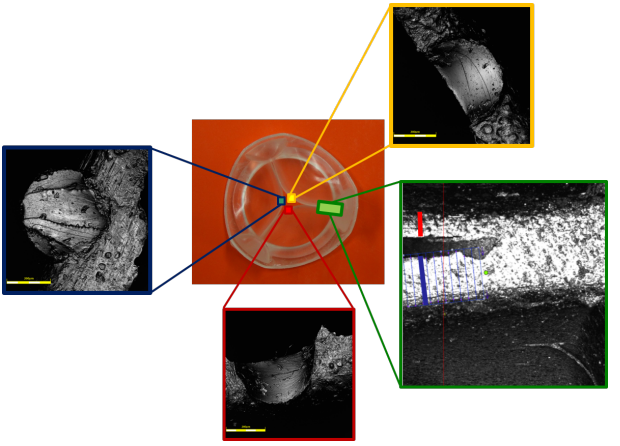

Figure 6.35 SEPS-22 prototypes analysed using a confocal Laser Scanning Microscope (Olympus LEXT OLS4100). Are shown the defect on the top of the free-edge and the thickness difference.

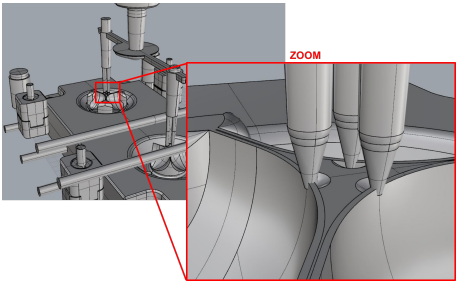

Figure 6.36 3D cad of the internal view of the injection moulding. The injection points are zoomed

However, as described below, this defect has not been the cause of the failure of the valve leaflets.
Performing quasi-real fatigue test it was not easy to keep the back pressure at the constant value of 100 mmHg. As reported in Table 6.7, the back pressure supported for the 10% of the cycle ($BP_{d10\%}$) was always reached but sometimes the maximum back pressure (BP_{MAX}) was double.

Table 6.7 Quasi real-time durability testing results for SEPS-22 prototypes.

Valve	Size [mm]	$BP_{d10\%}$ [mmHg]	BP_{MAX} [mmHg]	Lifetime [10^6 cycles]
1	23	92	163	2.0
2	23	100	190	4.6
3	23	111	172	3.5
4	23	145	190	0.58
5	23	130	185	2.0
6	21	145	373	1.7

The valve 4,5 and 6 were tested in Cambridge using the same modified pulse duplicator used in Milan. Figure 6.37 show the breaking point of the valve.

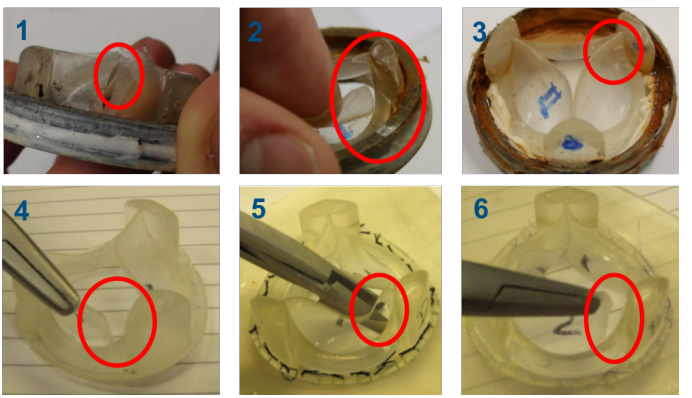

Figure 6.37 Images of failed valve. The red circle shows the breaking point. The valves tested both in Milan (1-2-3) and in Cambridge (4-5-6) failed at the leaflet stent boundary.

The valve showing the worst performance are the valve subjected to the highest peak of back pressure and mean back pressure on the 10% of the diastole, that can reach very high value (145 mmHg for valve # 4 and # 6).
Accelerated tests are being performed at the University of Cambridge and the results of these test are summarised in Table 6.8.

Table 6.8 Accelerated fatigue testing results for SEPS-22 prototypes.

Valve [#]	Size [mm]	$BP_{d10\%}$ [mmHg]	Lifetime [10^6 cycles]
7	23	100	3.6 ± 1.18
8	21	100	13 ± 8.51

All the valve failed having performed fewer than 200 million cycles, thus failing ISO 5840:2015 requirements.

6.4.3 Discussion

The injection moulding tool, and thus the valves which are produced were not within tolerance. As a matter of fact, the thickness is not uniform either in the leaflet or among different leaflet.
The design thickness is 300 μm but using a micrometer and performing micro-TAC the measured leaflet thickness goes from 240 μm to 350 μm. The increased thickness has been identified between the leaflet and the post, where all the valves ruptured.
On the other hand, the minimum thickness was found at the commissures.
The diastolic overpressure, that is not present in the fatigue tests performed using the Bose®DuraPulse™, may have contributed to the acceleration of failure.
However only the valves with the lower TAD, tested with the commercial tester, show a better performance even if failing ISO 5840:2015 requirements.
At present the fatigue tests are on-going and due to the positive preliminary results, the *in-vivo* test are scheduled for the next summer. For that reason the *in-vivo* tests will not be described in this work.

Chapter 7

General conclusions

7.1 Discussion and Conclusions

Fully synthetic polymeric prosthetic heart valve, with lifelong durability without the need for anticoagulant therapy would be the ideal alternative to mechanical and biological valves, which are currently used.
In this Ph.D. thesis a new trileaflet polymeric heart valve was designed, developed and tested. In particular, the classic engineering design process mixed with the scientific method was proposed with the purpose to achieve the ideal prosthesis. Since the seventies, the properties of polymeric materials have been studied in order to develop an ideal polymeric heart valve that combines the fluid dynamic properties of the tissue valve with the durability of mechanical ones.
The choice of the material is an essential step because influences the manufacturing technique and thus the design.
Soft block copolymer, based on styrene micro-chains, if well oriented, can be used to reproduce the collagen architecture of the native valve leaflet which contributes to its flexibility and durability.
Three nanostructured styrene based block copolymer were chosen as promising materials for cardiovascular application.
The mechanical properties of these polymer were evaluated in order to obtain all the needed parameters to be used for the numerical model. The formulation of the constitutive model does not account for dissipative behaviour or viscous mechanism (Zaffora, 2011).
Moreover these testing procedures were useful to better understand the effect of styrene content and its orientation. As a matter of fact, three different styrene fractions were taken into account: 19%, 22% and 30% and two manufacturing techniques. SI/BS-19 and SIS-30 were manufactured by compression moulding while SEPS-22 was manufactured by injection moulding.
Using small angle X-ray scattering (SAXS), the microstructure of the three polymer were investigated, observing a novel layered biaxial structure in the injection moulded material (SEPS-22).
The design of a new prosthesis required advanced experimental and computational methods. Starting from a previously computational method presented by the research group I belong to Zaffora (2011), a new polymeric heart valve was designed. Keeping constant the leaflet geometry, three different prototypes were compared. While SI/BS-19 and SIS-30 prototypes, obtained by compression moulding, have the same stent geometry, SEPS-22 prototypes were manufactured by injection moulding using the design that showed the lowest deformation in the numerical model during diastole.

With the purpose to obtain circumferentially micro-chain orientation inside the valve leaflet, mimicking the collagen architecture, a computational model reproducing the injection moulding technique was proposed. The rheology of the polymer melt was characterised and the Carreau model was selected to best fit the experimental data.
The computational model was set comparing the micro-chain orientation inside a thin membrane manufactured by injection moulding. Several configurations with different *Inlets* and *Outlets* positions, in order to determine which configuration leads to a predominantly circumferential orientation of the polymer chains, were analysed. Biaxial orientation was found along the leaflet thickness and the differences in the polymeric chains orientation among the different configurations resulted negligible.
Low flow rates led to a layered biaxial structure which mimicked the collagen orientation mostly in the concave region. The main difference was observed in the stent - leaflet boundary regions, where the presence of the injector point is very influential. In these regions it is possible to observe different *weld line*, the lines along which there has been the conjunction of two flow fronts. They are considered as defects, both for structural reasons and for aesthetic reasons, since it interrupts the continuity of the material, especially if the two fronts at the time of junction were at low temperatures. Interestingly, all the valves which underwent fatigue testing have buckled along these lines.
Three groups of prototypes were manufactured: 16 prototypes made by SI/BS-19 and SIS-30 were manufactured by compression moulding technique (Group A and B respectively) while 8 prototypes made by SEPS-22 were manufactured by injection moulding (Group C).
The valves were tested *in vitro* according to ISO5840:2015 Standard and met the minimum requirements imposed by the Standard (EOA greater than $1,05cm^2$ and regurgitation lower than 10% of the stroke volume). Group C showed the best pulsatile performance in the opening behaviour ($1.49cm^2 \pm 0.16cm^2$) while showed the highest regurgitation volume ($9.13\% \pm 0.78\%$).
In general, the PHVs behaviour is much better compared to the mechanical prosthesis and is comparable (at least the EOA and MSPD) with the one of tissue valve.
Two prototypes belonging of each groups underwent 2D-PIV continuous flow tests. The valves with the lower amount of styrene fraction showed the best performance, and in particular the prototypes manufactured by injection moulding showed a central orifice jet larger than the one observed in the tissue valve tested.
The best injection moulded prototype underwent also Tomo-PIV, performed in

pulsatile condition. This technique is very interesting as it allows the observation of how the fluid passes through the device along time.
The flow fields through this prototypes were compared to the velocity fields observed with the same technique in one tissue valve (Hasler et al., 2016) and among other polymeric prototypes (Leo et al., 2005). Similar three-lobe configuration of the central orifice jet was observed even if further tests would be needed to better investigate this phenomenon.
Durability tests on 21 new prototype made by SEPS-22 were also performed. Both *quasi-real time* durability tests and accelerated tests were performed, the first at the test frequency of 200 bpm, the latter at the test frequency of 20Hz. The valves survived at a maximum of thirteen million cycles which was less then the minimum Standard requirements of 200 millions of cycle at the back pressure of 100 mmHg.
The durability of the polymeric heart valves not only depends on the mechanical properties of the materials but also on the manufacturing technique and on the stress distribution within the material. It was observed a correlation between the region with the maximum stress and the breaking or tearing zone.
This work shows a methodology to follow in order to achieve a new polymeric heart valve, through an engineering iterative process. The proposed bioinspired styrene based heart valve prosthesis seems to have the potential to overcome the issue of durability and need for anticoagulation therapy.
Therefore, it is necessary to go over again the proposed algorithm until you get the desired result. At the present time, the next stages in development should focus on increasing durability to an acceptable level.
This PhD work puts the basis for the development of further activities either theoretical or experimental. In particular, based on this work results, it is possible to develop a fluid-structure interaction model and also optimise the manufacturing process.
Leaflet thickness, filet between leaflet and stent, weld lines obtained during manufacturing are fundamental steps in the fatigue life assessment. Some of these parameters could influence not only the fatigue behaviour but also the short term performance. Incorporating fluid-structure interaction (FSI) into a hyperelastic, viscoelastic and anisotropic model is a big step for modelling but would allow to optimise the PHV design.
It is important not only obtain a model of the ideal prosthesis, but also be able to achieve it. During these years a lot of prototypes were manufactured at the University of Cambridge and there has always been a constant improvement in the manufacturing phase. Pushing the manufacturing phase in the right direction, it will be possible get excellent prototypes.

Bibliography

Balguid, A., Rubbens, M. P., Mol, A., Bank, R., Bogers, J., Van Kats, J. P., De Mol, B. A., Baaijens, F. P., and Bouten, C. V. (2007). The Role of Collagen Cross-Links in Biomechanical Behavior of Human Aortic Heart Valve Leaflets - Relevance for Tissue Engineering. *Tissue Engineering*, 13(7):1501–1511.

Bansal, N., Kumar, S. R., Baker, C. J., Lemus, R., Wells, W. J., and Starnes, V. A. (2015). Age-Related Outcomes of the Ross Procedure Over 20 Years. *The Annals of Thoracic Surgery*, 99(6):2077–2085.

Bellhouse, B. J. (1972). Fluid mechanics of a model mitral valve and left ventricle. *Cardiovascular Research*, 6(2):199–210.

Bernacca, G., Mackay, T., Wilkinson, R., and Wheatley, D. (1997a). Polyurethane heart valves: Fatigue failure, calcification, and polyurethane structure. *Journal of Biomedical Materials Research*, 34(3):371–379.

Bernacca, G. M., Mackay, T. G., Gulbransen, M. J., Donn, A. W., and Wheatley, D. J. (1997b). Polyurethane heart valve durability: effects of leaflet thickness and material. *The International journal of artificial organs*, 20(6):327–31.

Bernacca, G. M., O'Connor, B., Williams, D. F., and Wheatley, D. J. (2002a). Hydrodynamic function of polyurethane prosthetic heart valves: Influences of Young's modulus and leaflet thickness. *Biomaterials*, 23(1):45–50.

Bernacca, G. M., Straub, I., and Wheatley, D. J. (2002b). Mechanical and morphological study of biostable polyurethane heart valve leaflets explanted from sheep. *Journal of Biomedical Materials Research*, 61(1):138–145.

Bezuidenhout, D., Williams, D. F., and Zilla, P. (2015). Polymeric heart valves for surgical implantation, catheter-based technologies and heart assist devices. *Biomaterials*, 36:6–25.

Billiar, K. L. and Sacks, M. S. (2000). Biaxial mechanical properties of the natural and glutaraldehyde treated aortic valve cusp–Part I: Experimental results. *Journal of biomechanical engineering*, 122(1):23–30.

Boden, M., Richard, R., Schwarz, M. C., Kangas, S., Huibregtse, B., and Barry, J. J. (2009). In vitro and in vivo evaluation of the safety and stability of the TAXUS? Paclitaxel-Eluting Coronary Stent. *Journal of Materials Science: Materials in Medicine*, 20(7):1553–1562.

Bouten, C. V. C., Dankers, P. Y. W., Driessen-Mol, A., Pedron, S., Brizard, A. M. A., and Baaijens, F. P. T. (2011). Substrates for cardiovascular tissue engineering. *Advanced Drug Delivery Reviews*, 63(4):221–241.

Braunwald, N. S. and Morrow, A. G. (1965). A late evaluation of flexible teflon prostheses utilized for total aortic valve replacement. postoperative clinical, hemodynamic, and pathological assessments. *The Journal of thoracic and cardiovascular surgery*, 49:485–96.

Brubert, J. (2015). *A novel polymeric prosthetic heart valve: design, manufacture, and testing*. Phd thesis, University of Cambridge.

Brubert, J., Krajewski, S., Wendel, H. P., Nair, S., Stasiak, J., and Moggridge, G. D. (2016). Hemocompatibility of styrenic block copolymers for use in prosthetic heart valves. *Journal of Materials Science: Materials in Medicine*, 27(2):1–12.

Cacciola, G., Peters, G. W. M., and Schreurs, P. J. G. (2000). A three-dimensional mechanical analysis of a stentless fibre-reinforced aortic valve prosthesis. *Journal of Biomechanics*, 33(5):521–530.

Carew, E. O., Barber, J. E., and Vesely, I. (2000). Role of preconditioning and recovery time in repeated testing of aortic valve tissues: validation through quasilinear viscoelastic theory. *Annals of Biomedical Engineering*, 28(9):1093–1100.

Carew, E. O., Talman, E. a., Boughner, D. R., and Vesely, I. (1999). Quasi-Linear Viscoelastic theory applied to internal shearing of porcine aortic valve leaflets. *Journal of biomechanical engineering*, 121(4):386–92.

Castano, M. (2016). Synthesis of polyisobutylene-polycaprolactone block copolymers using enzyme catalysis. *Express Polymer Letters*, 10(8):693–700.

Claiborne, T. E., Girdhar, G., Gallocher-Lowe, S., Sheriff, J., Kato, Y. P., Pinchuk, L., Schoephoerster, R. T., Jesty, J., and Bluestein, D. (2011). Thrombogenic potential of Innovia polymer valves versus Carpentier-Edwards Perimount Magna aortic bioprosthetic valves. *ASAIO Journal*, 57(1):26–31.

Claiborne, T. E., Sheriff, J., Kuetting, M., Steinseifer, U., Slepian, M. J., and Bluestein, D. (2013a). In Vitro Evaluation of a Novel Hemodynamically Optimized Trileaflet Polymeric Prosthetic Heart Valve. *Journal of Biomechanical Engineering*, 135(2):021021.

Claiborne, T. E., Xenos, M., Sheriff, J., Chiu, W.-C., Soares, J., Alemu, Y., Gupta, S., Judex, S., Slepian, M. J., and Bluestein, D. (2013b). Toward optimization of a novel trileaflet polymeric prosthetic heart valve via device thrombogenicity emulation. *ASAIO journal (American Society for Artificial Internal Organs : 1992)*, 59(3):275–83.

Cornhill, J. F. (1977). An aortic left ventricular pulse duplicator used in testing prosthetic aortic heart valves. *Journal of Thoracic and Cardiovascular Surgery*, 73(4):550–558.

Daebritz, S. H., Fausten, B., Hermanns, B., Franke, A., Schroeder, J., Groetzner, J., Autschbach, R., Messmer, B. J., and Sachweh, J. S. (2004). New flexible polymeric heart valve prostheses for the mitral and aortic positions. *Heart Surgery Forum*, 7(5):371–378.

Darling, S. B. (2007). Directing the self-assembly of block copolymers. *Progress in Polymer Science (Oxford)*, 32(10):1152–1204.

Dasi, L. P., Simon, H. A., Sucosky, P., and Yoganathan, A. P. (2009). Fluid mechanics of artificial heart valves. *Clinical and Experimental Pharmacology and Physiology*, 36(2):225–237.

De Gaetano, F., Bagnoli, P., Zaffora, A., Pandolfi, A., Serrani, M., Brubert, J., Stasiak, J., Moggridge, G. D., and Costantino, M. L. (2015a). A Newly Developed Tri-Leaflet Polymeric Heart Valve Prosthesis. *Journal of Mechanics in Medicine and Biology*, 15(02):1540009.

De Gaetano, F., Serrani, M., Bagnoli, P., Brubert, J., Stasiak, J., Moggridge, G. D., and Costantino, M. L. (2015b). Fluid dynamic characterization of a polymeric heart valve prototype (Poli-Valve) tested under continuous and pulsatile flow conditions. *The International journal of artificial organs*, 38(11):600–6.

De Hart, J., Cacciola, G., Schreurs, P. J., and Peters, G. W. (1998). A three-dimensional analysis of a fibre-reinforced aortic valve prosthesis. *Journal of biomechanics*, 31(7):629–638.

De Hart, J., Peters, G. W. M., Schreurs, P. J. G., and Baaijens, F. P. T. (2004). Collagen fibers reduce stresses and stabilize motion of aortic valve leaflets during systole. *Journal of Biomechanics*, 37(3):303–311.

D'Souza, S. S., Butterfield, M., and Fisher, J. (2003). Kinematics of synthetic flexible leaflet heart valves during accelerated testing. *The Journal of heart valve disease*, 12(1):110–9; discussion 119–20.

Duan, B., Hockaday, L., Kang, K., and Butcher, J. (2014). Aortic Heart Valve Tissue Regeneration. In *Tissue and Organ Regeneration*, number November 2015, pages 645–694. Pan Stanford Publishing.

Duraiswamy, N., Choksi, T. D., Pinchuk, L., and Schoephoerster, R. T. (2008). A Phospholipid-modified Polystyrene-Polyisobutylene- Polystyrene (SIBS) Triblock Polymer for Enhanced Hemocompatibility and Potential Use in Artificial Heart Valves. *Journal of Biomaterials Applications*, 23(4):367–379.

El Fray, M., Prowans, P., Puskas, J. E., and Altstädt, V. (2006). Biocompatibility and fatigue properties of polystyrene-polyisobutylene-polystyrene, an emerging thermoplastic elastomeric biomaterial. *Biomacromolecules*, 7(3):844–850.

Feindel, C. M. and David, T. E. (2004). Aortic valve sparing operations: Basic concepts. *International Journal of Cardiology*, 97:61–66.

Fisher, J., Jack, G. R., and Wheatley, D. J. (1986). Design of a function test apparatus for prosthetic heart valves. Initial results in the mitral position. *Clinical Physics and Physiological Measurement*, 7(1):63–73.

Gabbay, S., McQueen, D. M., Yellin, E. L., Becker, R. M., and Frater, R. W. (1978). In vitro hydrodynamic comparison of mitral valve prostheses at high flow rates. *Journal of Thoracic and Cardiovascular Surgery*, 76(6):771–787.

Gallocher, S. L., Aguirre, A. F., Kasyanov, V., Pinchuk, L., and Schoephoerster, R. T. (2006). A novel polymer for potential use in a trileaflet heart valve. *Journal of biomedical materials research. Part B, Applied biomaterials*, 79(2):325–34.

Ghanbari, H., Viatge, H., Kidane, A. G., Burriesci, G., Tavakoli, M., and Seifalian, A. M. (2009). Polymeric heart valves: new materials, emerging hopes. *Trends in Biotechnology*, 27(6):359–367.

Ghazanfari, S., Driessen-Mol, A., Sanders, B., Dijkman, P. E., Hoerstrup, S. P., Baaijens, F. P., and Bouten, C. V. (2015). In Vivo Collagen Remodeling in the Vascular Wall of Decellularized Stented Tissue-Engineered Heart Valves. *Tissue Engineering Part A*, 21(15-16):2206–2215.

Glasmacher-Seiler, B., Reul, H., and Rau, G. (1992). In vitro evaluation of the calcification behavior of polyurethane biomaterials for cardiovascular applications. *Journal of long-term effects of medical implants*, 2(2-3):113–26.

Guyton, A. C. and Hall, J. E. (2006). *Textbook of Medical Physiology*. Elsevier Inc., 11 edition.

Hansen, J. T. (2010). *Netter's Clinical Anatomy*. SAUNDERS Elsevier, Philadelphia, PA, 2 edition.

Hasan, A., Ragaert, K., Swieszkowski, W., Selimović, Š., Paul, A., Camci-Unal, G., Mofrad, M. R. K., and Khademhosseini, A. (2014). Biomechanical properties of native and tissue engineered heart valve constructs. *Journal of Biomechanics*, 47(9):1949–1963.

Hasler, D., Landolt, A., and Obrist, D. (2016). Tomographic PIV behind a prosthetic heart valve. *Experiments in Fluids*, 57(5):1–13.

Hutchison, C., Sullivan, P., and Ethier, C. R. (2011). Measurements of steady flow through a bileaflet mechanical heart valve using stereoscopic PIV. *Medical and Biological Engineering and Computing*, 49(3):325–335.

Jansen, J. and Reul, H. (1992). A synthetic three-leaflet valve. *Journal of Medical Engineering and Technology*, 16(1):27–33.

Jansen, J., Willeke, S., Reiners, B., Harbott, P., Reul, H., and Rau, G. (1991). New J-3 flexible-leaflet polyurethane heart valve prosthesis with improved hydrodynamic performance. *International Journal of Artificial Organs*, 14(10):655–660.

Jiang, H., Campbell, G., Boughner, D., Wan, W.-K., and Quantz, M. (2004). Design and manufacture of a polyvinyl alcohol (PVA) cryogel tri-leaflet heart valve prosthesis. *Medical engineering & physics*, 26(4):269–77.

Katz, L. N. and Feil, H. (1923). Clinical observations on the dynamics of ventricular systole. *Archives of Internal Medicine*, 32(5):672.

Kheradvar, A., Groves, E. M., Dasi, L. P., Alavi, S. H., Tranquillo, R., Grande-Allen, K. J., Simmons, C. A., Griffith, B., Falahatpisheh, A., Goergen, C. J., Mofrad, M. R. K., Baaijens, F., Little, S. H., and Canic, S. (2015). Emerging Trends in Heart Valve Engineering: Part I. Solutions for Future. *Annals of Biomedical Engineering*, 43(4):833–843.

Lanzarone, E., Vismara, R., and Fiore, G. B. (2009). A new pulsatile volumetric device with biomorphic valves for the in vitro study of the cardiovascular system. *Artificial Organs*, 33(12):1048–1062.

Leat, M. E. and Fisher, J. (1994). A synthetic leaflet heart valve with improved opening characteristics. *Medical Engineering and Physics*, 16(6):470–476.

Lecommandoux, S., Lazzari, M., and Liu, G. (2006). *Block Copolymers in Nanoscience*. Wiley-VCH Verlag GmbH & Co. KGaA, Weinheim, Germany.

Lee, J. c., Kim, H. c., Kim, J. c., and Lee, S.-H. b. c. (2016a). Soft implantable microelectrodes for future medicine: Prosthetics, neural signal recording and neuromodulation. *Lab on a Chip - Miniaturisation for Chemistry and Biology*, 16(6):959–976.

Lee, L., Cui, J. Z., Cua, M., Esfandiarei, M., Sheng, X., Chui, W. A., Xu, M. H., Sarunic, M. V., Beg, M. F., Van Breemen, C., Sandor, G. G. S., and Tibbits, G. F. (2016b). Aortic and cardiac structure and function using high-resolution echocardiography and optical coherence tomography in a mouse model of Marfan syndrome. *PLoS ONE*, 11(11):1–19.

Lee, S.-G., Lee, J. H., Choi, K.-y., and Rhee, J. M. (1998). Glass transition behavior of polypropylene/polystyrene/styrene-ethylene-propylene block copolymer blends. *Polymer Bulletin*, 40(6):765–771.

Leo, H. L., Dasi, L. P., Carberry, J., Simon, H. A., and Yoganathan, A. P. (2006). Fluid dynamic assessment of three polymeric heart valves using particle image velocimetry. *Annals of Biomedical Engineering*, 34(6):936–952.

Leo, H. L., Simon, H., Carberry, J., Lee, S. C., and Yoganathan, A. P. (2005). A comparison of flow field structures of two tri-leaflet polymeric heart valves. *Annals of Biomedical Engineering*, 33(4):429–443.

Liu, Y., Kasyanov, V., and Schoephoerster, R. T. (2007). Effect of fiber orientation on the stress distribution within a leaflet of a polymer composite heart valve in the closed position. *Journal of Biomechanics*, 40(5):1099–1106.

Lockie, K. J., Butterfield, M., Fisher, J., Juster, N. P., Watterson, K., and Davies, G. A. (1993). Geometry of homograft valve leaflets: Effect of dilation of the aorta and the aortic root. *The Annals of Thoracic Surgery*, 56(1):125–130.

Mackay, T., Wheatley, D. J., Bernacca, G. M., a.C. Fisher, and Hindle, C. (1996). New Polyurethane Heart Valve Prosthesis: design, manufacturing and evaluation. *Biomaterials*, 17(19):1857–1863.

Martin, C. and Sun, W. (2012). Biomechanical characterization of aortic valve tissue in humans and common animal models. *Journal of Biomedical Materials Research - Part A*, 100 A(6):1591–1599.

Matheny, R. G., Hutchison, M. L., Dryden, P. E., Hiles, M. D., and Shaar, C. J. (2000). Porcine small intestine submucosa as a pulmonary valve leaflet substitute. *Journal of Heart Valve Disease*, 9(6):769–775.

Matin, M. L., Daivis, P. J., and Todd, B. D. (2000). Comparison of planar shear flow and planar elongational flow for systems of small molecules. *The Journal of Chemical Physics*, 113(20):9122–9131.

Mavrilas, D. and Missirlis, Y. (1991). An approach to the optimization of preparation of bioprosthetic heart valves. *Journal of biomechanics*, 24(5):331–9.

Mohammadi, H. and Mequanint, K. (2011). Prosthetic aortic heart valves: Modeling and design. *Medical Engineering and Physics*, 33(2):131–147.

Nishimura, R. A., Otto, C. M., Bonow, R. O., Carabello, B. A., Erwin, J. P., Guyton, R. A., O'Gara, P. T., Ruiz, C. E., Skubas, N. J., Sorajja, P., Sundt, T. M., and Thomas, J. D. (2014). 2014 AHA/ACC guideline for the management of patients with valvular heart disease: Executive summary: A report of the American college of cardiology/American heart association task force on practice guidelines. *Journal of the American College of Cardiology*, 63(22):2438–2488.

Nistal, F., Garcia-Martinez, V., Arbe, E., Fernandez, D., Artinano, E., Mazorra, F., and Gallo, I. (1990). In vivo experimental assessment of polytetrafluoroethylene trileaflet heart valve prosthesis. *Journal of Thoracic and Cardiovascular Surgery*, 99(6):1O74–1081.

O'Connor, B., Wheatley, D. J., Bernacca, G. M., and Haworth, W. S. (2006). Heart Valve Prosthesis and Method of Manufacure.

Pandolfi, A. and Vasta, M. (2012). Fiber distributed hyperelastic modeling of biological tissues. *Mechanics of Materials*, 44:151–162.

Pinchuk, L., Wilson, G. J., Barry, J. J., Schoephoerster, R. T., Parel, J. M., and Kennedy, J. P. (2008). Medical applications of poly(styrene-block-isobutylene-block-styrene) ("SIBS"). *Biomaterials*, 29(4):448–460.

Rahmani, B., Tzamtzis, S., Ghanbari, H., Burriesci, G., and Seifalian, A. M. (2012). Manufacturing and hydrodynamic assessment of a novel aortic valve made of a new nanocomposite polymer. *Journal of Biomechanics*, 45(7):1205–1211.

Reul, H. and Potthast, K. (2000). The dilemma of accelerated bioprosthetic and polymeric valve testing. *Journal of Heart Valve Disease*, 9(1):159–160.

Ribeiro, P. A., Al Zaibag, M., Idris, M., Al Kasab, S., Davies, G., Mashat, E., Wareham, E., and Al Fagih, M. (1986). Antiplatelet drugs and the incidence of thromboembolic complications of the St. Jude Medical aortic prosthesis in patients with rheumatic heart disease. *Journal of Thoracic and Cardiovascular Surgery*, 91(1):92–98.

Rock, C. A., Han, L., and Doehring, T. C. (2014). Complex collagen fiber and membrane morphologies of the whole porcine aortic valve. *PLoS ONE*, 9(1):1–9.

Roe, B. B., Owsley, J. W., and Boudoures, P. C. (1958). Experimental results with a prosthetic aortic valve. *The Journal of thoracic surgery*, 36(4):563–570.

Sachweh, J. S. and Daebritz, S. H. (2006). Novel "biomechanical" polymeric valve prostheses with special design for aortic and mitral position: a future option for pediatric patients? *ASAIO journal (American Society for Artificial Internal Organs : 1992)*, 52(5):575–580.

Sacks, M. S., Merrryman, W. D., and Schmidt, D. E. (2010). On the Biomechanics of Heart Valve. *Journal of biomechanics*, 42(12):1804–1824.

Sacks, M. S., Smith, D. B., and Hiester, E. D. (1998). The aortic valve microstructure: Effects of transvalvular pressure. *Journal of Biomedical Materials Research*, 41(1):131–141.

Schoen, F. J. and Butany, J. (2016). Chapter 13 - Cardiac Valve Replacement and Related Interventions. In Buja, L. M. and Butany, J., editors, *Cardiovascular Pathology (Fourth Edition)*, pages 529–576. Academic Press, San Diego, fourth edi edition.

Schoen, F. J. and Gotlieb, A. I. (2016). Heart valve health, disease, replacement, and repair: a 25-year cardiovascular pathology perspective. *Cardiovascular Pathology*, 25(4):341–352.

Stasiak, J., Brubert, J., Serrani, M., Nair, S., de Gaetano, F., Costantino, M. L., and Moggridge, G. D. (2014a). A bio-inspired microstructure induced by slow injection moulding of cylindrical block copolymers. *Soft matter*, 10(32):6077–86.

Stasiak, J., Moggridge, G. D., Zaffora, A., Pandolfi, A., and Costantino, M. L. (2010). Engineering Orientation in Block Copolymers for Application to Prosthetic Heart Valves. *Functional Materials Letters*, 03(04):249–252.

Stasiak, J., Nair, S., and Moggridge, G. D. (2014b). Mechanical strength of sutured block copolymers films for load bearing medical applications. *Bio-Medical Materials and Engineering*, 24(1):563–569.

Stasiak, J., Squires, A. M., Castelletto, V., Hamley, I. W., and Moggridge, G. D. (2009). Effect of stretching on the structure of cylinder- and sphere-forming styrene-isoprene-styrene block copolymers. *Macromolecules*, 42(14):5256–5265.

Stella, J. A., Liao, J., and Sacks, M. S. (2007). Time-dependent biaxial mechanical behavior of the aortic heart valve leaflet. *Journal of Biomechanics*, 40(14):3169–3177.

Swanson, W. and Clark, R. E. (1974). Dimensions and Geometric Relationships of the Human Aortic Value as a Function of Pressure. *Circulation Research*, 35(6):871–882.

Syedain, Z., Reimer, J., Lahti, M., Berry, J., Johnson, S., and Tranquillo, R. T. (2016). Tissue engineering of acellular vascular grafts capable of somatic growth in young lambs. *Nature communications*, 7:12951.

Syedain, Z., Reimer, J., Schmidt, J., Lahti, M., Berry, J., Bianco, R., and Tranquillo, R. T. (2015). 6-Month aortic valve implantation of an off-the-shelf tissue-engineered valve in sheep. *Biomaterials*, 73:175–184.

Syedain, Z. H., Meier, L. A., Reimer, J. M., and Tranquillo, R. T. (2013). Tubular heart valves from decellularized engineered tissue. *Annals of Biomedical Engineering*, 41(12):2645–2654.

Szelest-Lewandowska, A., Masiulanis, B., Klocke, A., and Glasmacher, B. (2003). Synthesis, physical properties and preliminary investigation of hemocompatibility of polyurethanes from aliphatic resources with castor oil participation. *Journal of biomaterials applications*, 17(3):221–36.

Trebbin, M., Steinhauser, D., Perlich, J., Buffet, A., Roth, S. V., Zimmermann, W., Thiele, J., and Förster, S. (2013). Anisotropic particles align perpendicular to the flow direction in narrow microchannels. *Proceedings of the National Academy of Sciences of the United States of America*, 110(17):6706–11.

Tseng, H. and Grande-Allen, K. J. (2011). Elastic fibers in the aortic valve spongiosa: A fresh perspective on its structure and role in overall tissue function. *Acta Biomaterialia*, 7(5):2101–2108.

Vesely, I. (1997). The role of elastin in aortic valve mechanics. *Journal of Biomechanics*, 31(2):115–123.

Vesely, I., Gonzalez-Lavin, L., Graf, D., and Boughner, D. (1990). Mechanical testing of cryopreserved aortic allografts. Comparison with xenografts and fresh tissue. *The Journal of Thoracic and Cardiovascular Surgery*, 99(1):119–23.

Vesely, I. and Noseworthy, R. (1992). Micromechanics of the fibrosa and the ventricularis in aortic valve leaflets. *Journal of Biomechanics*, 25(1):101–113.

Visai, L., Rindi, S., Speziale, P., Petrini, P., Farè, S., and Tanzi, M. C. (2002). In vitro interactions of biomedical polyurethanes with macrophages and bacterial cells. *Journal of biomaterials applications*, 16(3):191–214.

Wang, G., Zhao, G., and Guan, Y. (2013). Thermal response of an electric heating rapid heat cycle molding mold and its effect on surface appearance and tensile strength of the molded part. *Journal of Applied Polymer Science*, 128(3):1339–1352.

Wang, Q., McGoron, A. J., Bianco, R., Kato, Y., Pinchuk, L., and Schoephoerster, R. T. (2010). In-vivo assessment of a novel polymer (SIBS) trileaflet heart valve. *The Journal of heart valve disease*, 19:499–505.

Wheatley, D. J., Raco, L., Bernacca, G. M., Sim, I., Belcher, P. R., and Boyd, J. S. (2000). Polyurethane: Material for the next generation of heart valve prostheses? *European Journal of Cardio-thoracic Surgery*, 17(4):440–448.

Wisman, C. B., Pierce, W. S., Donachy, J. H., Pae, W. E., Myers, J. L., and Prophet, G. A. (1982). A polyurethane trileaflet cardiac valve prosthesis: in vitro and in vivo studies. *Transactions - American Society for Artificial Internal Organs*, 28:164–8.

Yanagawa, B. and Christakis, G. T. (2012). Bioprosthetic Aortic Valve Replacement: Stented Pericardial and Porcine Valves. In Cohn, L., editor, *Cardiac Surgery in the Adult*, chapter 33, page 695. New York, McGraw Hill, 4th edition.

Yin, W., Gallocher, S., Pinchuk, L., Schoephoerster, R. T., Jesty, J., and Bluestein, D. (2005). Flow-induced platelet activation in a St. Jude mechanical heart valve, a trileaflet polymeric heart valve, and a St. Jude tissue valve. *Artificial organs*, 29(10):826–31.

Zaffora, A. (2011). *Computational method for the design of innovative materials for heart valve prostheses*. PhD thesis, Politecnico di Milano.

Zhao, Y., Su, B., Chen, F., and Fu, Q. (2015). Evolution of unique nanocylindrical structure in poly(styrene-b-isoprene-b-styrene) prepared under "dynamic packing injection moulding". *Soft matter*, 11(11):2300–7.

List of Figures

List of Tables

Publications

Papers

G. Luraghi, W. Wu, **F. De Gaetano**, J. F. R. Matas, G. Moggridge, M. Serrani, J. Stasiak, M. L. Costantino and F. Migliavacca. Evaluation of an aortic valve prosthesis: Fluid-structure interaction or structural simulation? *Journal of Biomechanics*, 2017, xxx, xxx-xxx

M. Serrani, J. Brubert, J. Stasiak, **F. De Gaetano**, A. Zaffora, M. L. Costantino and G. Moggridge. A computational tool for the microstructure optimization of a polymeric heart valve prosthesis. *Journal of Biomechanical Engineering*, 2016, 138, 061001-8

F. De Gaetano, M. Serrani, P. Bagnoli, J. Brubert, J. Stasiak, G. Moggridge and M. L. Costantino. Fluid dynamic performances of a new polymeric heart valve prototype (poli-valve) tested under continuous and pulsatile flow conditions. *International Journal of Artificial Organs*, 2015, 38(11), 600-606

J. Stasiak, J. Brubert, M. Serrani, A. Talhat, **F. De Gaetano**, M. L. Costantino and G. Moggridge. Structural changes of block copolymers with bimodal orientation under fast cyclical stretching as observed by synchrotron SAXS. *Soft Matter*, 2015, 11, 3271-3278

F. De Gaetano, P. Bagnoli, A. Zaffora, A. Pandolfi, M. Serrani, J. Brubert, J. Stasiak, G. Moggridge and M. L. Costantino. A newly developed tri-leaflet polymeric heart valve prosthesis. *Journal of Mechanics in Medicine and Biology*, 2015, Vol.15, No. 2, 154009-1:8

J. Stasiak, J. Brubert, M. Serrani, Sukumaran Nair, **F. De Gaetano**, M. L.

Costantino and G. Moggridge. A bio-inspired microstructure induced by slow injection moulding of cylindrical block copolymers. *Soft Matter*, 2014, 10, 6077-6086.

Proceedings

F. De Gaetano, M. Serrani, J. Brubert, J. Stasiak, G. Moggridge, and M. L. Costantino. Fluid Dynamic assessment if new PHVs prototypes under pulsatile flow condition and using PIV. *Proceedings of the 5th national group of bioengineering conference, GNB 2016*, 20th-22nd June 2016.

F. De Gaetano, M. Serrani, J. Stasiak, J. Brubert, G. Moggridge, and M. L. Costantino. Injection moulding process: cfd evaluation on the orientation of polymeric chains for manufacturing heart valves. *Proceedings of the 42nd Annual Congress European Society for Artificial Organs, ESAO 2015*, 2nd-5th September 2015.

F. De Gaetano, M. Serrani, J. Brubert, J. Stasiak, G. Moggridge, and M. L. Costantino. Computational evaluation of polymer chains orientation in styrene block copolymers treated by injection moulding technique. *Proceedings of the 23rd Congress of the European Society of Biomechanics, ESB 2015*, 5th-9th July 2015.

F. De Gaetano, P. Bagnoli, A. Zaffora, M. Serrani, J. Brubert, J. Stasiak, G. Moggridge and M. L. Costantino. Design of a new polymeric heart valve prosthesis. *Proceedings of the XIX International Conference on Mechanics in Medicine and Biology, ICMMB 2014*, 3rd-5th September 2014.

F. De Gaetano, M. Serrani, J. Stasiak, J. Brubert, P. Bagnoli, G. Moggridge and M. L. Costantino. Hydrodynamic investigation of new polymeric heart valves prototypes. *Proceedings of the 41st- Annual Congress European Society for Artificial Organs, ESAO 2014*, 17th-20th September 2014.

F. De Gaetano, M. Serrani, J. Stasiak, J. Brubert, G. Moggridge, and M. L. Costantino. Hydrodynamic assessment of new polymeric heart valves prototypes under continuous and pulsatile flow rate. *Proceedings of the 7th World Congress of Biomechanics, WCB 2014*, 6th-11th July 2014

F. De Gaetano, M. Serrani, P. Bagnoli, J. Brubert, J. Stasiak, G. Moggridge, and M. L. Costantino. Fluid Dynamic Performance of New Polymeric Heart Valves Prototypes tested under Continuous and Pulsatile Flow Condition. *Proceedings of the 4th national group of bioengineering conference, GNB 2014*, 25th-27th June 2014.